12-2015

The Effect of Graphite Nanoplatelets on the Barrier and Mechanical Properties of LLDPE Films

Wilson Sansbury
Clemson University, wsansbu@g.clemson.edu

THE EFFECT OF GRAPHITE NANOPLATELETS ON THE BARRIER AND MECHANICAL PROPERTIES OF LLDPE FILMS

A Thesis
Presented to
the Graduate School of
Clemson University

In Partial Fulfillment
of the Requirements for the Degree
Master of Science
Packaging Science

---

by
Wilson Ferrel Wright Sansbury
December 2015

Accepted by:
Duncan Darby, Committee Chair
Robert Kimmel
Kay Cooksey
Rupert Hurley

ABSTRACT

Polymer nanocomposites for packaging applications have gained significant research interest over the previous decade. More recently, graphite nanoplatelets (GNP) have attracted interest as potential multipurpose fillers in polymer matrices because of their superb mechanical, thermal, and gas barrier properties that could potentially be transferred to a polymer composite at relatively low loadings. The purpose of this research was to determine the effect that GNP had on the mechanical and barrier properties of 3.5 ± 0.4 mil Dow® Elite™ 5230G Enhanced Polyethylene (EPE) films that were produced by letting down a 20% GNP filled Dow® Elite™ 5230G masterbatch into a base of 5230G resin via a 24:1 single screw cast film extruder. Films were extruded into batches consisting of 0.5%, 1.0%, 2.0%, 3.0%, and 5.0 % by weight of graphite nanoplatelet content as well as a 0.0% control film batch. Optical microscopy revealed poor distribution as well as regions of agglomeration due to a lack of shear provided by single screw extrusion and poor distribution of GNP in the masterbatch. X-ray diffraction results revealed that the films displayed a phase separated morphology, without intercalation or exfoliation of GNP throughout the films. TEM imagery revealed that agglomerations existed in the film and masterbatch samples, but small isolated regions of exfoliated graphite were also present. DSC analysis revealed that the presence of GNP in the matrix acted as a nucleation aid for the LLDPE structure, where cold crystallization occurred 8.0°C higher in the 0.5% film sample and at a maximum of 11.0° C higher in the 5.0% sample. The LDPE crystallinity remained unchanged. OTR results indicated a reduction in oxygen transmission with increasing GNP content. The maximum reduction

of OTR was found in the 5.0 % sample, where the OTR was reduced from 166.4019 ± 2.434 CC / [100in² - day] to 135.2405 ± 7.38 CC / [100in² - day]. WVTR results displayed no significant changes with added GNP content. Tensile analysis revealed a reduction in the plasticity of the films with added GNP content. Increases in 1.0% Secant moduli were observed in all samples containing GNP content, with a maximum increase of 87.5% in the 2.0% GNP sample in the MD and 94.3% in the TD. Insignificant changes in tensile strength were observed in both the MD and TD. Puncture resistance testing displayed similar reductions in compressive extension prior to puncture in samples containing GNP content. The reductions in elongations during puncture and tensile testing may be due to the GNP reducing polymer mobility, while the reduction in tensile strength and puncture resistance is likely due to an inhomogeneous distribution of GNP agglomerates within the matrix, leading to premature cracking and subsequent failure. These agglomerates are likely present due to inhomogeneous distribution of GNP in the masterbatch and lack of shear applied by single screw extrusion.

DEDICATION

I dedicate this paper to Robert Truett Moore.

ACKNOWLEDGMENTS

I would like to thank my advisor, Dr. Duncan Darby, as well as Dr. Robert Kimmel, Dr. Kay Cooksey, and Dr. Andrew Hurley for their time spent serving on my graduate committee. I would also like to express my appreciation to Patricia Marcondes and Girard Stoner for their assistance with the testing procedures performed in this study.

I would like to extend my gratitude to Xolve, Inc. for producing the graphite nanoplatelets and compounding the masterbatch used in this research. I would also like to thank the Dow Chemical Company® for providing resin materials.

I would like to thank George Wetzel of the Clemson Advanced Materials Research Lab for his tremendous assistance with the electron microscopy work, as well as Colin McMillen of the Clemson University Department of Chemistry's Molecular Structure Center for his assistance with x-ray diffraction analysis. I also would like to thank Russell Cooper for his assistance throughout the course of this research.

TABLE OF CONTENTS

Page

Table of Contents (Continued) Page

Table of Contents (Continued) Page

LIST OF TABLES

LIST OF FIGURES

List of Figures (Continued)

List of Figures (Continued)

List of Equations

CHAPTER ONE

INTRODUCTION

The trade of goods across distances became commonplace as economies grew and economic specialization influenced the development of modern civilization. To ensure that these goods remained in tradable condition during transportation and storage, a means to preserve and protect perishable products required that they were contained within some medium. Glass, ceramics, metals, and wooden containers have historically been utilized for this purpose. In more recent times, the use of polymers as packaging materials has become commonplace. Polymers can be produced in bulk at relatively low cost and can be converted into a wide variety of lightweight containers and films to preserve and protect the products they contain. Polyethylene, polypropylene, polystyrene, polyvinyl chloride, and polyethylene terephthalate are some of the most widely used polymers in packaging. Compared to wood, glass, and ceramic materials, polymers are able to be produced using a small fraction of the energy, materials, and cost. (Selke, 2004) Despite these advantages, the applications of polymeric materials are limited in some cases due to high gas and solvent permeability, thermal instability, low stiffness, and transparency (Vasileiou, Kontopoulou, & Docoslis, 2014).

To improve the properties of polymeric materials, they can be blended with other plastics and property altering additives, mixed with inorganic fillers to create filled systems, and processed with fibers and other materials. This blending yields composite

and hybrid materials with a wide range of useful property attributes. (Gupta & Mukhopadhyay, 2011)

Dissimilar polymeric films can be laminated together to form multicomponent structures. A metallized layer is often used to significantly improve barrier properties, but metallized layers are not a perfect solution. Metallized films and foil laminates are not commonly recyclable and require additional processing and materials to produce. (Selke, 2004) Foil structures are also subject to pin holes and stress cracks, which can lead to pathways of significant oxygen ingress, potentially degrading the contents. (Murray, 2006)

In the late 1980's, Toyota Motors Central R&D introduced polymers filled with organically modified layered silicates with very fine thicknesses (in the nanometer range). These new composites were deemed "nanocomposites" and have been of significant research interest since that time because of potential improvements in mechanical, barrier, and thermal properties. Despite the ample research in this field, the commercial application of layered silicate nanocomposites has been limited due to the difficulty in adapting the techniques required to adequately distribute layered silicate materials throughout a polymer matrix using traditional extrusion processes. (Mukhopadhyay & Gupta, 2011)

Recently, the use of nanoscale graphite based materials as fillers in polymers has gained much attention, especially after the recent surge of research following the

successful isolation of monolayer graphite, which is called graphene. Graphene and small clusters of graphene, deemed graphite nanoplatelets (GNP), display excellent thermal, mechanical, barrier, and electron transport properties. Adding these materials to polymers could potentially transfer many of these properties if GNP were adequately distributed throughout a polymer matrix.

Many packaging applications require that materials possess a sufficient combination of barrier, thermal, and mechanical properties to protect the products they contain. GNP-based polymer nanocomposites could potentially be utilized as recyclable, cost effective packaging materials if GNP can be adequately dispersed in a polymer via conventional extrusion methods. Pre-compounded GNP-polymer masterbatches are now commercially available in a variety of commodity polymer resins, but little research exists that investigates whether these masterbatches are capable of being sufficiently dispersed and distributed by the widely used process in the packaging industry of single screw film extrusion.

Objectives

The surge of interest in GNP based composites is broad in focus and much research exists that displays improvements in barrier, mechanical, thermal, and electrical properties in small-scale GNP polymer composite materials produced by direct twin screw extrusion or micro-planing. Unlike monolayer graphene, GNP can currently be

produced economically and in bulk from naturally mined graphite, an inexpensive precursor.

The purpose of this research is to examine how the addition of graphite nanoplatelets to Dow® 5230G EPE™ films affects the barrier and mechanical properties of the films compared to an unmodified control sample while also investigating the morphology of the films to examine if single screw extrusion adequately dispersed the masterbatch. Single screw extrusion was chosen as the means of film production for this research because it is the most common film production method used to produce packaging films (Giles, Wagner, & Mount, 2013). If GNP polymer masterbatches were to be used in packaging film production, then it is critical they are capable of being adequately distributed by means of single screw extrusion.

CHAPTER TWO

REVIEW OF LITERATURE

Polyethylene in Packaging

Polyethylene (PE) is one of the most widely used commodity polymers because of its low cost of processing, non-toxic nature, and good recyclability. It is produced from ethylene gas, which is usually derived from petroleum byproducts or natural gas. Ethylene is polymerized to form several forms of polyethylene that are classified by their density and side chain branching. Low density polyethylene (LDPE), high density polyethylene (HDPE) and linear low density polyethylene (LLDPE) are some of the most common forms of polyethylene used in packaging. (Selke, 2004) The densities of PE differ because of differences in their amount of side chain branching which can be composed of long and or short side chains. The length of the side chains is determined by the polymerization method of the ethylene monomer and in some cases, the comonomer. Ethylene can be polymerized by either a low pressure, Ziegler-Natta process, or a high pressure, free radical process. During the free radical polymerization process, LDPE is formed with long side chain branching and reduced crystallinity compared to HDPE, which is formed via the Ziegler-Natta process with little side chain branching. As the long chain branching increases, the density and crystallinity decreases. LDPE's reduced crystallinity allows for greater clarity which is desirable in certain consumer packaging applications. HDPE's minimal side branching allows for tighter chain packing, greater density (0.940-0.970 g/cm^3), and a more crystalline structure, resulting in increased haze, and improved barrier properties. LLDPE consists of high amounts of short chain

branching as comonomers are added during polymerization of the ethylene. Butene, hexene, and octene, are commonly used as comonomers to form LLDPE. LLDPE shares a similar density to LDPE (0.915 – 0.930 g/cc) and LLDPE typically has a narrower molecular weight distribution, which reduces processability. (Giles, Wagner, & Mount, 2013) In summary, the mechanical, thermal, barrier, and optical properties of polyethylene are greatly influenced by the degree and type of side chain branching, which in turn affects the crystallinity. LLDPE and LDPE are typically ~30% to 55% crystalline, while HDPE can be up to 85% crystalline. (Frey, 2009)

Table 1: Property Changes due to Crystallinity Changes (Source: Frey, 2009)

As Crystallinity Increases:	
Barrier Properties (Gas, water vapor, light)	Increases
Density	Increases
Tensile Strength	Increases
Chemical Resistance	Increases
Heat Resistance	Increases
Tear Strength (Machine Direction)	Decreases
Impact Strength	Decreases
Puncture Resistance	Decreases
Clarity	Decreases
Coefficient of Friction	Decreases

Today, polyethylene's largest market segment is film, where almost half of all LDPE and LLDPE produced is used in film manufacturing. Films can be defined as stand-alone, thin layers of materials that can provide sufficient strength to maintain their thin structure, typically less than 0.003 inches. (Selke, 2004) PE films are used widely throughout food packaging, agricultural films, liners, garbage bags, and merchandise packaging (Zhong, Janes, Zheng, Hetzer, & Kee, 2007). PE film can be produced by cast or blown film extrusion processes. Blown film is a more common manufacturing process for PE packaging films, while cast film is reserved for specialty PE applications where high clarity is required, such as bakery and bread bag film. (Giles, Wagner, & Mount, 2013) Films can be manufactured into pouches, bags, wraps, capsules, and liners as packaging materials to contain and protect products. LDPE and LLDPE films are easily heat sealed and are often used as sealing layers in multilayer structures. (Selke, 2004) Different forms of PE, such as LDPE and LLDPE, can be blended together for improvements in sealing, tensile strength, barrier, processability and other desired properties. LDPE is often blended into LLDPE to increase melt strength during extrusion, which allows for higher throughput.

While PE is nonpolar and provides a sufficient barrier to water vapor, it is highly permeable to oxygen ingress. LLDPE is often considered a "screen door" to oxygen permeation. (Selke, 2004)

Polymer Composites and Laminations

While PE is widely used as a multipurpose packaging material, the current demand of high performance materials requires properties uncharacteristic to the common forms of PE. To meet these demands, composite polymers have been developed that can display properties of both the polymer and the filler, resulting in properties such as increased modulus, dimensional stability, opacity, and heat stability. Composites should not be confused with polymers that contain additives for property modifications that constitute a small portion of the polymer's makeup. Additives are typically added to polymers to alter processing characteristics or final application needs, such as UV absorbency or plasticity, while composites are defined as structural materials that consist of two or more combined non-soluble constituents. It is desired that the manufacturing of composites should allow for precise control of the final material's properties which are dictated by the desired final application. (Gupta & Mukhopadhyay, 2011)

A composite consists of at least two phases. For example, if strength is the desired attribute, a composite would consist of a reinforcing phase and a matrix phase. This reinforcing phase can consist of fillers such as fibers, particles, platelets, or flakes, while the matrix phase can consist of polymers, metals, or ceramics. (Thomas, 2012) A polymer containing a significant portion or amount of a solid additive can be deemed a filled polymer. Composite polymers can be classified as a subgroup of filled polymers. (Gupta & Mukhopadhyay, 2011)

In most cases, mechanical property improvements are the primary objective of a composite, however other properties can be modified including electrical conductivity, gas and moisture barrier properties, thermal properties, antimicrobial properties, etc. The composite's strength and stiffness depend heavily upon the mechanical properties and distribution of the reinforcing filler material, as well as the interfacial bonding that allows for adequate load transfer from the matrix to the reinforcement. (Gupta & Mukhopadhyay, 2011)

Polymer films can be coated or laminated to aluminum, paper, or other films to form multilayer, laminar composite structures that are bonded together by an adhesive or a jointly compatible polymer. Lamination and coating provide a means to combine various material properties of the individual layers into one structure. These laminations and coated materials are commonly used in the food, pharmaceutical, and medical packaging industries, as they allow for an economic means to produce flexible packaging materials with a wide range of material properties. For example, a laminate could combine the superb barrier properties of an aluminum layer with the toughness of a biaxially oriented nylon layer, and with the heat sealing properties of a polyethylene layer. (Selke, 2004) Lamination and coating, however, require additional processing and materials, such as adhesives, primers, and extrudate resins. Instead, the continuous process of multilayer coextrusion allows the converter to potentially skip the lamination process and extrude up to 11 different layers into a film, covering a wide range of material attributes. While coextrusion allows for an efficient manufacturing process, the

capital investment required for multiple extruders for barrier, tie, and sealing layers can be very high. One, two, and three layer film extrusion lines are still commonly found throughout the flexible packaging industry. (Giles, Wagner, & Mount, 2013)

Polymer Nanocomposites

Particulate composites can be classified according to the size of the solid filler. If all of the filler's dimensions are in the micron level or higher, the composite is classified as a microcomposite. Most conventional polymer composites filled with inorganic materials can be classified as microcomposites. A relatively new class of composite materials, deemed nanocomposites, has been the subject of significant research in the previous two decades. If the composite contains a phase consisting of a dimensionally stable material that displays at least one dimension less than 100 nanometers, the composite is classified as a nanocomposite. In a more relatable scale, a human hair is roughly 100,000 nanometers in thickness. (Silvestre, Duraccio, & Cimmino, 2011)

Many nanomaterials of different forms and origins have been examined as potential fillers in polymeric matrices. Layered silicates, such as montmorillonite, have gained much research attention because of their high aspect ratio, low cost, and wide availability, however montmorillonite's highly hydrophilic surface complicates adequate distribution in a hydrophobic polymer matrix. (Azeredo, 2009). Table 2 summarizes some of the most widely researched nanomaterials for use in polymer nanocomposites.

Table 2: Classification of Various Nanomaterials Used in Polymer Nanocomposites.

Adapted from: Gupta & Mukhopadhyay, 2011

Nano-Material	Structure	Brief Description	Drawbacks
Layered Silicates	Platelets	Inexpensive, high cation exchange capacity, high aspect ratio, allow intercalation of polar organic compounds for surface modification	Sufficient dispersion in polymers is difficult to achieve (clays are hydrophilic while many polymers are hydrophobic)
Carbon Nanotubes	Fibers	Outstanding mechanical strength, electrical conductivity	Costly, have tendency to agglomerate within polymer due to strong van der Waals forces between tubes
Graphite Nanoplatelets	Platelets	Inexpensive, thermally and electrically conductive, based on sp2 hybridized carbon.	Reduce polymer clarity
Metallic Nanoparticles	Particles and Rods	Wide variety of accessible metallic nanoparticles, can enhance thermal and electrical conductivity properties at low loadings.	Can be costly (ie, silver & gold nanoparticles), high surface energy leads to agglomeration and instability, environmental concerns upon disposal.
Polyhedral Oligomeric Silsesquioxane (POSS)	Cage-like structure, cubes, hexagonal or octagonal prisms	Inorganic core, can enhance cross linking and crystallinty in host polymer.	Environmental concerns.

During the remainder of this thesis, only nanomaterials with a platelet-like structure will be referenced.

Polymer nanocomposites offer four distinct advantages over conventional composites according to Gupta & Mukhopadhyay:

1) Lighter weight due to low filler loading rates and masses (≤1%-5% mass fraction)

2) Lower cost due to reduced material requirement.

3) Improved properties compared to conventional composites.

4) Combination of multiple property enhancements such as higher tensile and flexural modular strength, improved barrier properties, enhanced flame resistance, etc.

Many of the advantages of polymer nanocomposites can be specifically attributed to interaction at the molecular level between the high interfacial area of a nanoscale filler and the polymer matrix, potentially resulting in only minor changes to the processability of the polymer. While this molecular level interaction is preferred, it is difficult to achieve and depends heavily upon the chemical composition of the constituents and the processing method. (Potts, Dreyer, Bielawski, & Ruoff, 2011)

Maximizing the properties of the polymer at low mass fraction loadings of a nanoscale filler requires that it is thoroughly distributed throughout the polymer matrix and that complete exfoliation of the filler's layers has occurred. Complete exfoliation allows for maximum surface area exposure between the filler and the polymeric structure. Sufficient interaction between the filler and polymer must also be achieved for adequate dispersion. (Mukhopadhyay & Gupta, 2013)

Theoretical modeling can be used to predict the potential modulus improvements of adding a filler to a matrix. In polymer nanocomposite research, the Halpin-Tsai model has been used for this purpose. The model accounts the modulus for the filler, the volume

fraction of the filler, and the orientation of the filler within the matrix. (Mukhopadhyay & Gupta, 2013)

Similar to conventional composites, the distribution of the nanoscale reinforcement within the matrix can be random, (anisotropic) or aligned (isotropic), depending on the intended application. An aligned, anisotropic distribution of the reinforcement will allow for improved strength in the direction of the filler's alignment in the matrix, but weakened strength in the direction perpendicular to the reinforcement's alignment. Isotropic composites consist of a more randomly distributed reinforcement and bidirectional strength improvements can be observed (Thomas, 2012). For example, the orientation of a nanoscale filler induced during cast film processing is likely to result in a film with measurable differences between the machine and transverse direction mechanical properties. This is due to the alignment applied by the extensional shear between the die and casting drum.

In regard to packaging applications, nanocomposites can provide for improvements in gas barrier properties, the potential to down gauge films, reduction of overall package weight, reduction of waste, and improvement in recyclability. (Potts, Dreyer, Bielawski, & Ruoff, 2011) With these potential advantages, nanocomposites could allow for additional opportunities for a coextruded film to replace a lamination, reducing processing and material costs. Nanocomposite films also have the potential to

widen the versatility of monolayer film lines, allowing a converter to produce barrier film in a single layer.

Graphene and Graphite Nanoplatelets

Graphene and graphite nanoplatelets (GNP) have attracted significant interest in recent years for their extraordinary electrical, mechanical, thermal, and barrier properties. Graphene consists of a one atom thick sheet of sp2 hybridized carbon atoms arranged in a planar, honeycomb structure. (Kim, Abdala, & Macosko, 2010) This recent surge of interest in graphene and GNP related research follows Andre Geim and Konstantin Novoselov's 2010 Nobel Prize in Physics for their work in isolating these single atom sheets in 2004. (Kim et al., 2011)

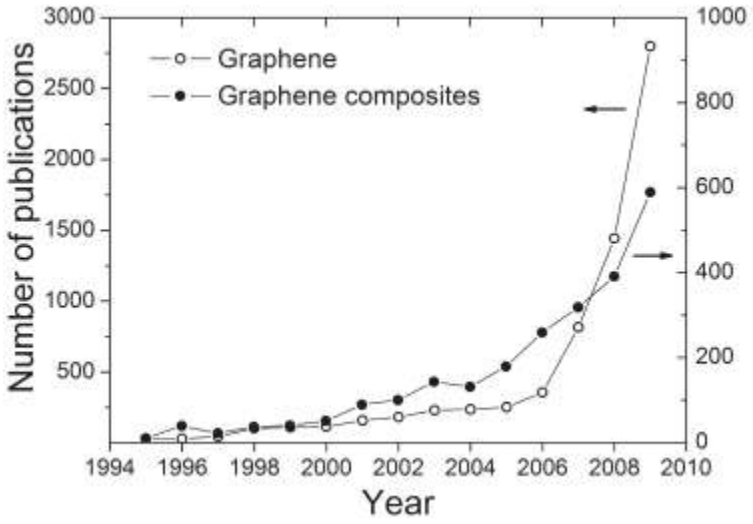

Figure 1: Graphene and Graphene Composite Publications

(Source: Kim, Abdala, & Macosko, 2010)

Much of the research attention given to single layer graphene regards potential use in electronic devices because graphene possesses superb electrical conductivity of up to 6000 Siemens per centimeter. Single layer graphene is also one of the strongest materials discovered, with a Young's modulus of 1 Pa and an ultimate strength of 130 GPa, roughly 200 times the strength of steel. It also has a thermal conductivity of 5000 W/(m•k), which is comparable to values found for single walled carbon nanotubes. (Kim, Abdala, & Macosko, 2010) Because of the high electron density of its aromatic rings, graphene is impermeable to all gases, including helium (Yoo, Shin, Yoon, & Park, 2014). Graphene also exhibits a very high surface area to mass ratio, with a theoretical value of 2630 m^2/g (Kim, Abdala, & Macosko, 2010).

To understand graphite and its characteristics, the properties of crystalline carbon must first be considered. Graphite and diamond are the naturally occurring crystalline forms of carbon and can be distinguished by their electron configurations. Diamond consists of carbon atoms that are covalently bonded with their four unpaired electrons. This results in an sp^3 electron configuration which forms a tetrahedral structure where each atom is separated by 1.54 Å. Graphite consists of carbon atoms that are covalently bonded to each other in an sp^2 hybridized electron configuration, forming hexagonal rings. This results in a planar structure with planes separated by 3.35Å, while the carbon atoms within the plane are separated by 1.42 Å. Within this structure, each carbon atom is bonded to three adjacent carbon atoms within the plane, while the fourth bonding electron participates in weaker, pi bonds that result in van der Waals interactions between the

planes. (Callister & Rethwisch, 2010) Each single atomic planar layer is called a "graphene" layer (Mukhopadhyay & Gupta, 2013).

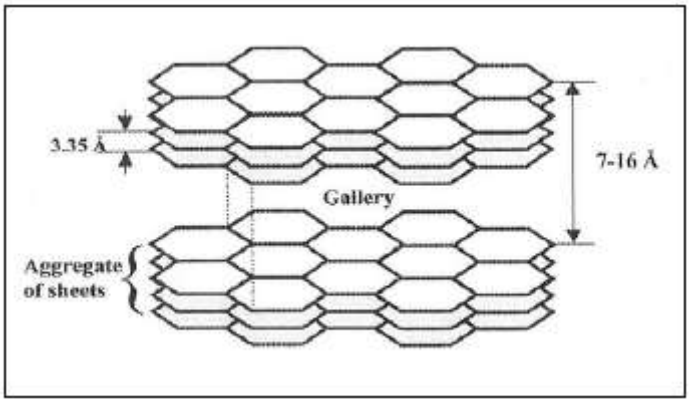

Figure 2: Graphitic Basal Spacing and Structure (Source: Etmimi, 2009)

Because of the electron configuration, graphite is electrically conductive along the graphene layers, but not conductive perpendicular to the layers. (Gupta & Mukhopadhyay, 2011) The bond strength within the layers is also much higher than between them, resulting in a high degree of anisotropy. These property differences within the planes versus between the planes give graphite its unique properties and uses. For example, graphite is used as an industrial lubricant because the planes are able to slide across each other, but maintain their structure to endure wear and degradation. (Etmimi, 2009)

Single layer graphene sheets and GNP clusters can be isolated from graphite via a wide variety of techniques via a "top down" approach. Graphene can also be produced in bulk by the exfoliation and reduction of graphite oxide. Another form of graphene, graphene oxide, can be produced from graphite oxide, which consists of graphene sheets

stacked together similarly to pure graphite, but the sheets are separated by epoxide and hydroxyl functional groups between the planes, resulting in a larger interlayer spacing between 6 and 10 Å. While displaying some degree of polarity, the use of graphene oxide as a filler in polymers has also gained research attention because it is capable of strong interaction with polar polymers. Graphene oxide, however, does not share the same electrical conductivity or superb strength that pure graphene possesses. (Kim, Abdala, & Macosko, 2010)

A "bottom up" approach can also be used to produce graphene from gaseous carbon precursors, such as carbon monoxide and methane.

Table 2 and table 3 describe some of the most common techniques used to produce graphene and graphite nanoplatelets. (Kim, Abdala, & Macosko, 2010)

Method	Thickness	Diameter	Advantages	Drawbacks
Chemical Vapor Deposition	Few Layers	Centimeter range	Ability to Produce large scale, high quality few layer graphene sheets	Small scale production limitations
CO Reduction	Multiple Layers	Sub-micron	Pure, unoxidized sheets can be produced	Likely contamination by Al_2O_3 and Al_2S
"Unzipping" Carbon Nanotubes	Multiple Layers	Several microns	Size can be controlled by carbon nanotube precursors	Costly

Table 3: Bottom Up Production Graphene Production Processes

Source: Source: Kim, Abdala, & Macosko, 2010

Method	Thickness	Diameter	Advantages	Drawbacks
Micromechanical Cleavage	Few Layers	Micron to centimeter range	Ability to produce large size, unmodified graphene sheets. Relatively simple process.	Small scale production limitations
Direct Graphite Sonication	Single to multiple layers	Micron to submicron	Inexpensive, produced unmodified graphene	Not capable of industrial production of single layer graphene
Super acid dissolution of graphite	Largely single layer	Nanometer range	Scalable, produces unmodified graphene	Uses strong, hazardous acids such as chlorosulfonic acid, and requires acid removal process
Chemical Reduction of Graphite Oxide	Single and multiple layer	Micron to submicron range	Can produce large sheets	Will only disperse in hydrophilic polymers, some methods require hazardous chemicals
Thermal Exfoliation/Reduction of Graphite Oxide	Single and few layers	~500 Nanometer range	Only requires one step for exfoliation and reduction	Requires high heating temperature and produces relatively small sheets

Table 4: Top Down Approaches to Graphene and GNP Production

Source: Kim, Abdala, & Macosko, 2010

Considering the wide range of graphene production methods, the final application should determine the production method utilized, especially when used in polymer composites. Platelet thickness, diameter, and presence of remaining organic functional groups are all determined by the production process. (Richards, 2014)

Small clusters of graphene sheets, deemed graphite nanoplatelets, can currently be produced via super acid dissolution, thermal and chemical reduction from graphene oxide, as well as from direct sonication of graphite. The size of GNP can be controlled through the production process and can range from 0.5 microns to 40 microns in diameter by two to several atomic layers in thickness. Unlike pure graphene, GNP can be economically produced and could potentially transfer some of graphene's superior properties to a polymer if adequately dispersed. (Mukhopadhyay & Gupta, 2013)

There has been some ambiguity in the nomenclature between graphene and GNP, since the isolation of graphene from graphite. More recently, it has been presented in related literature that the term graphene should be reserved for the true monolayer of sp2 hybridized carbon atoms, while any minor stacking of these layers should be classified as GNP. Figure 3 displays the various forms of nanostructures based on graphite and their associated dimensions.

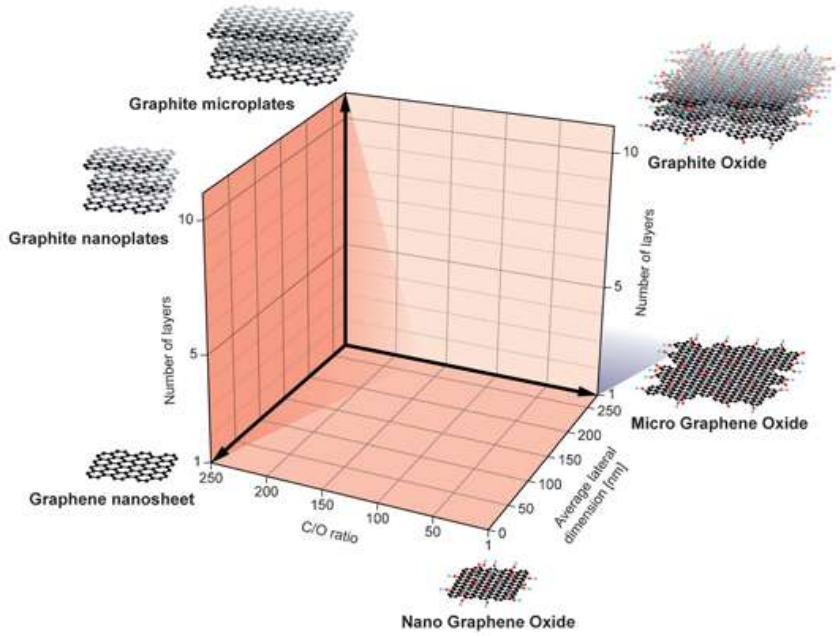

Figure 3: Graphene and Graphite Nanoplatelet Nomenclature (Source: Richards, Chemistry World, 2014)

Preparation of GNP - Polymer Nanocomposites

There are three general approaches to preparing GNP-polymer nanocomposites: in situ polymerization, solvent blending, and melt blending. Melt and solvent blending are the two most common introduction methods of GNP into various polymer matrices. In situ polymerization requires that the GNP is present during the polymerization reaction, where a high degree of GNP dispersion can be obtained. (Kim, Abdala, & Macosko, 2010) Solvent blending can also result in thorough dispersion where graphene is exfoliated and co-dissolved within a common low viscosity solvent with the host polymer. The solvent is removed by evaporation with high heating, leaving the exfoliated GNP and polymer together, forming a nanocomposite. Melt compounding can be

considered as the most widely available and environmentally sound introduction method, as it does not require additional solvents or changes to the polymerization process. Melt compounding utilizes extrusion processing to combine dry, powdered state GNP with the polymer resin in the molten state. Due to graphene's low bulk density, thorough dispersion can be difficult to achieve compared to in situ polymerization or solvent blending. (Potts, Dreyer, Bielawski, & Ruoff, 2011) To date, there has not been a published study directly comparing dispersion among solvent blending, in situ polymerization, and melt compounding introduction techniques within polyolefin-graphene nanocomposites (Kim et al., 2011).

The ultimate goal of the introduction method is twofold; GNP should be exfoliated and well distributed throughout the polymer matrix. Very similarly to silicate nanoclays, three distinct morphological arrangements can occur once GNP is incorporated into a polymer matrix; phase separation, intercalation, and exfoliation, as shown in Figure 4.

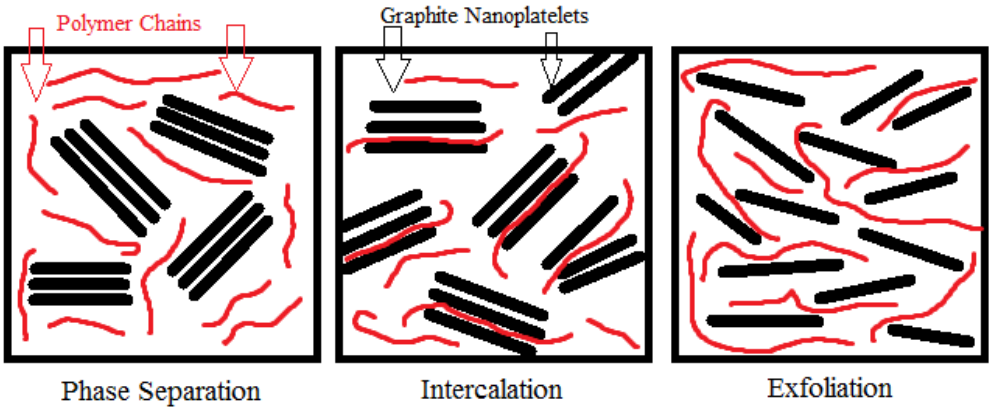

Figure 4: Morphologies of GNP Polymer Nanocomposites (Source: Modified from Etmimi)

GNP share similar morphologies within a polymer to those of layered silicates, such as montmorillonite, due to their similar platelet-like structures. Phase separation results in a microcomposite, while both intercalated and exfoliated dispersion yield a nanocomposite material. These special distributions are largely determined by the interfacial interactions between GNP and the polymer matrix as well as the production and processing methods utilized (Silvestre, Duraccio, & Cimmino, 2011). An intercalated morphology is achieved when a polymer chain or group of polymer chains have inserted themselves in between the stacked graphene layers, but the GNP maintain a stacked structure. Intercalation allows opportunity for an improved interfacial area between the polymer and GNP compared to a phase separated morphology. (Azeredo, 2009) In research with compatibilized clay-polyolefin nanocomposites, intercalation has been the most commonly achieved morphology (Zhong, Janes, Zheng, Hetzer, & Kee, 2007). An exfoliated morphology is achieved when all layers have been separated to their smallest state and all agglomerates are broken down to their smallest unit. Exfoliation offers the greatest improvement in both mechanical and barrier properties because the greatest allowable surface area of the filler is exposed, maximizing the interfacial area between the polymer and filler. Exfoliation also allows for much lower loading rates of the filler and is the usually the desired result of research in this field. (Potts, Dreyer, Bielawski, & Ruoff, 2011) Complete exfoliation is difficult to achieve in a final product because of the strong interlayer cohesive forces between the planar lattices that exist in most platelet-like nanomaterials. The mixing forces applied during extrusion processing oftentimes contribute to agglomeration of nanomaterials, as nanomaterials come back into contact

with each other and agglomerate due the strong bonds between planar lattices. To achieve complete exfoliation in a final product, these interlayer forces between the filler's planar sheets must be overcome, while sufficient interaction between the polymer and the filler is required to maintain exfoliation during processing. Both the particle-particle and particle-polymer interactions are key factors in this regard. (Mukhopadhyay & Gupta, 2013) It is for this reason that it is common to organically modify the surface of the filler or to utilize a compatibilizer to facilitate hydrogen bonding or covalent interaction between the filler and polymer (Kim et al., 2011). A compatibilizer is a substance that is used to facilitate chemical bonding and stabilization between two otherwise immiscible substances (Giles, Wagner, & Mount, 2013). However, compatibilizers have been shown to reduce barrier properties in compatibilized polyolefin nanocomposites. (Zhong, Janes, Zheng, Hetzer, & Kee, 2007)

Processing techniques can have a significant effect on the degree of dispersion and exfoliation of a nanoscale filler. Generally, it has been known that high shear and extensional mixing are required to achieve good dispersion and exfoliation when mixing a thermoplastic and nanomaterial in a powdered form. This typically requires a counter rotating twin screw extruder when combining a thermoplastic resin with a powdered nanomaterial. The greater viscosity of higher molecular weight polymers can also assist with breaking down and separating the layers of the nanofiller. Little research exists regarding dispersion characteristics when mixing a nanomaterial with a polymer from a concentrated polymer-nanomaterial masterbatch via a single or twin screw extruder.

Permeation through Polymers and Polymer Nanocomposites

A sufficient barrier that can prevent degradation has become more important in many applications such as food and pharmaceutical packaging (Selke, 2004). As already described, polymeric materials are widely used in packaging. However, their performance is hindered due to relatively high permeability of gases such as CO_2, O_2, and N_2 in addition to flavors and aromas. (Darby, Cooksey, & Kimmel, 2007). Permeation is defined as the quantification of permeant transmission, gas, or vapor through a resisting material (Siracusa, 2012). A product's shelf life can be significantly affected due to permeation, causing an uptake of moisture by normally dry products, the loss of CO_2, or the oxidation of oxygen-sensitive products (Stevens, 2012).

Oxygen is a reactive gas that plays a large role in food spoilage. Many reactions that result in food spoilage, such as oils turning rancid, and flavor degradation require oxygen to occur. There are two primary methods for reducing a product's exposure to oxygen in flexible packaging: modified atmosphere packaging (MAP) and vacuum packaging. MAP replaces the atmosphere in a packaging with a nonreactive gas, such as nitrogen, prior to sealing the package. This is a common method employed in potato chip and shredded cheese packaging. Vacuum packaging removes the entire atmosphere prior to sealing, leaving minimal degradative gases within the package. This is a common method for packaging meats, cheeses, and salty snacks. Both methods require a sufficient barrier as well as sufficient seal integrity to prevent oxygen ingress throughout the product's shelf life. (Selke, 2004)

In many situations, the permeability of the packaging materials plays a significant role in determining the shelf life of the contained product. The proper packaging material must be selected to withstand handling forces during processing as well as maintaining a sufficient barrier to degradative gases and vapors (Siracusa, 2012). According to Selke, et al., six key variables affect permeability within a polymer; the chemical structure of the polymer, the chemical structure of the permeant molecule, temperature, humidity, permeant concentration, and the physical structure of the polymer. While some of these factors are uncontrollable, others are closely tailored to optimize the product's shelf life while balancing the associated cost. (Selke, at al., 2004)

When a package is sealed, a concentration gradient may be created. There is a natural tendency to eliminate this concentration gradient by mass transfer at a molecular level. (Selke, 2004) For a permeant to pass through a homogeneous film, it first dissolves within the film on the side with the higher permeant concentration, then diffuses through the polymer matrix. It is in this stage where the size, shape, and polarity of the permeant as well as the polymer crystallinity and crosslinking play a critical role in the rate of diffusion (Siracusa, 2012). Almost all of the permeation occurs through the polymer's amorphous region, as there is more free volume that allows for gases to transfer through the material. The crystalline regions are less permeable, as the crystallites create a tortuous pathway that slows permeant diffusion. (Selke, 2004) A tortuous pathway is a diffusion pathway that has been significantly lengthened by the addition of higher density crystallites, or other impermeable materials. Crystallite and filler orientation play a key

role in creating a tortuous pathway for permeants. In the last stage of the diffusion process, the permeant desorbs or evaporates back to a vapor or gaseous state. (Siracusa, 2012)

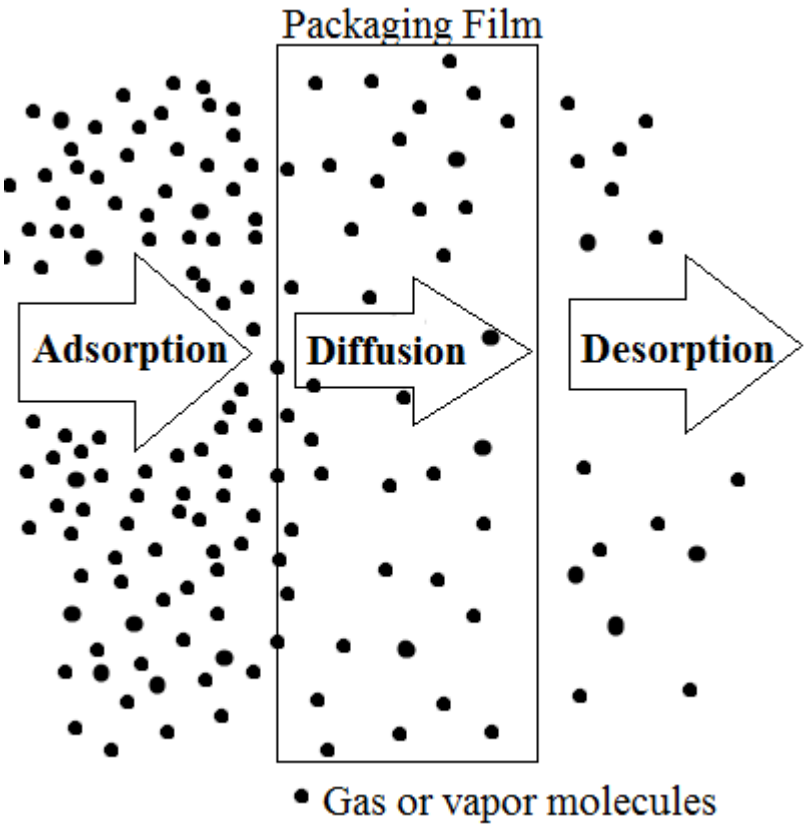

Figure 5: Stages of Permeation (Source: Adapted from Siracusa, 2012)

The addition of impermeable platelets within a polymer can provide improved barrier properties by creating a more tortuous, lengthy pathway for permeants while also filling regions of free volume in the polymer through which gases would otherwise diffuse (Azeredo, 2009). Compared to other nanomaterials such as carbon nanotubes, platelets provide a maximum reduction in diffusion because of their high surface area and aspect ratio at a given mass (Silvestre, Duraccio, & Cimmino, 2011). Nielsen proposed

the original tortuous pathway model based on plate-like fillers as depicted below in the two dimensional image of the diffusion process (Zhong, Janes, Zheng, Hetzer, & Kee, 2007).

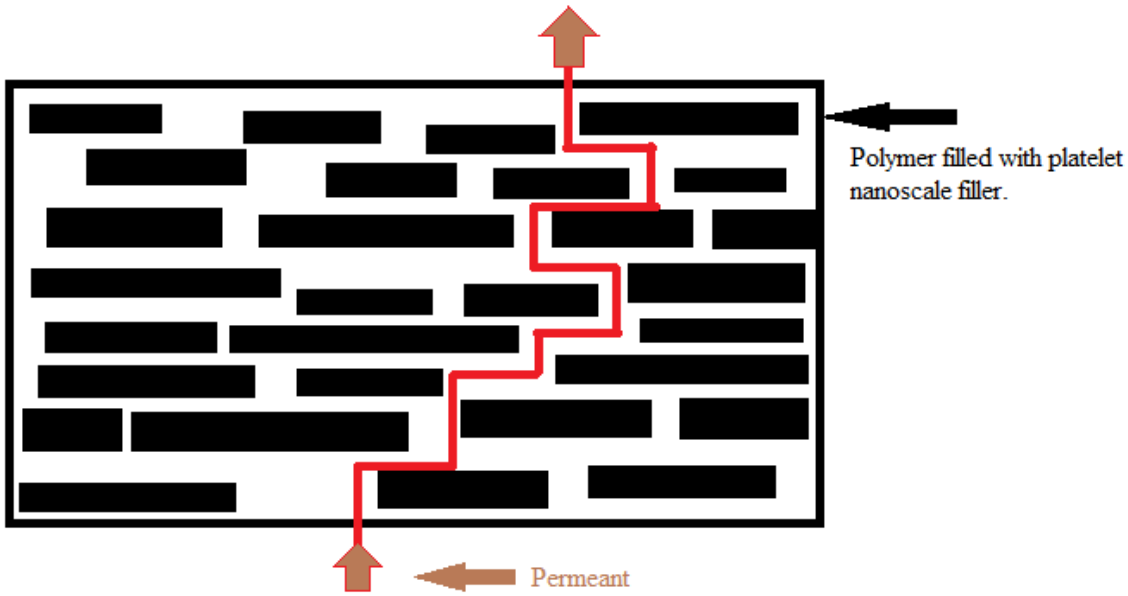

Figure 6: Platelet – Filled Tortuous Pathway Model

(Source: Adapted from Azeredo, 2009)

The permeability of a filled system can be estimated using Nielson's equation, where P_c is the permability of the filler, P_m is the permeability of the polymer matrix, ϕ is the volume fraction of the platelet filler, and $\alpha(N)/2$ refers to the aspect ratio of the filler. (Nielsen, 1967)

$$\frac{P_c}{P_m} = \frac{1-\phi}{1+\frac{\alpha(N)}{2}\phi}$$

Equation 1: Nielson Model

While Nielson's model provided a theoretical understanding of the role of high aspect ratio platelets in polymer systems, it is very limited in realistic predictive value because it assumes that the platelets are arranged with the faces of the greatest surface area aligned perpendicularly to the direction of mass transfer. It also assumes that there is minimal overlap of the platelets and that all platelets are monodispersed and aligned in a regular array. These morphologies are very difficult to obtain with polymer nanocomposites and cannot be assumed. (Zhong, Janes, Zheng, Hetzer, & Kee, 2007) Due to the varied morphologies that nanomaterials adopt during processing, experimental permeation analysis is much preferred over theoretical models for investigation of changes in permeability using an oxygen or water vapor transmission testing unit.

Related Studies

Zehetmeyer et al. observed a small decrease in permeability of O_2, in their study with ~25 µm polypropylene homopolymer - organically modified montmorillonite films. Zehetmeyer et al. produced the nanocomposite resin by melt compounding the polypropylene and MMT in a counter rotating twin screw film prior to injection molding 1, 2, and 5 wt% MMT-PP film samples. O_2 permeation was reduced from 89.9±5.1 $cm^3/[m^2\text{-day}]$ to 81.8± $cm^3/[m^2\text{-day}]$ in a 5 wt % MMT-PP film sample. Water vapor permeability remained unchanged. (Zehetmeyer et al, 2012)

Montmorillonite layered clay fillers have been well researched as potential flexible packaging materials that have shown improvements in barrier and mechanical

properties with sufficiently exfoliated clays, but little literature exists that investigates graphite-based polymer nanocomposites for these same packaging applications.

The properties of a polymer nanocomposite are heavily determined by the degree of dispersion and exfoliation of the nanoscale filler. The introduction method plays a critical role in this regard. (Silvestre, Duraccio, & Cimmino, 2011) Due to the van der Waals forces between graphene layers, Carotenuto, et al (2012) described that the best embedding mediums are polymers that are capable of interacting with these forces, such as polyolefins. The introduction method must provide sufficient dispersion of GNP for property improvements since there is a lack of chemical interaction between the nonpolar GNP and a nonpolar polyolefin matrix. (Carotenuto et al., 2012)

Carotenuto et al. (2012) examined the mechanical properties of blown and compression molded LDPE films filled with graphite nanoplatelets sized ~1um in diameter and 20nm in thickness. The graphite nanoplatelets were introduced into a concentrated masterbatch of LDPE by first dispersing expanded graphite within octane (C_8H_{18}) and applying intensive sonication to further exfoliate the graphitic structure. A small amount of LDPE was then dissolved into the solution at octane's boiling point of 104ºC. The remaining octane was then removed by heating small grains of the material to 160ºC while under an oil pump. This masterbatch was then let down into a base LDPE resin and extruded via blown film extrusion. This is one of the few published studies

where the properties of a GNP-polyolefin film produced from extrusion processing have been analyzed.

A significant reduction in plasticity of the films resulting in reduced elongation, and an increase in Young's modulus was observed. The modulus was increased from 180 to 425 MPa in the transverse direction and 187 to 477 in the machine direction of the blown film sample. DSC investigation concluded that no increase in percent crystallinity had occurred in the films containing GNP content. (Carotenuto et al., 2012)

Jiang and Drzal uniformly coated graphene nanoplatelets with paraffin wax to improve dispersion in an HDPE matrix. Flexural coupons were prepared using two separate batches of GNP of varying dimensions. One batch used GNP of 15 μm in diameter by 5-10nm thickness and the other batch used GNP of 1μm in diameter by 5-10 nm in thickness. Composites were formed with loading rates of 1 vol%, 3 vol%, 5 vol%, 10 vol%, and 15 vol% by injection molding after extrusion in a twin screw extruder. DSC analysis revealed a higher crystallization temperature of 3° C at low GNP loading levels of 1 vol %, which suggests that the presence of GNP particles acted as a nucleating agent within the HDPE matrix. The nucleating effect was higher at the 1 vol% and 3 vol% than the 10 vol% and 15 vol% loading levels, which suggests that the formation of nucleation sites may be hindered at higher GNP loadings. At the same loadings, the composites formed from 1μm diameter GNP display greater percent crystallinity than the 15 μm GNP composites. This was described as being due to the increase in particles in

the 1µm GNP composites compared to the 15 µm composites, where a more heterogeneous distribution of nucleating sites is present to facilitate crystallization. In regard to mechanical properties, Jiang and Drzal observed a 116% increase in flexural strength (15µm GNP) and a 90% increase at the 15vol% loading (1µm GNP). At all other loadings, the 1µm GNP proved superior to the 15µm GNP. A reduction in Izod impact strength was observed in all GNP composites compared to the unmodified HDPE sample. The impact strength declined as loadings increased, which is expected when adding a rigid filler to a relatively tough polymer. (Jiang & Drzal, 2011)

Wang, et al, observed significant improvements in both modulus and barrier properties by utilizing an organofunctional silane, vinyl triethoxysilane (VTES), as a coupling agent to facilitate covalent interaction between reduced graphene oxide and VTES within an LDPE matrix. Separate batches of LDPE -VTES-graphene and LDPE -graphene were co-dissolved in toluene and intensive sonication was applied prior to slow heating and vacuum drying to evaporate the toluene solvent. Final 1 wt%, 3 wt%, 5 wt%, and 7 wt% of non- compatibilized and compatibilized graphene-LDPE nanocomposites were made with a plate vulcanizing machine. The samples with the VTES coupling agent displayed superior nonpolar solvent barrier properties to toluene compared to the neat and non-compatibilized graphene-LDPE samples. The compatibilized sample resulted in a more homogeneous distribution throughout the LDPE matrix, resulting in a more tortuous pathway, slowing the diffusion of permeants. (Wang, et al.)

The non compatibilized graphene-LDPE sample displayed a brittle behavior under tensile stress with significantly reduced elongation compared to the neat and compatibilized samples due to the poor dispersion and weak interaction of graphene in the non compatibilized matrix. The VTES-graphene samples displayed a maximum improved tensile strength (of 27%) with an improved toughness (of 17.7%) in the 7wt% sample. (Wang et al., 210)

Theoretical Methods and Materials

Extrusion

Extrusion is typically the first step in converting solid resin pellets into a melt that can be used for the next step in processing. Extruders use heat, pressure, and shear to convert the solid resin pellets into a melt, as if it were a pump for plastic materials. (Selke, 2004)

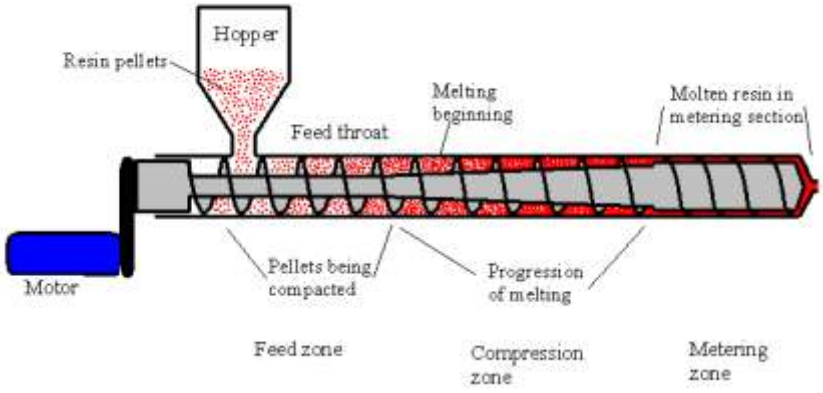

Figure 7: Schematic of Extruder (Source: Darby PKGSC 430)

Mixing is an essential step to almost every polymer extrusion process. Three types of mixing forces are applied during extrusion: dispersive, distributive, and extensional. Dispersive mixing are the forces that break apart agglomerates and minor

components within a melt. This is achieved by mechanical forces applied by the shear stress in the flow. Distributive mixing distributes all components homogeneously throughout the melt. Extensional mixing can be described as the continuous pulling and stretching forces applied to a polymer melt that results in high shear and mixing. It is considered that extensional mixing can only be achieved with a twin screw extruder. Standard extrusion screws will generally always provide some degree of both dispersive and distributive mixing, but more specialized designs can allow for greater degrees of both mixing forces. Single screw extruders are typically limited to imparting distributive forces upon a melt, therefore it is essential that additives and particulates within masterbatches are thoroughly dispersed prior to mixing in single screw extrusion. A masterbatch is a mixture of additives, pigments, particulates and other compounds that are concentrated in a carrier resin and mixed with compatible unmodified polymer during extrusion processing. (Giles, Wagner, & Mount, 2013)

Successfully transferring GNP nanocomposites from lab to commercial scale requires that they can be distributed within readily available commodity polymer resins via an introduction method that would suit commercial extrusion mixing methods. This could entail two approaches; directly mixing powdered GNP with a polymer resin, or mixing from a prepared nanocomposite-polymer masterbatch that is mixed with a base resin. Direct mixing would require a twin screw extruder, as previous studies indicate that high shear and extensional mixing would be required (Jiang & Drzal, 2011). Twin screw extruders are not nearly as common in commercial lines as single screw extruders,

leaving the masterbatch mixing method as potentially being the most widely adaptable approach if GNP can be sufficiently dispersed from a masterbatch via single screw extrusion. Since a masterbatch is a concentrated mixture of additives, it could be produced via any of the three primary introduction methods; in situ polymerization, solvent blending, and melt blending because a lower volume would be required. (Jiang & Drzal, 2011)

Cho et al. demonstrated thorough distribution of a 50% MMT-PP masterbatch that was let down into a base of PP homopolymer by a single screw extruder. The d-spacing between clay layers in the samples produced by single screw extrusion were very similar to the d-spacing observed in the masterbatch. D-spacing refers to distance between platelet planes. This study is significant because it reveals that nanocomposites can potentially be successfully distributed from a masterbatch via conventional single screw extrusion, opening routes for potential commercial implementation. (Cho et al. 2012)

Microstructure and Morphology Characterization

As with any nanocomposite, the morphology of the nano-filler within the matrix significantly influences the material's properties. This morphology must be characterized in order to understand the material's behavior.

Optical Microscopy

Optical microscopy can be used to characterize the distribution and dispersion of GNP on a microscopic scale. Single and double layer graphene cannot be observed with

an optical microscope, as they only absorb ~2.3% of light regardless of wavelength, however as the number of graphene layers increases to form stacks of graphite, more light is absorbed and they become clearly visible as dark regions.

X-Ray Crystallography

X-Ray diffraction is a non-destructive technique that is commonly used to characterize the molecular structure of crystalline materials. Crystalline materials are characterized by their unique atomic arrangements and will diffract x-ray radiation in characteristic patterns that can be used to determine certain features of a material, such as graphitic basal plane spacing or changes in polymer crystalline structure.

Upon exposure to x-ray radiation, the scattering of x-ray radiation from the atomic structure of the crystalline material provides insight to the structure's arrangement. The diffraction peak positions provide information regarding the atomic arrangements within a crystalline lattice while the peak heights provide insight to the atomic arrangement within the crystalline lattice. A perfectly crystalline material will display sharp diffraction peaks, while a more semi-crystalline material will display broad peaks known as an "amorphous halo." (Callister and Rethwisch, 2010)

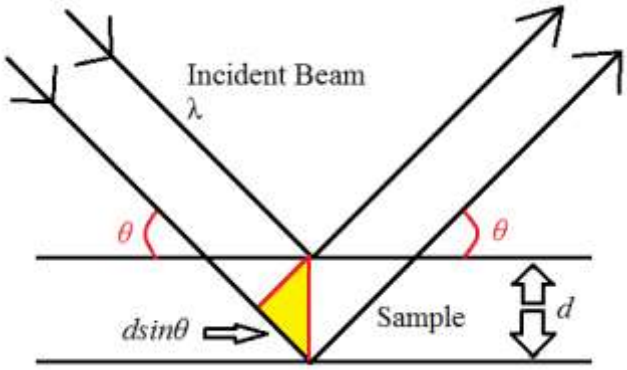

Figure 8: Basic diagram of x-ray diffraction. (Modified from Callister and Rethwisch)

Graphite consists of graphene layers that have a basal spacing of 3.31Å and will display defined diffraction peaks at 26°, 42°, and 46° of 2θ. The 26° angular position is the most prominent and characteristic peak for graphite materials. The height of a diffraction peak can be attributed to the intensity of the occurring diffraction, which in combination with the peak location can give insight to the interlayer distance between graphene layers and the resultant morphology of GNP. A shift of this 26° peak to a lower angular position of 2θ is indicative of an intercalated structure with a larger interlayer spacing, while a loss of this peak is indicative of an exfoliated, monolayer structure that is not diffracting x-ray radiation. (Kim et al., 2011)

Crystalline diffraction can be calculated using Braggs Law:

$$2\,d \sin\theta = n\,\lambda$$

Equation 2: Bragg's Law

λ is the wavelength, θ is the glancing angle of diffraction, n is the order of reflection, and d is the crystalline lattice spacing in Angstroms in Bragg's Law. (Callister and Rethwisch, 2010) It should be expected that GNP will display a prominent graphitic peak at the 26° angular position, as they still retain a crystalline graphitic structure of several atomic layers that will diffract x-ray radiation. (Kim et al., 2011)

The diffraction of semicrystalline structures can be determined with a Debye function, which accounts for radial distribution.

Equation 3: Debye Function

Crystallite dimensions perpendicular to the crystallographic plane, hkℓ, can also be estimated with x-ray diffraction techniques using the Debye-Scherrer equation:

Equation 4: Debye-Scherrer Equation

In which case, $L_{hk\ell}$ is the dimension in Angstroms of the crystalline structure perpendicular to the crystalline planes, hkℓ. K is a constant of 0.89, λ is the wavelength of radiation used, $\lambda_{CuK\alpha,}$ and is the half width of the diffraction peak associated with the hkℓ crystallographic plane in radians. β is found by dividing the peak at its full width by half of its maximum intensity (the maximum height).

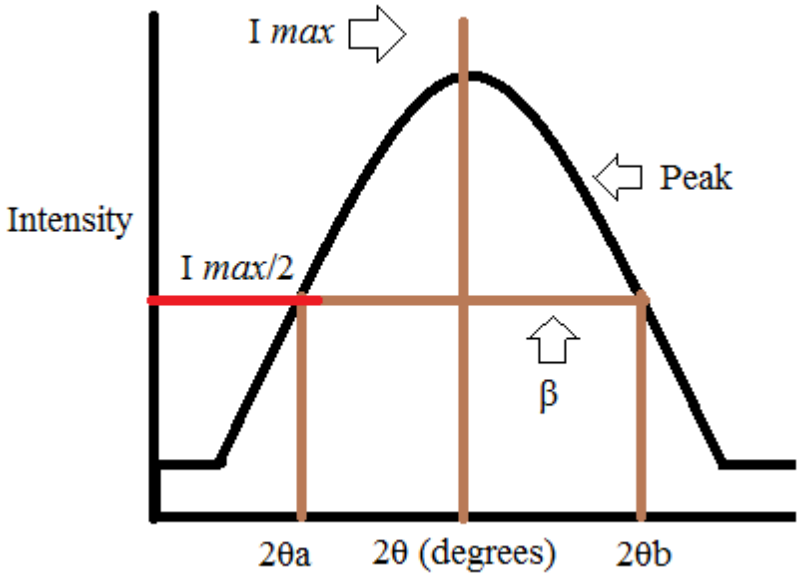

Figure 9: Division diffraction peak for β calculation. (Source, redrawn from Polymer Technology)

Transmission Electron Microscopy

Transmission electron microscopy (TEM) is an imaging technique where a beam of electrons is transmitted through a very thin sample, interacting with the components of the sample as they pass through it, forming an image on a phosphorus plate that is detected through an imaging device, such as a charge coupled camera. TEM is capable of capturing high resolution images of fine atomic details. (Callister & Rethwisch, 2010)

Sample preparation is a key step in obtaining quality TEM images, as with any electron microscopy. For TEM images of polymeric film samples containing GNP

content, cross sections of the film must first be sliced into micron thick samples and placed onto a copper grid within the apparatus of the microscope. (Etmimi, 2009)

When inspecting for GNP within a polymer matrix using TEM, graphite materials will be displayed as much darker shaded regions in contrast to the polymer, which will be displayed as a much lighter shade. This is due to high atomic density of graphite that is preventing fewer electrons from reaching the phosphorus plate.

TEM is a widely used technique for inspecting the distribution and morphology of nanoparticles within polymer nanocomposites. The images obtained display valuable information, such as whether agglomerations have been formed, particulate size, and particle morphology.

Thermal Properties

Differential Scanning Calorimetry

Differential Scanning Calorimetry (DSC) is a method to determine the thermal transitions of a polymer, such as glass transition (T_g), crystallization temperature (T_c), and melting temperature (T_m). DSC operates by adding or removing heat to maintain a constant rate of temperature change of a polymer sample and a reference as shown in Figure 10. The reference will have a known heat capacity to which the polymer sample's temperature is compared. Heat capacity is the amount of thermal energy required to raise

the temperature of one gram of material by one degree Celsius. (US Patent US 3263484 A)

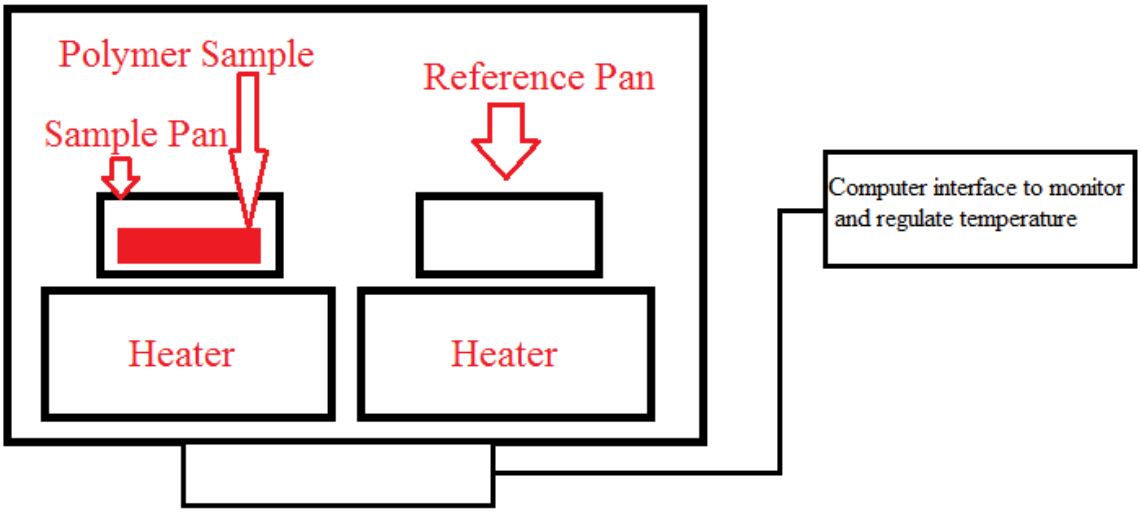

Figure 10: Basic Diagram of DSC Apparatus (Source: Redrawn from O'neill, 1962)

When a polymeric material undergoes a phase transition such as crystallinity changes, more or less heat will be required to maintain a constant temperature change with the reference sample. If a material melts, it is undergoing an endothermic reaction and it will require additional heat to increase its temperature at the same rate as the reference. If a material undergoes an exothermic reaction such as crystallization, then less heat is required to maintain the temperature change at the same rate as the reference. This difference of heat flows between the sample and reference allows the amount of heat absorbed or released to be measured as one sample undergoes phase changes. (Selke, 2004)

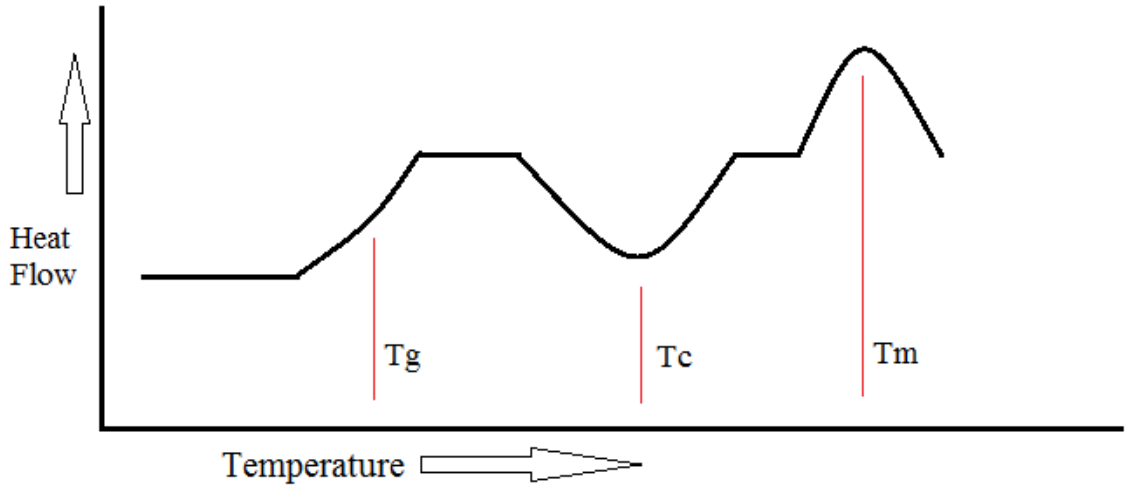

Figure 11: Idealized DSC Plot (Source: Redrawn from Selke, 2004)

Above T_g, a polymer is soft and pliable, while below T_g, a polymer is brittle. T_g is a transition displayed by amorphous polymers or amorphous regions of semicrystalline polymers. Polymers will display a higher heat capacity above T_g, where more heat is required to raise the temperature of the sample. The glass transition temperature will occur gradually over a small range of temperatures as indicated in the plateau in the example DSC plot in Figure 11.

T_c is the temperature where a polymer may organize from an amorphous structure into a highly ordered structure, resulting in greater density, reduced clarity, and improved barrier properties. T_c is displayed by a large drop in heat flow, as shown in Figure 11. A polymer's crystallinity depends upon several factors; the structure and intermolecular forces between polymer chains, molecular weight, thermal history, and physical treatment. (Selke, 2004) Crystallization from a melt is a two-step process. First, there is

the onset of crystallization, known as nucleation, followed secondly by rapid crystallite growth. (Jiang & Drzal, 2011)

A semicrystalline polymer sample will eventually reach its T_m, where the polymer chains arranged in crystalline structures will disarrange themselves from their more ordered structure as the material becomes melts and is capable of viscous flow. T_m will be displayed on a DSC plot as a peak in an increase in thermal energy required, as more heat flow is necessary to melt the polymer. (Selke, 2004)

Jiang and Drzal found a higher degree of crystallinity with the addition of GNP to HDPE at low loadings between 1% and 5% by weight. Since the mechanical and barrier properties of a polymer are strongly determined by the degree of crystallinity, it should be determined if the microstructure of the polymer has been affected by the addition of GNP to the polymer. Determining whether the crystallinity has been altered should better isolate GNP as the cause to any changes in mechanical or barrier properties. (Jiang & Drzal, 2011)

Mechanical Properties

Polymers display a wide range of mechanical properties that are determined by their structure and composition. These properties can be greatly affected by changes in temperature and speed of the test when testing these properties. (Selke, 2004)

Tensile Strength

A polymer's mechanical properties can be evaluated by its stress-strain characteristics when stress is applied to the material. The most common stress strain analysis for packaging films is the tensile test, per ASTM method D882. This stress can be measured in force per unit area, such as Pascals or pounds per square inch, while the strain is a fractional length increase that is dimensionless. Stress-strain curves are oftentimes generated at low strain rates. The ratio between the applied stress and the resulting strain in the elastic region is known as the modulus of elasticity, while the maximum amount of stress a material can undergo without permanent deformation is known as the elastic limit. The point after the elastic limit where the material begins to undergo an increase in strain without an increase in the applied stress is known as the yield point. A material's resilience is its ability to absorb energy and return to its original dimensions, which is a property that is primarily attributed to the amorphous regions of a polymer. A polymer's resilience decreases with increasing crystallinity. The breaking point of a material is the point where the material undergoes mechanical failure. The tensile strength is the maximum stress a material can withstand, which is the breaking point of the material. Percent elongation at break (EB) is the percentage of elongation relative to its original dimension that a film sample undergoes just prior to breaking. (Selke, 2004) A material can be described as being "strong" if it has a high tensile strength value and "tough" if it can undergo significant deformation prior to yielding, which corresponds to the area under the stress-strain curve. (Cheruvathur, 2009.)

A material's secant modulus of elasticity is its ratio of stress to strain at any point on a stress-strain curve. The secant modulus can serve as a performance indicator when the load elongation curve is not straight. For a 1% secant modulus, it is the material's ratio of stress to strain when the material is extended to 1% of its original length. (Callister and Rethwisch 2010)

Testing methods for the tensile properties of a polymeric film are described in ASTM D882. A tensile tester is often used to evaluate a material's tensile properties.

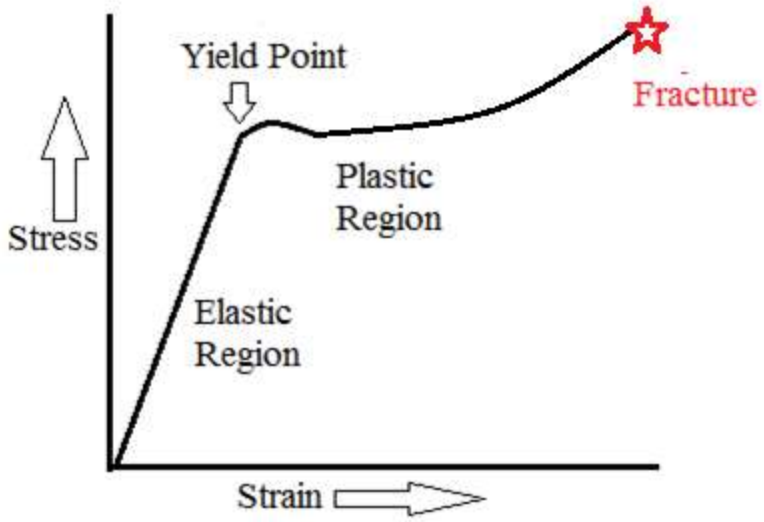

Figure 12 : Stress-Strain Curve Example (Credit: Redrawn from Selke, 2004)

Figure 12 depicts a stress strain curve of polymer displaying plastic characteristics, as it is capable of elongation beyond its elastic region. In comparison, a brittle material will yield with minimal elongation.

Puncture Resistance

The ability of a packaging film to resist punctures during manufacturing or distribution is essential to maintaining the integrity of the package and protecting the enclosed product. Products such as bones within cuts of meat and sharp edges on processing equipment can lead to film punctures. A film's resistance to puncture is heavily dependent upon the presence of strong intermolecular forces within the polymer. Puncture resistance is also very speed dependent, as slow rate punctures allow for the polymer chains to rearrange prior to puncture, whereas fast rate punctures do not. High strength and high elongation to puncture can both result in high puncture resistance. In applications where resistance to punctures is essential, it is common that polymers such as nylon and PET are used. Puncture resistance tests can be performed according to ASTM F 1306 using a testing instrument such as an Instron® Universal Testing machine. (Cheruvathur, 2009)

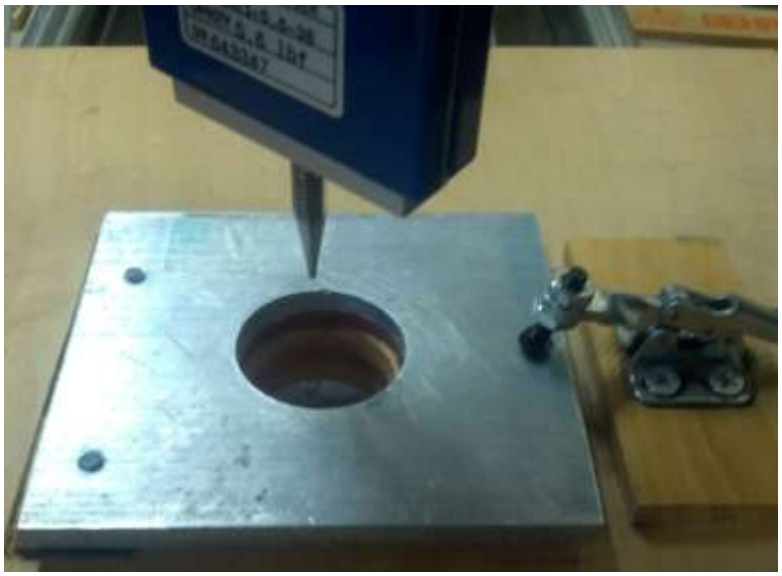

Figure 13: Image of puncture resistance testing apparatus.

Barrier Properties

Oxygen Permeability

The oxygen transmission rate (OTR) of a material or package can be determined with an oxygen transmission rate testing module, such as a Mocon 2/21. ASTM test method D 3958 provides common standards for the testing method. Oxygen transmission rate testing measures the amount of oxygen that has passed through a film in a given time. The module consists of a chamber with two sides which are separated by the film sample. A mixture of 20% oxygen and 80% nitrogen gas is circulated inside one of the chambers, while pure nitrogen is circulated on the opposite side as shown in figure 14. The oxygen then diffuses through the film sample and is carried by the nitrogen to the coulometric oxygen sensor. From the resulting data, the oxygen transmission rate is determined. (Stevens, 2012)

The transmission of oxygen is reported in units of cc/100in^2/24 hr-atm, which are commonly used to compare oxygen barrier properties of packaging films. A material is considered as a high oxygen barrier if it has an OTR less than 1 cc/100in^2/24. (Stevens, 2012)

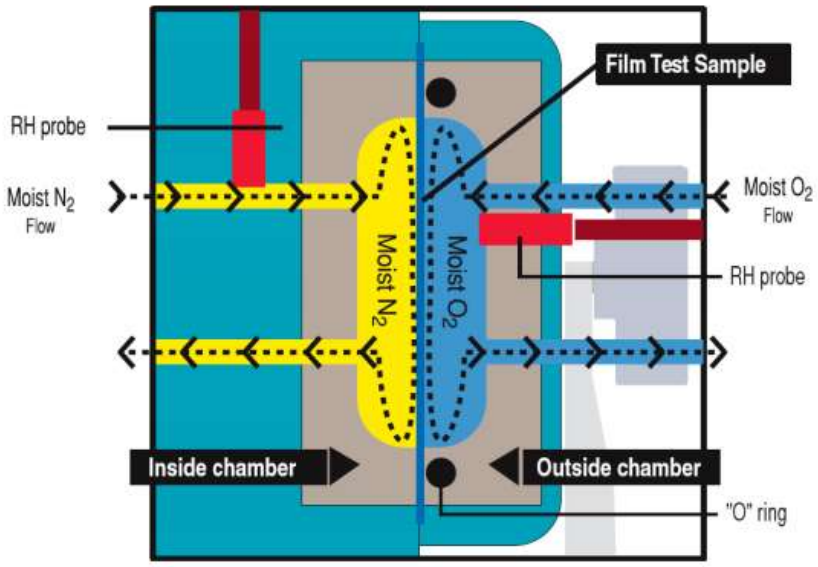

Figure 14: Oxygen Transmission Rate Testing Module (Source: Mocon Ox-Tran Manual – with permission)

Water Vapor Permeability

Permeability to water vapor can be determined using a water vapor transmission rate testing module, which operates in a similar fashion to an oxygen transmission rate testing module. The test cell is divided into an inner and outer test chamber, which are separated by the test sample film as shown in figure 15. The inner chamber is filled with nitrogen gas, which acts as a carrier, and the outer chamber is filled with water vapor from a source of high performance liquid chromatography water (Sigma-Aldrich, St. Louis, MO, USA). Relative humidity and pressure are maintained at a constant throughout the testing cycle. Water molecules then diffuse through the film sample and are carried by the nitrogen carrier gas to the test sensor where water vapor transmission rate is recorded. (Stevens, 2012)

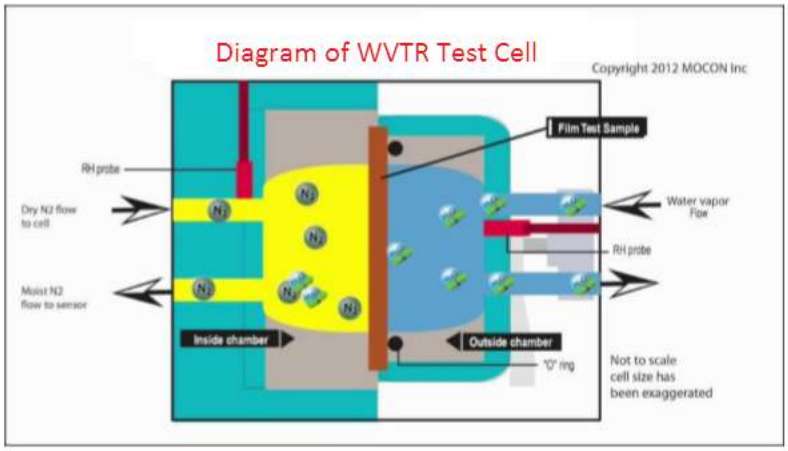

Figure 15: Water Vapor Transmission Rate Testing Module

(Source: Mocon Instructional Manual – with permission)

CHAPTER 3

EXPERIMENTAL DESIGN

Materials

For this study, 1.8 kg of a 20% GNP / 80 % Dow® 5230G Enhanced Polyethylene (EPE) masterbatch were obtained from Xolve Technologies® of Middleton, Wisconsin. The GNP used in the masterbatch were produced by direct sonication of graphite and originally ranged from 2 nm to 4 nm in thickness by 0.5 µm to 2 µm in diameter. The GNP and PE in the masterbatch were combined by a proprietary solvent mixing method without a compatibilizing agent. Upon solvent removal, the masterbatch was compounded for one cycle in a twin screw extruder.

Additional Dow® 5230G EPE resin was obtained from The Dow Chemical Company (Midland, Mi). Dow® 5230 EPE is a film grade polyethylene blend and has a density of 0.916 g/cm^3 (ASTM D792) and a melt index of 4.0 g/10 min (ASTM D1238). Dow® 5230G EPE is a proprietary metallocene-catalyzed octene LLDPE that contains both linear and long chain branched polyethylene.

Processing

The masterbatch was mixed with additional Dow® Elite™ 5230G EPE to produce films of 0.5%, 1.0%, 2.0%, 3% and 5.0% GNP content by percent weight via cast film extrusion with a 24:1 Maddock mixing screw within a Killion extruder. (Davis Standard, Somerset, New Jersey, USA). A Maddock mixing screw resembles a standard PE screw, however the melt passes through a narrow region just prior to the metering

section where the melt undergoes higher shear, resulting in a small degree of dispersive mixing. The melt is split, recombined several times, and reoriented to also provide distributive mixing prior to exiting the barrel. (Giles, Wagner, & Mount, 2013)

Figure 16: Image of Maddock Mixing Screw

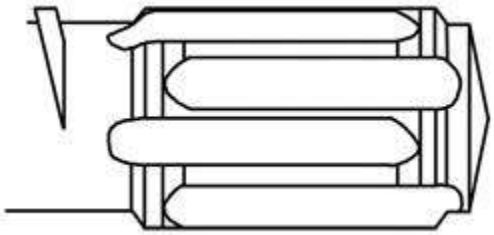

Figure 17: Diagram of Maddock Mixing head. Credit: Frankland, 2010

Methods

Once the films were produced, microstructural analysis was performed using x-ray diffraction, TEM, and optical microscopy to characterize and inspect the morphology and masterbatch distribution within the films. These analysis methods were also used to inspect for homogeneous distribution within the GNP masterbatch. X-ray diffraction was performed on three film samples per loading rate, including unmodified control sample and masterbatch.

Tensile strength and puncture resentence testing were performed on 10 film samples per loading %. Oxygen permeability and water vapor permeability were tested

on 5 film samples per loading rate. These tests and methods will be later described in greater detail.

Thermal Properties

Differential Scanning Calorimetry

DSC was performed using a TA Instruments 2920 Modulated DSC (TA Instruments, USA). DSC analyses were performed on the 0% control sample, as well as all samples containing GNP content. 6 – 8 mg samples were cut from the center of each web using a hole-punch and weighed on a digital balance (Explorer, Ohaus Corporation, Switzerland). The samples were sealed inside aluminum DSC sample pans (TA Instruments, USA). The reference consisted of an empty aluminum sample pan. All DSC testing was performed under nitrogen atmosphere.

The samples were first ramped to 25° C at a rate of 1.00° C/min and held isothermally for 1 minute. The temperature was then ramped to 150.0° C at a rate of 10° C/min and held for 1 min isothermally to remove any thermal history in the samples. The temperature was then dropped to 25.0° C at a rate of 10° C/min and held isothermally for 1 min before ramping back to 150.0° C at 10° C/min. Percent crystallinty of a sample can be calculated using the following formula:

$$\%\ \text{Crystallinity} = \frac{[\Delta \text{Hm} - \Delta \text{Hc}]}{\Delta \text{Hm}^0}\ x\ 100\%$$

Equation 5: % Crystallinity Calculation using Differential Scanning Calorimetry

In this equation, ΔH_m is the enthalpy of melting in Joules per gram (J/g), ΔH_c is the enthalpy of crystallization in J/g, and $\Delta H_m°$ is the heat of melting if the polymer were 100% crystalline. However, since the Dow® 5230G resin contains both linear and branched polyethylene that will display two distinct crystalline peaks that are merged into each other, deconvolution of the two merged peaks is not an accurate means to determine percent crystallinity. Instead, changes in crystallinity were compared for changes in peak height, width, and temperatures between the control sample and the samples with added GNP content.

Tensile Properties

Tensile properties were measured using an Satec T10000 according to ASTM D882, "Tensile Properties of Thin Plastic Sheeting" (Instron Corporation, Canton, MA, USA). 10 film samples were taken from the center, flattest section of the web and cut into 2.54 cm x 10 cm strips and were conditioned in a controlled atmospheric chamber for 48 hours at 23° C and 50% RH. The initial jaw separation distance was 5 cm and the head speed was 12.5 mm/min.

To compare the observed tensile properties to theoretical values, the Halpin-Tsai model was used. The Halpin-Tsai model provides a predictive estimation of the modulus of a platelet-filled reinforced composite. Several versions of the Halpin-Tsai model can be used depending on the orientation of the filler. It is expected that cast film extrusion

would provide some degree of orientation of the nanopartiles, thus the Halpin-Tsai equation which accounts for a unidirectionally distributed filler was used:

Equation 6: Halpin-Tsai Model for a unidirectionally distributed filler

E is the modulus of the LLDPE film sample, E_G, is the modulus of the GNP filler (an estimation of ~1 TPa). α is the aspect ratio of the filler, which is the length of the platelet divided by the width of each platelet section. Due to the varying GNP sizes within the matrix, platelet width was established at 1.25 μm and 2 nm was established for the thickness. V_G is the volume fraction of the filler within the matrix, which can be obtained by converting the mass fraction to volume fraction:

Equation 7: Mass Fraction to Volume Fraction Conversion

represents the density of the matrix (0.916 g/cm^3), represents the density of the GNP filler (2.2 g/cm^3) and *w* represents the mass fraction of the filler.

Barrier Properties

Oxygen Transmission

Transmission of oxygen through the films was determined using a Mocon OX-TRAN 2/21 (Minneapolis, MN) at 23° C and 0% relative humidity using 20% O_2 synthetic air. All tests were conducted according to ASTM D-3958. A coulometric oxygen sensor was used to detect oxygen and the tests were performed continuously until the OTR reached consecutive values of within 1%. Each test was allowed 24 hours and oxygen transmission rate (OTR) was recorded in cc/[100^2-day]. Five OTR tests were performed per GNP loading.

Water Vapor Transmission

Transmission of water vapor was determined using a Mocon PERMATRAN-W 3/33 (Minneapolis, MN). The tests were conducted according to ASTM F-1249 at 37.8° C and 100% relative humidity. An infrared sensing detector was used to detect water vapor content and the test was terminated automatically after WVTR reached consecutive values within 1% of each other. Five WVTR tests were performed per GNP loading.

Microstructure and Morphology Characterization

Optical Microscopy

Film samples containing GNP content were examined with a Nikon (Tokyo, Japan) Optiphot integrated circuit microscope at magnifications of 100x, 200x, and 400x.

X-Ray Diffraction

X-ray diffraction was utilized to inspect for changes in the distance spacing between graphene platelets within the masterbatch and film samples. XRD was also used to estimate polymer crystallite size. A Rigaku Ultima IV X-Ray diffractometer (Rigaku-MSC, Houston TX) was used. The diffraction was conducted using Cu target Kα radiation with a wavelength of 1.5406 Å. The diffraction patterns were analyzed with Rigaku Measurement Monitor for Windows v1.0 and Rigaku PDXL version 1.8.1.0. The x-ray source was operated at 40 kV and 40 mA with an exposure time of 60 minutes from 0-60° 2θ at a rate of 1° 2θ/minute. Three samples per GNP loading were tested, as well as three samples of the masterbatch and control. The masterbatch samples were compressed to into thin, flat disks for x-ray diffraction using a Carver press.

TEM

The masterbatch and film samples to be investigated with TEM were first encased in a medium grade LR White® embedding resin (London Resin Products, England) that was allowed to cure for 24 hours. The samples were cut to a thickness of ~90 nm using an ultra-microtome (Reichert Jung, Germany) equipped with a glass knife. The samples were placed on a carbon coated mesh copper grid (Electron Microscopy Sciences, Hatfield, PA, USA) prior to imaging on a Hitachi 7600T (Hitachi, Ltd., Tokyo, Japan) transmission electron microscope operating at 120 kV. Images were obtained at varying magnifications and captured using Advanced Microscopy Techniques Advantage Image Capture Engine software version 5.4.2.259 (AMT Corporation, Woburn, Massachusetts).

TEM images were obtained of both the masterbatch and film samples containing GNP content to inspect the GNP distribution and morphology.

Statistical Analysis

Statistical analysis was performed on the results from all mechanical and barrier testing. Statistically significant differences within the data were determined using analysis of variance (ANOVA) procedures. The Tukey Kramer honestly significantly different (HSD) test was conducted using SAS Software Version 9.0 (SAS Institute, Cary, NC) to analyze for differences of the means at a defined significance level of $P = 0.05$. The Tukey Kramer HSD test was chosen, as it reveals statistically significant differences between control and sample groups and also significant differences within the sample group variables. Compared to a t-test, the Tukey-Kramer HSD test accounts for the experiment's error rate and is a preferred statistical analysis for experiments with multiple treatments, as the likelihood of a type 1 error is reduced.

Relationship modeling was performed using simple linear regression upon results displaying a clear trend using the below equation:

$$y = X\beta + \varepsilon$$

Equation 8: Linear Regression Model

Y is the dependent variable, being the measured results obtained, while X is the independent variable, being the loading rates of the film samples. β is the regression coefficient, in which case if $\beta \neq 0$, then the existence of a correlation between the loading

rate and obtained result could exist. ε is the error term that accounts for other extraneous factors that could influence the relationship between X and y.

CHAPTER 4

RESULTS AND DISCUSSION

The follow extrusion conditions were applied and observed during extrusion:

GNP Loading (% wt)	0.00%	0.50%	1.00%	2.00%	3.00%	5.00%
Barrel Zone 1 Temp (°F)	250	250	250	250	250	250
Barrel Zone 2 Temp (°F)	330	330	330	330	330	330
Barrel Zone 3 Temp (°F)	365	365	365	365	365	365
Adapter Temp (°F)	365	365	365	365	365	365
Back Pressure (PSI)	830	810	830	840	810	890
Melt Temp (°F)	365	366	367	366	367	367
Screw RPM:	65.5	65.8	65.7	65.6	65.6	65.5
Air Gap	1 7/8	1 7/8	1 7/8	1 7/8	1 7/8	1 7/8
Amperage	7.5	7.5	7.5	7.5	7.5	7.5
Take Off Roll FPM:	20.8	20.8	20.8	20.8	20.8	20.8
Web Width (inches)	5.75	4 7/8	4	4.125	4	4
Casting Drum Temp (°F)	59.6	59.6	59.6	59.6	59.6	59.6
Average Thickness (mils)	3.5	~3.5	~3.6	~3.7	~3.7	~3.9

Table 5: Observations and Conditions during Extrusion

Since the properties of a nanocomposite are heavily dependent upon the degree of exfoliation and dispersion of the nanoscale filler, these morphologies were first investigated with x-ray diffraction.

Appendix A contains x-ray diffraction patterns for all samples, including the control and masterbatch. Figure A-1 displays the x-ray diffraction pattern for the LLDPE sample without additives. The shoulder peak at ~20° displays the semi-crystalline structure of the unmodified PE film sample, while the steep peaks at 21° and 23° are representative of the crystallites within the film sample. The diffraction pattern of the 20% masterbatch displays a prominent graphitic peak at 26.5°, which corresponds to a d-spacing of 3.35 Å between the stacked graphite layers according to Bragg's law in equation #1. A 26.5° graphitic peak was expected in the masterbatch diffraction pattern, as the graphite nanoplatelets consist of several stacked graphite layers that retain a crystalline structure capable of x-ray radiation diffraction. The diffraction patterns of the film samples with an added GNP content display also display a graphitic peak at 26.5°, as shown below in the 5.00% GNP film sample diffraction pattern in Figure 17. Table 6 summarizes the findings of x-ray diffraction.

The absence of an additional peak at lower values in any of the diffraction patterns indicates that a greater interlayer spacing has not been achieved, thus an intercalated structure has not been formed in either the masterbatch or film samples. This intercalated structure is the most achievable morphology in a polyethylene – graphite

composite outside of phase separation. The lack of significant reduction in the 26.5° graphitic peak indicates that the graphene layers have not been delaminated to their monolayer, graphene form in either the masterbatch or the film samples. The reduction in the graphitic peak would have been caused by a significant increase in the interlayer distance between graphene planes that would be incapable of diffracting x-ray radiation. It was not expected that single screw extrusion would delaminate the GNP in the film samples. The primary purpose of x-ray diffraction was to determine if intercalation had occurred.

The intensity of the graphitic peak is consistent with the loading rate, as it is higher with higher loadings and especially apparent in the masterbatch diffractogram.

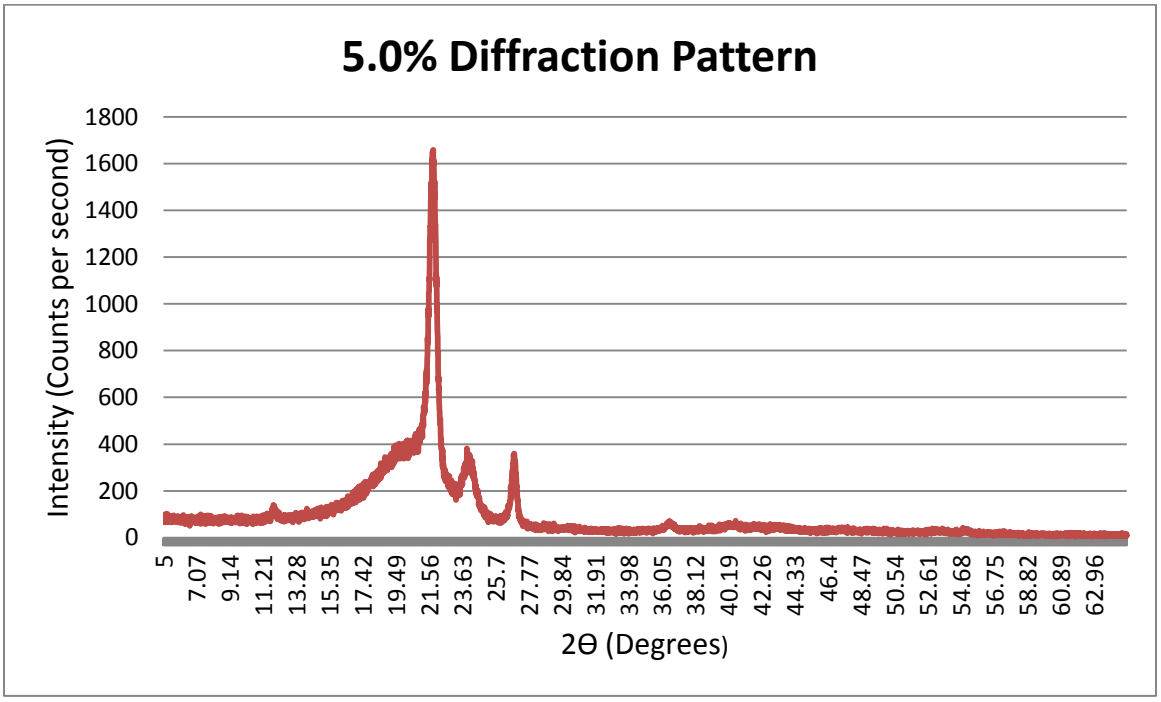

Figure 18: 5.00% X-Ray Diffraction Pattern

GNP Loading %	D-Spacing at 26.5° 2-theta (Angstroms)	Additional Peak < 26.5°	Loss of 26.5° Peak
0%	No peak	No	N/A
0.50%	3.33882	No	No
1.00%	3.30709	No	No
2.00%	3.331185	No	No
3.00%	3.1547	No	No
5.00%	3.31027	No	No
20.00%	3.3242	No	No

Table 6: Summary of X-Ray Diffraction Results

Optical Microscopy

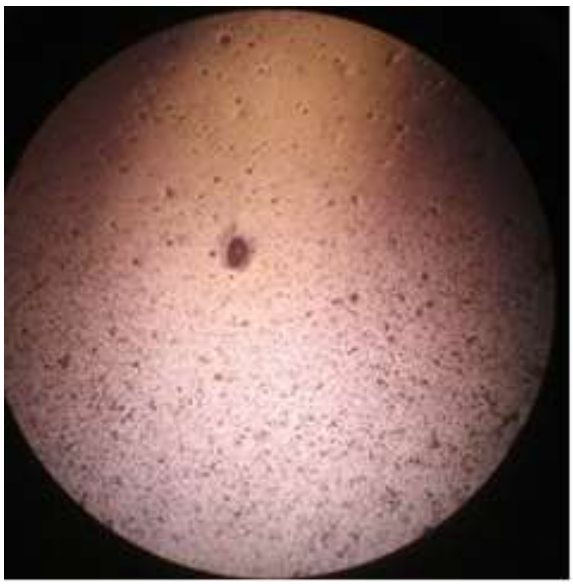

Figure 19: 200x Image of 2.0% Film

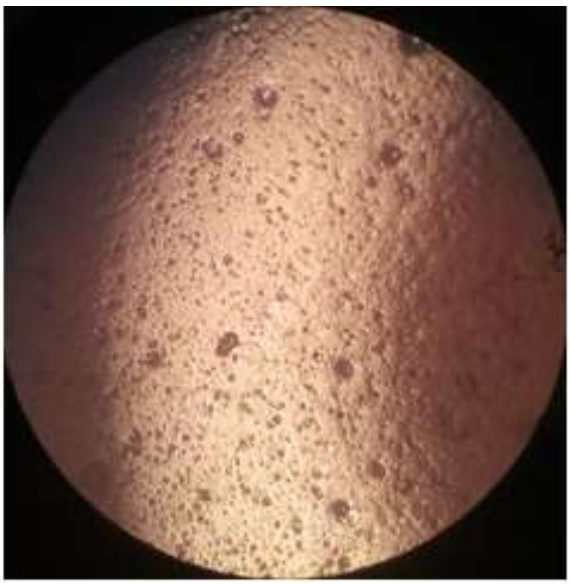

Figure 20: 200x Image of 3.0% Film

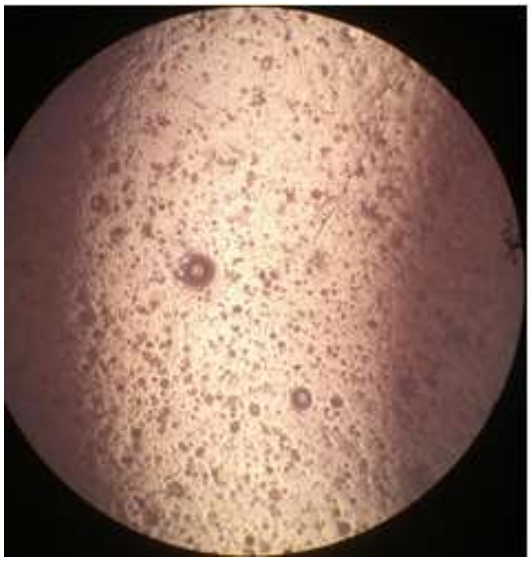

Figure 21: 200x Image of 2.0% Film

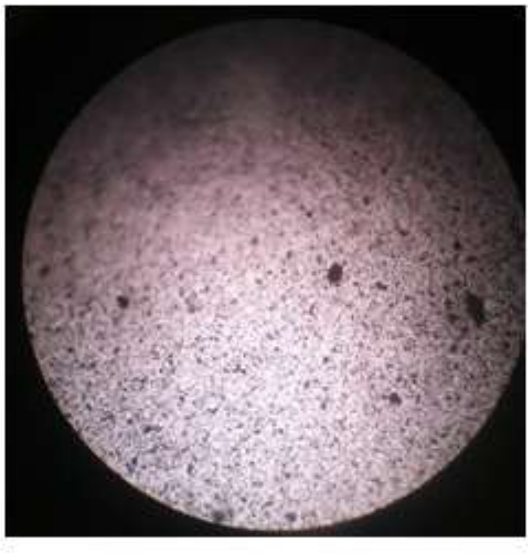

Figure: 22 200x Image of 3.0% Film

Figures 18 - 21 reveal poor distribution of the GNP masterbatch in the film samples produced by single screw extrusion. The large dark regions indicate undistributed masterbatch and graphite material, which is likely due to inadequate distribution of GNP within the masterbatch. Microscope images of the masterbatch were not obtainable, as the high density of GNP prevented light from passing through for imaging. Additional cycles of twin screw extrusion prior to pelletizing may have improved GNP distribution in the masterbatch and may have resulted in a more homogeneous arrangement upon single screw film production. TEM was used to confirm the results obtained by optical microscopy.

Transmission Electron Microscopy (TEM)

TEM was used to inspect the dispersion and distribution of GNP within the masterbatch and film samples. TEM can also confirm the morphology analysis obtained by x-ray diffraction.

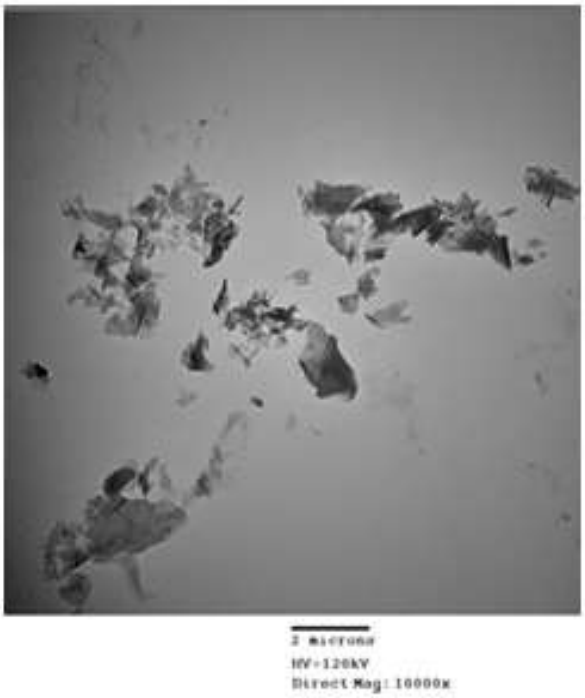

Figure 23: GNP in masterbatch.

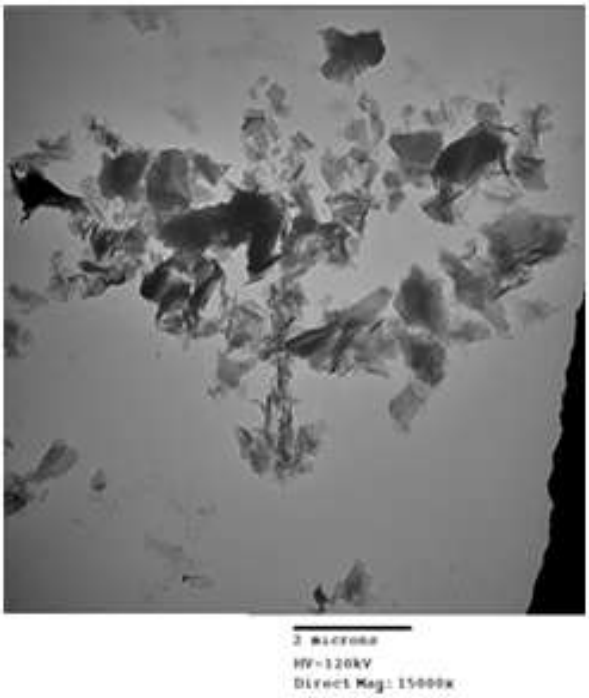

Figure 24: GNP cluster in masterbatch.

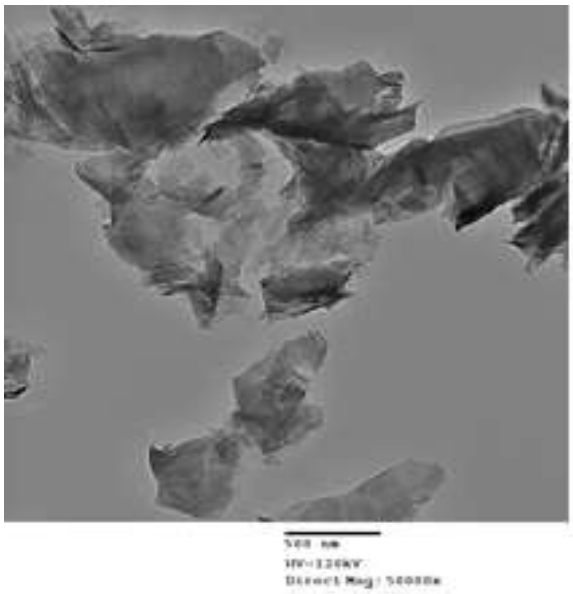

Figure 25: GNP in masterbatch.

Figure 26: GNP dispersion in masterbatch.

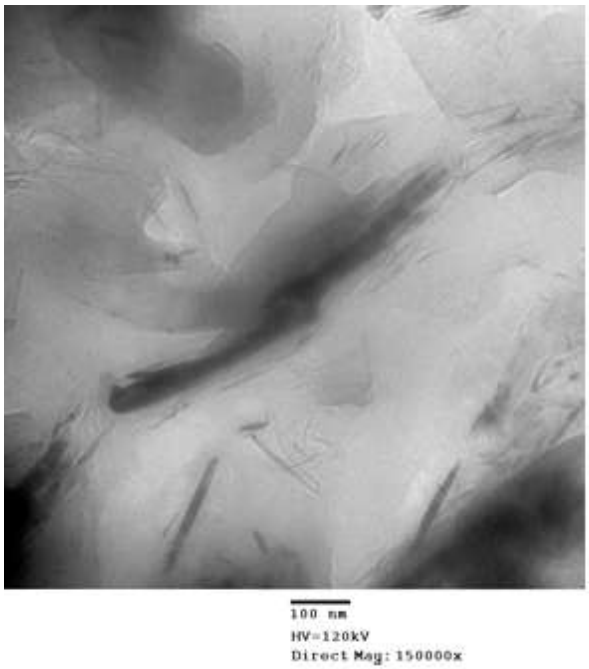

Figure 27: Cross Section of masterbatch.

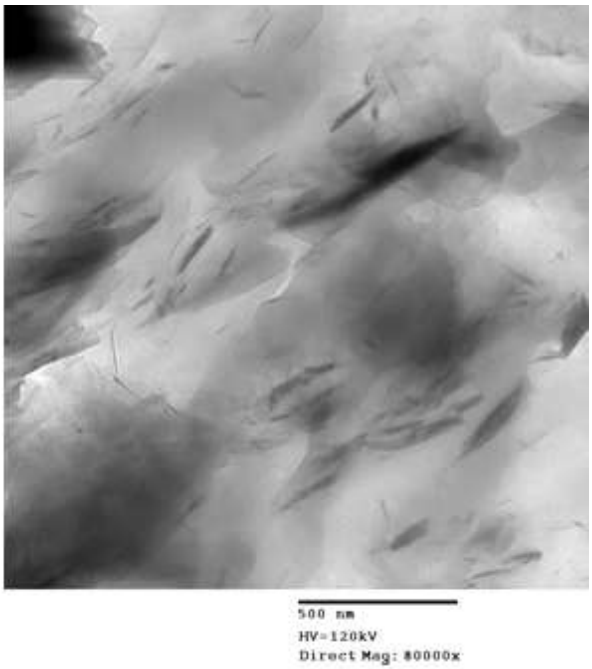

Figure 28: Cross Section of masterbatch.

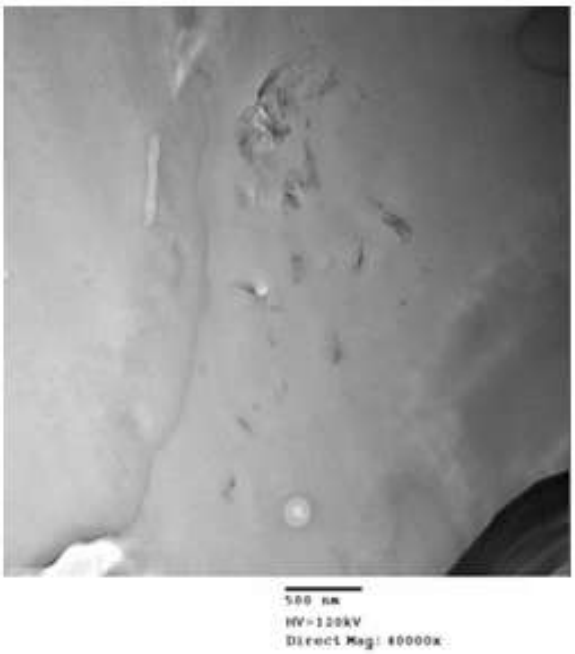

Figure 29: Dispersion in 0.5% film.

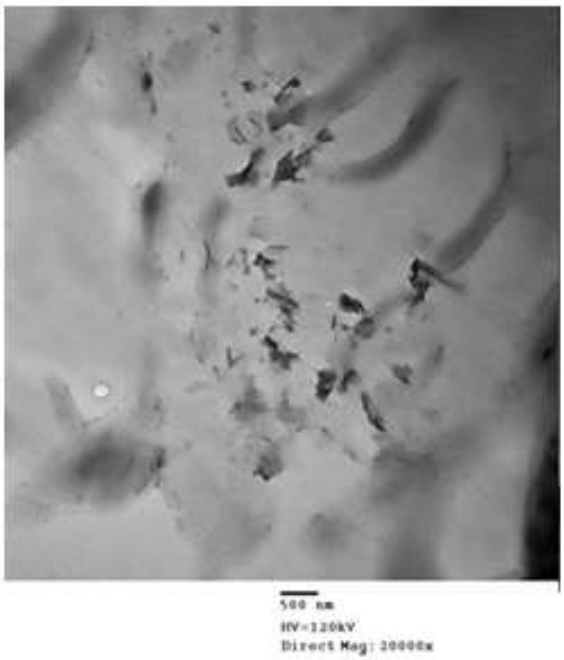

Figure 30: Dispersion in 0.5% film.

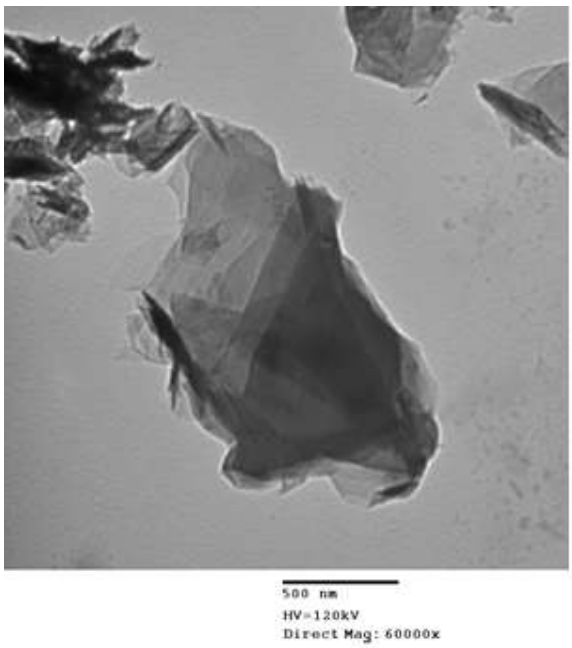

Figure 31: Platelet with thickness variations in masterbatch.

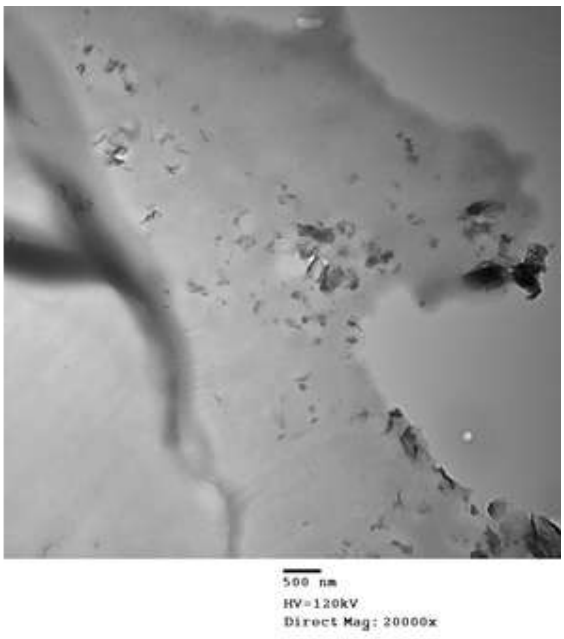

Figure 32: Dispersion in 1% film.

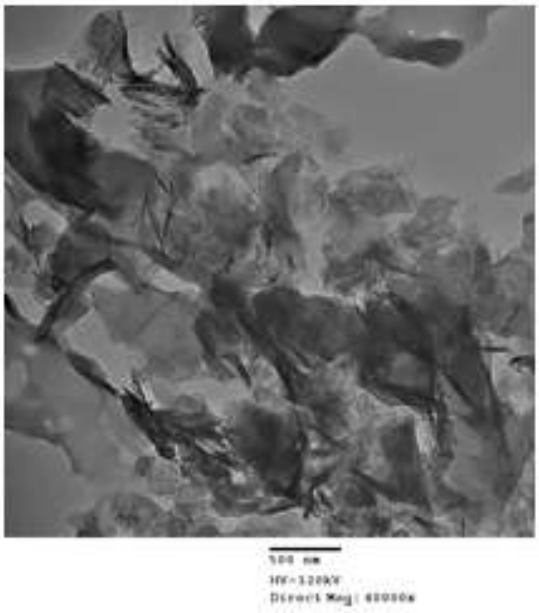

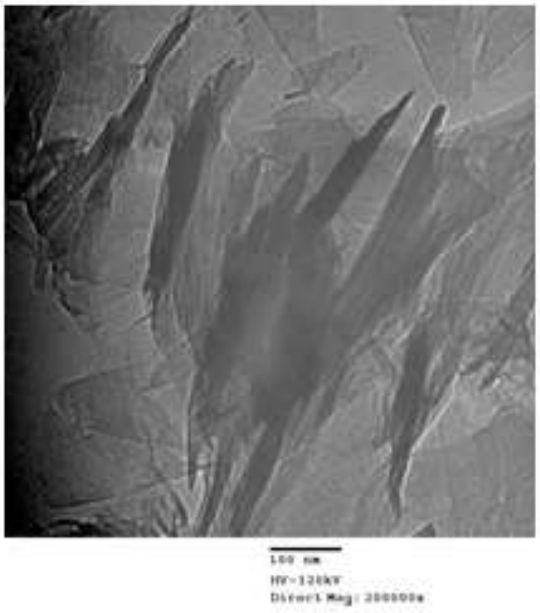

Figure 33: Agglomeration of GNP in 5% film. Figure 34: GNP in 5% film

The TEM images reveal inconsistent distribution of GNP within the masterbatch prior to single screw extrusion. Figures 32 - 25 display sections of the masterbatch where clusters of GNP have been inadequately dispersed and distributed. While some GNP can be observed as being several nanometers in thickness, most regions appear to consist of inhomogeneous regions of GNP agglomerates in the masterbatch.

The TEM images 29 - 34 reveal poor distribution and dispersion of GNP throughout the film samples as well. Both agglomerates as well as small regions of exfoliated GNP appear to be present. These regions of exfoliation are inhomogeneously distributed throughout the films. The agglomerations of GNP consist of multiple graphitic

layers, as dark, shaded regions due to their high electron density. The agglomerations also appear to be rather sizeable, containing significant graphite content.

The GNP agglomerates within the film samples are likely due to inadequate GNP distribution in the masterbatch prior to single screw extrusion. Single screw extrusion will not exert sufficient shear and dispersive forces upon the melt to impart significant changes on the GNP morphology if it is not adequately distributed in the masterbatch. Improved distribution in the masterbatch would have likely resulted in distribution improvements in the film samples.

The TEM imagery presented in Wang, et al.'s investigation reveals much improved distribution of GNP within a compatibilized LDPE matrix. The homogeneous distribution of GNP in Wang et al.'s research also resulted in significant improvements in mechanical properties. SEM micrographs presented in Wang, et al.'s research also display uniform surface morphology within the LDPE – GNP composite films, however it is important to note that these materials were produced via a plate vulcanizing machine and not by extrusion processing.

Microstructure Changes

Differential Scanning Calorimetry

Appendix F displays the DSC curves from all samples, including the masterbatch sample. Figures 35 and 36 summarize the key changes observed during crystallization.

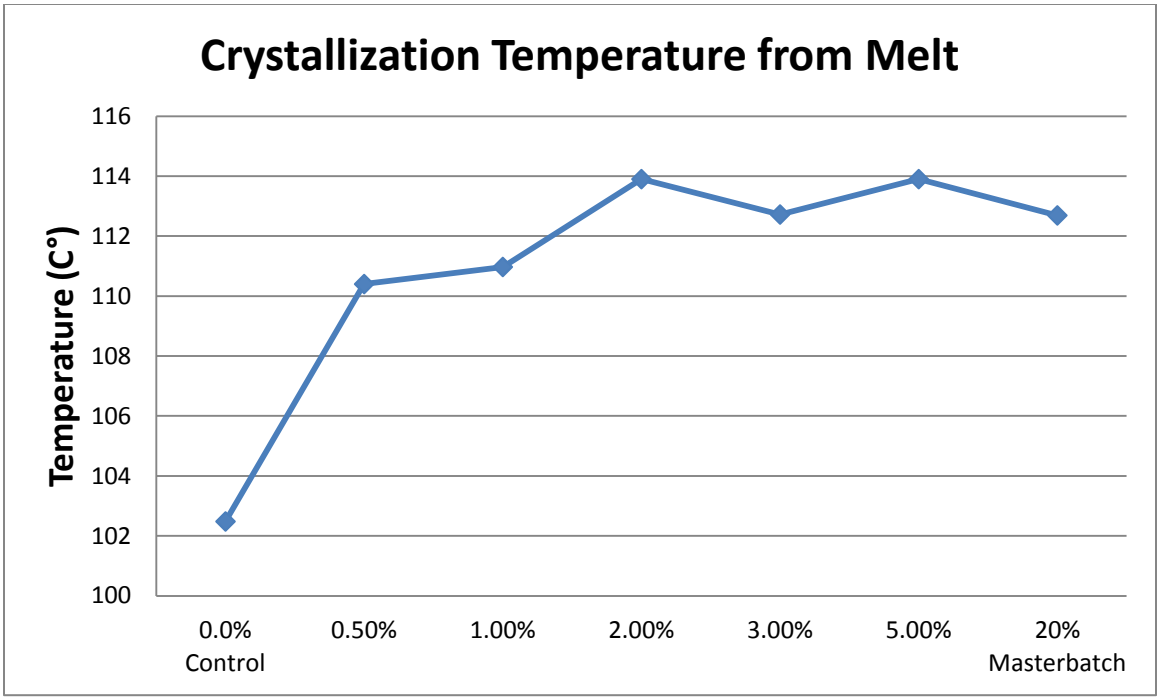

Figure 35: Crystallization Temperature from Melt

As the samples were cooled during DSC, the LLDPE crystallization temperature occurred at significantly higher temperatures in samples containing GNP content. It appears that the addition of GNP to the LDPE/LLDPE matrix is acting as a nucleating agent on the LLDPE structure. This was also observed in Jiang and Drzal's study where a similar trend was observed between HDPE and GNP. Interestingly, the crystallization peak of the LDPE appears unchanged by the addition of GNP. While even at very low loadings (0.5%), the LLDPE crystallization temperature is increased by around 8° C. The broader LLDPE crystallization peaks in the DSC curves of all samples containing GNP content may be due to the presence of GNP slowing the formation of crystallites compared to the narrow LLDPE crystallization peak in the control sample. This

nucleation and hindering phenomena was also observed and described by Jiang and Drzal where it was especially apparent in samples containing higher GNP content (>5% volume). The masterbatch sample displays a greater reduction in the heat of fusion and the smallest crystalline peak in the DSC curve. This may be due to the high volume of GNP within the matrix hindering the formation of crystalline structures.

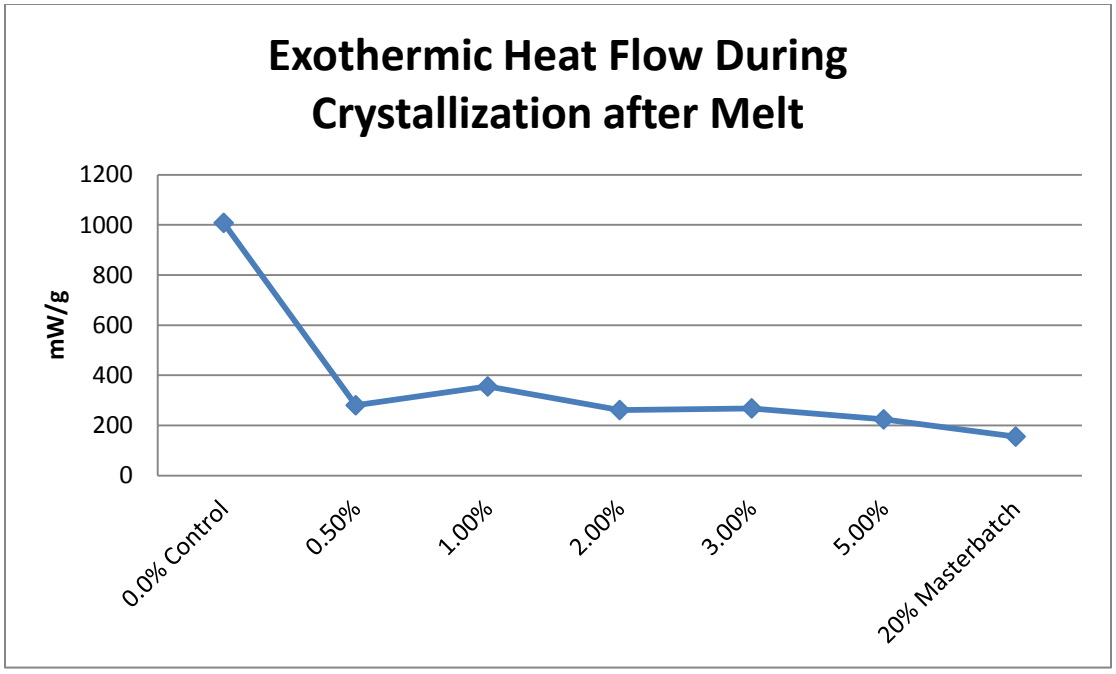

Figure 36: Heat Flow During Crystallization after Melt

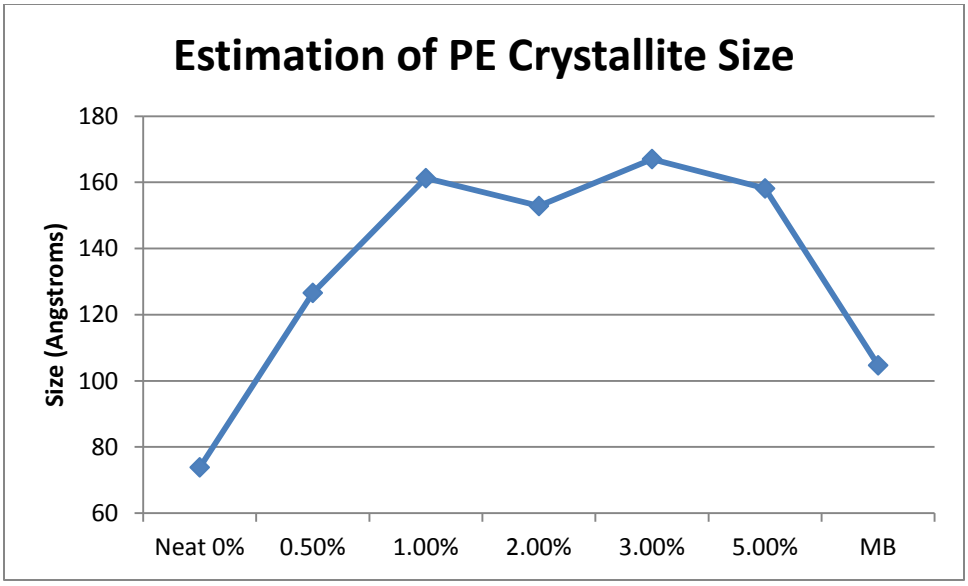

Figure 37: Estimation of Polyethylene Crystallite Size according to the Scherrer equation from X-Ray diffraction

Figure 37 displays the estimation of crystallite dimensions perpendicular to the crystallographic plane using data collected during x-ray diffraction according to the Scherrer equation. As the loading % of GNP increases in the LLDPE/LDPE matrix, the size of the crystallites increases. While the Scherrer equation only provides a rough estimation of crystalline spherulite sizes perpendicular to the diffraction direction, the increasing trend in crystallite size with added GNP content is a key observation.

The crystallite sizes in the masterbatch do not fall within the same trend. This could be due to the high volume of GNP hindering formation of crystallites as described by Jiang and Drzal, but it should also be noted that the masterbatch sample does not share the same processing history as the film samples.

Barrier Properties

Oxygen Transmission Rate

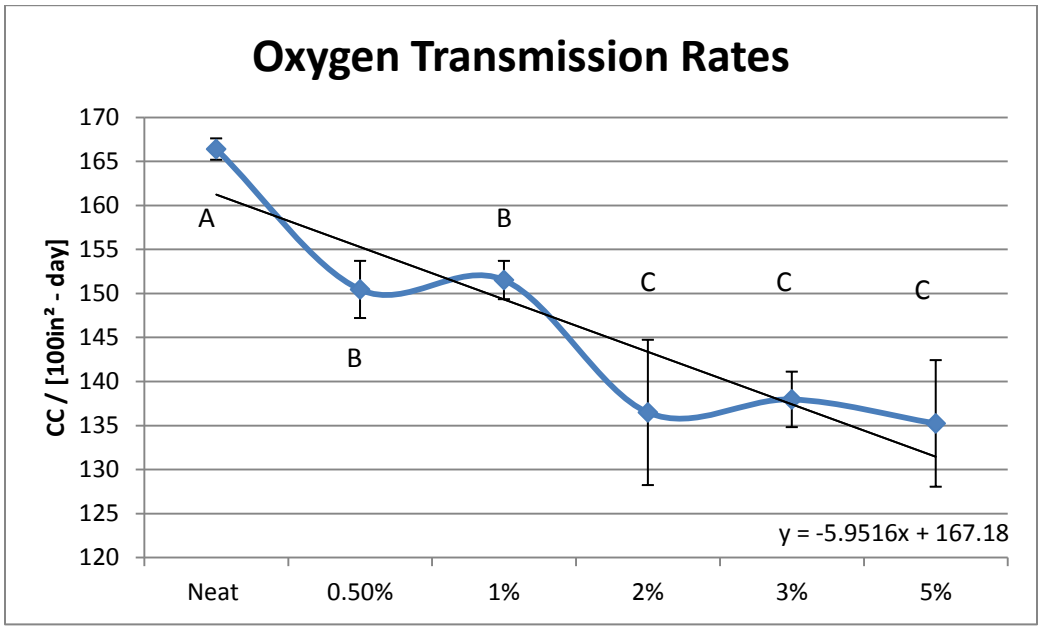

***Means with the same letter are not significantly different.

Figure 38: Oxygen Transmission Rates of Film Samples

The degree of dispersion and exfoliation of GNP within the polymer observed in the TEM images can directly affect the oxygen barrier properties of the film, as a more tortuous pathway for oxygen migration is created if greater surface area of the GNP is exposed. Figure 38 displays the oxygen transmission rates of the film samples. With higher GNP loadings, the oxygen transmission through the films was decreased. This reduction is likely due to the creation of a more tortuous pathway by additional platelets that block diffusion pathways. If greater dispersion and more homogeneous distribution had occurred, a greater improvement in the films' oxygen barrier properties would have

likely been observed. The decrease in oxygen transmission in the films could also be due to a higher percentage of crystallinity and larger crystallites as observed in the data acquired by x-ray diffraction using the Sherrer equation. Larger crystallites create a more tortuous pathway for permeants, reducing transmission rates.

While there are statistically significant reductions in oxygen transmission rates, the reductions are negligible relative to other common coextruded packaging films in the marketplace that do not require lamination or additional post extrusion processing. For example, a 3 mil 7 layer split nylon 66/6 film will display an oxygen transmission rate of roughly 7.0 CC / [100in² - day].

Water Vapor Transmission Rates

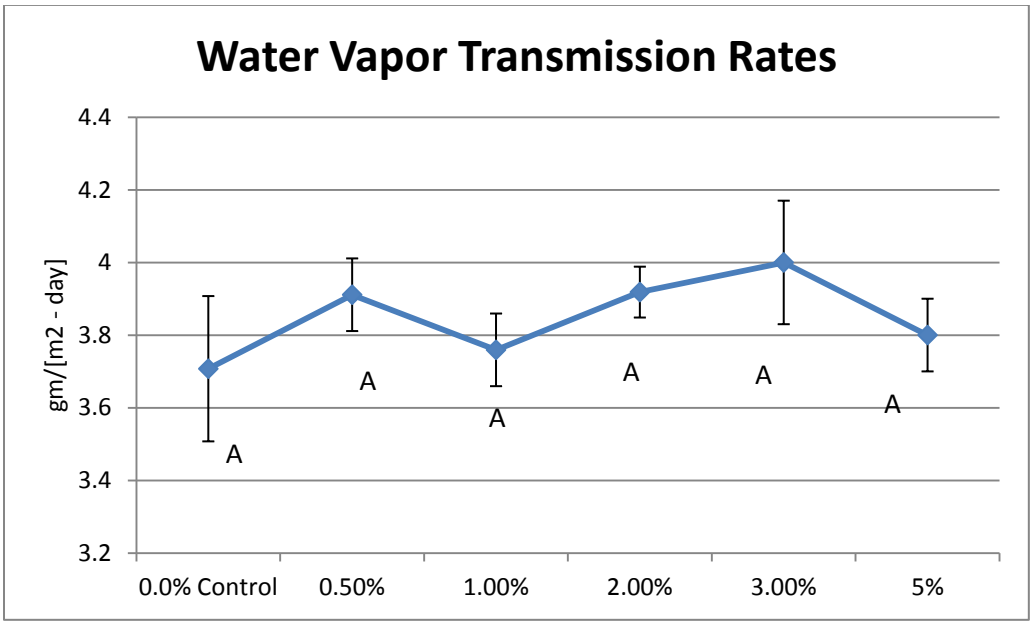

*****Means with the same letter are not significantly different.

Figure 39: Water Vapor Transmission Rates of Film Samples

No significant changes in WVTR was observed with samples containing GNP content. GNP can be highly permeable to water vapor if they contain impurities and structural defects. The sonication method of natural graphite used to produce the GNP in the masterbatch did not include a graphite purification step, thus impurities and defects could exist. Graphene oxide is considered to be "super permeable" to water vapor and is being researched for applications in water purification and desalination (Mukhopadhyay and Gupta, 2013).

Mechanical Properties

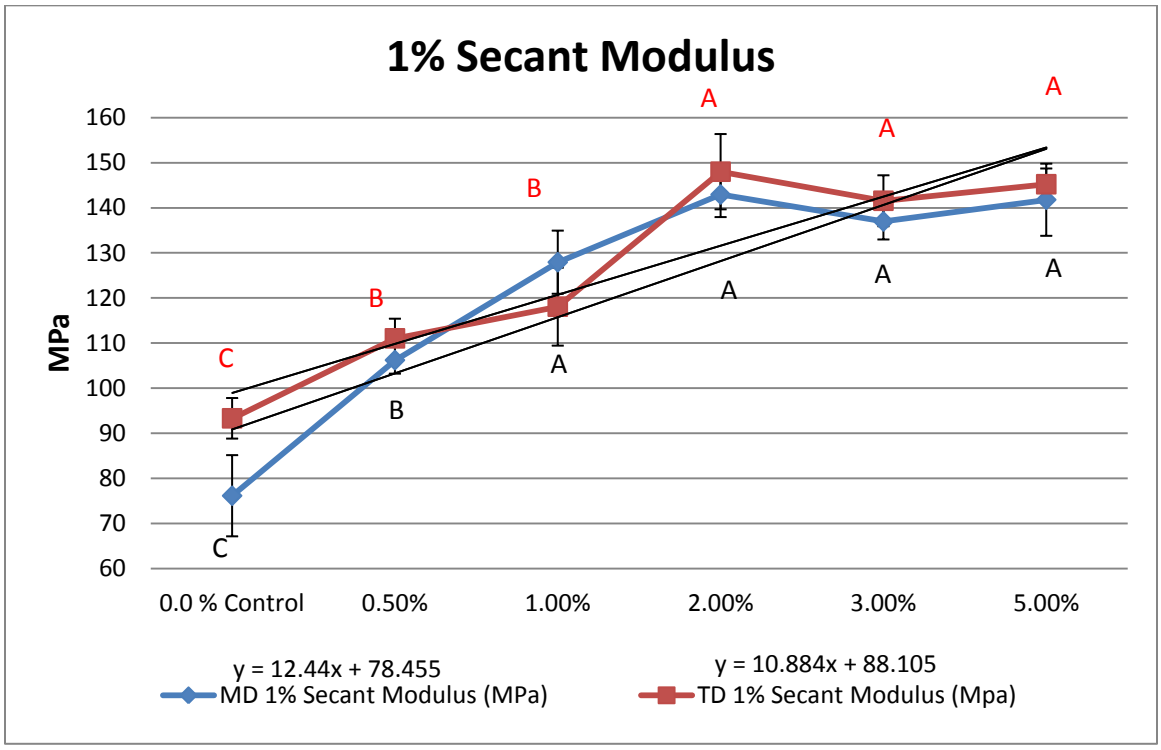

***Means with the same letter are not significantly different.

Figure 40: 1% Secant Modulus Summary

Figure 40 displays the secant moduli averages of each set of films in the machine and transverse directions where a greater resistance to deformation of films with GNP content can be observed. This may be due to the stiffening effect that the rigid GNP filler has imparted upon the film by reducing polymer mobility as described by Caroenuto, et al (2012). This has resulted in a more rigid film that displays more resistance to initial elastic deformation.

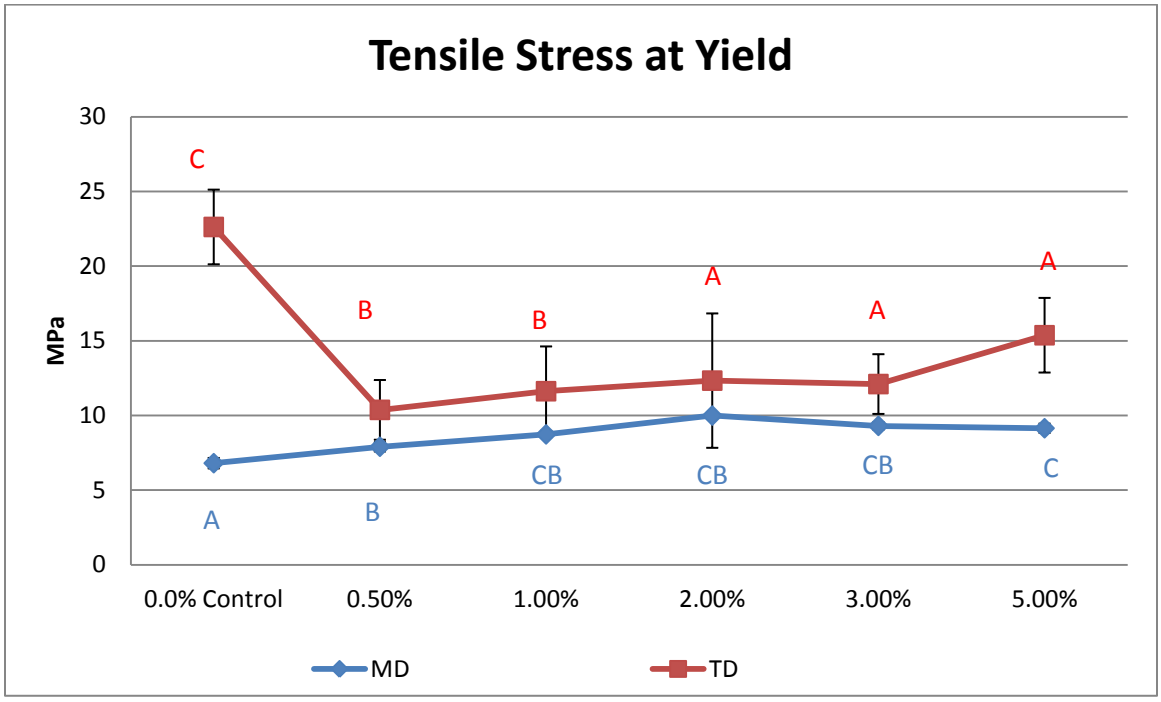

*Means with the same letter are not significantly different.

Figure 41: Tensile Stress at Yield

Tensile stress at yield is an important property in flexible packaging, as it refers to the point where a film begins to undergo an increase in strain without an increase in stress (Selke, 2004). In the MD, a slightly positive linear trend was observed where the GNP

reduced the polymer's mobility, requiring greater stress to deform it. Similar to the increase in 1% secant modulus, this may be due to the presence of GNP in the polymer, stiffening the film and acting to prevent the stretching and unfolding of polymer chains.

In the TD, the addition of GNP weakened the film's ability to resist plastic deformation. This difference in MD and TD in tensile stress at yield suggests a degree of anisotropy that cast film extrusion has imparted on the orientation of GNP in the film. It is interesting that few of the other tensile properties have displayed such differentiation between TD and MD properties as the tensile stress at yield.

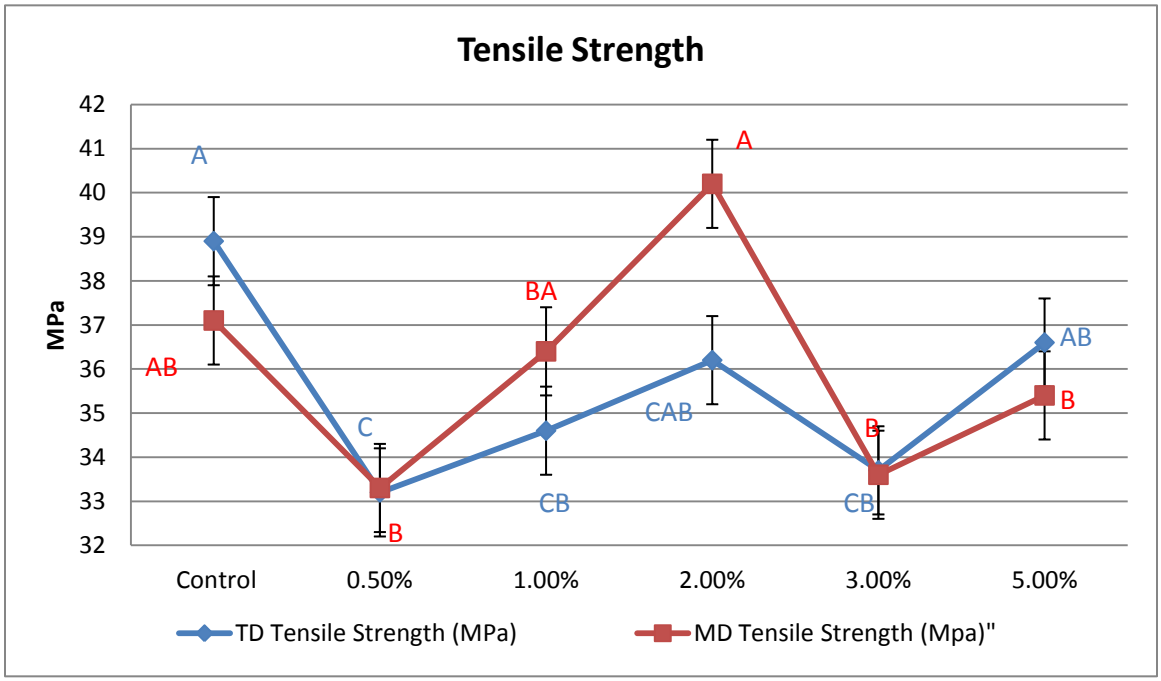

***Means with the same letter are not significantly different.

Figure 42: Tensile Strength of GNP-Film Samples

There were no significant trends apparent in the tensile strength values. Despite sizeable agglomerates observed in the microscope and TEM images, major reductions in

the film tensile strengths in the MD or TD were not observed. The significant variation in the tensile strength data could be due to the uneven distribution of the masterbatch during film extrusion.

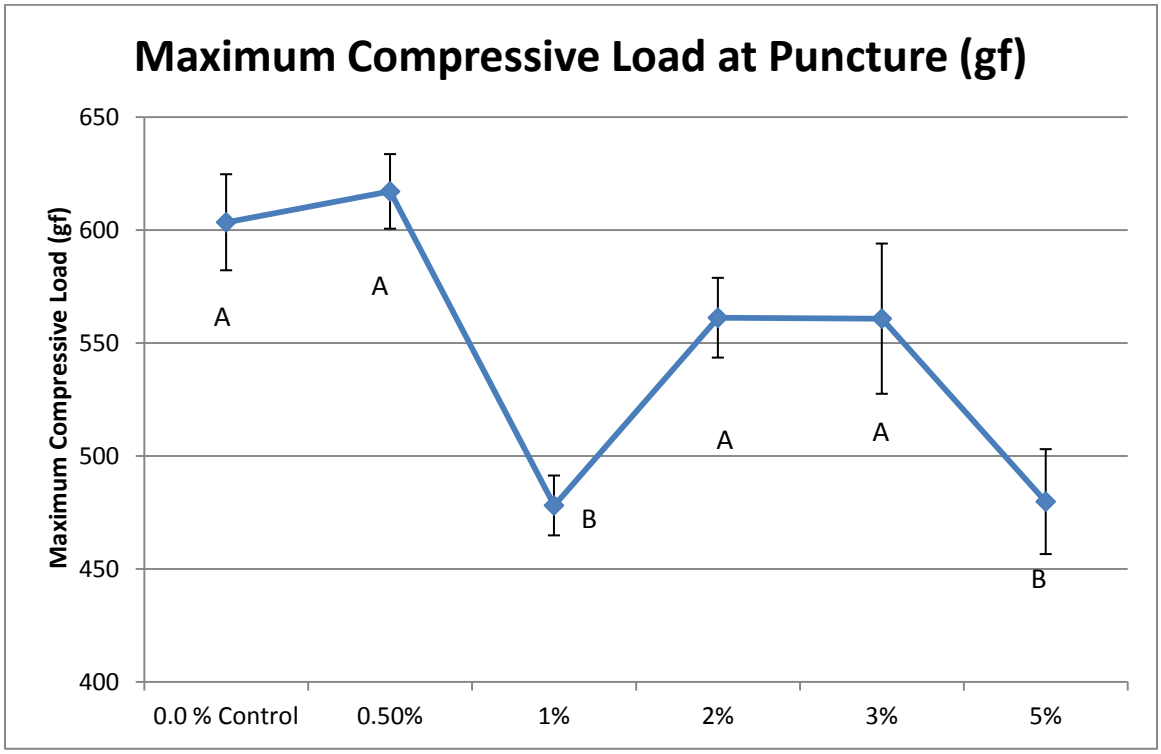

***Means with the same letter are not significantly different.

Figure 43: Maximum Compressive Load at Puncture

A reduction in puncture resistance of the films containing GNP content may be due to two causations; an inhomogeneous distribution and agglomerations of GNP, or a higher degree of crystallinity of the LLDPE structure. Agglomerations of GNP within the polymer matrix could cause structural imperfections allowing premature cracking, embrittlement, and subsequent puncture, while greater crystallinity could reduce puncture

resistance as the polymer's structure becomes denser and stiff which is less capable of resisting puncture.

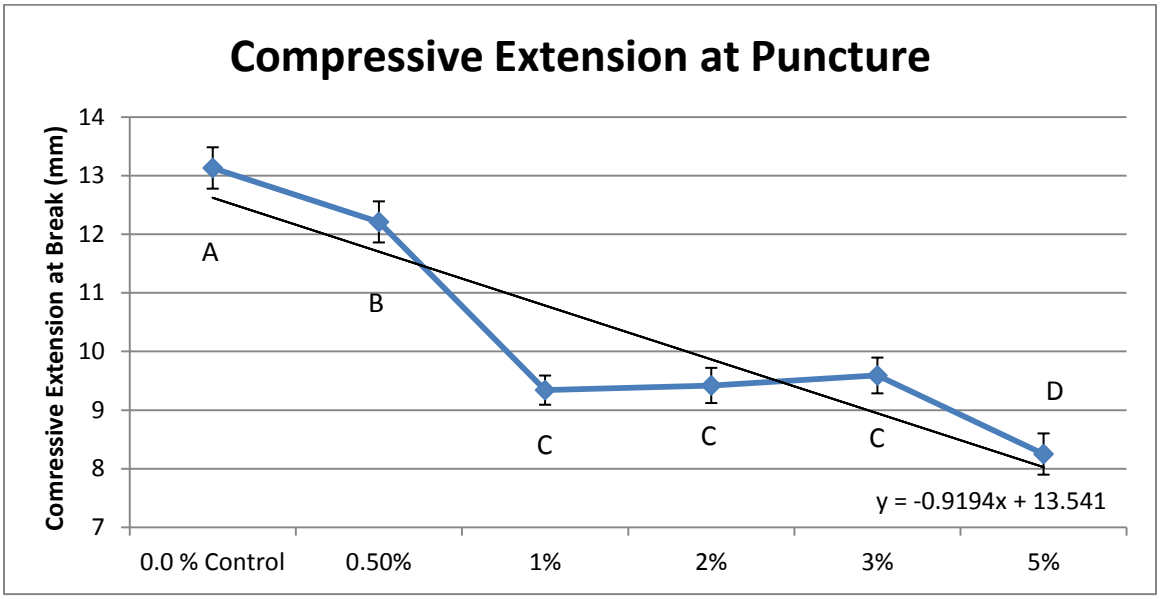

***Means with the same letter are not significantly different.

Figure 44: Maximum Compressive Extension at Puncture

The reduction in compressive extension prior to puncture parallels the reduction in polymer mobility displayed in the tensile property changes. Again, the presence of GNP in the polymer matrix reduced the extensibility of the film.

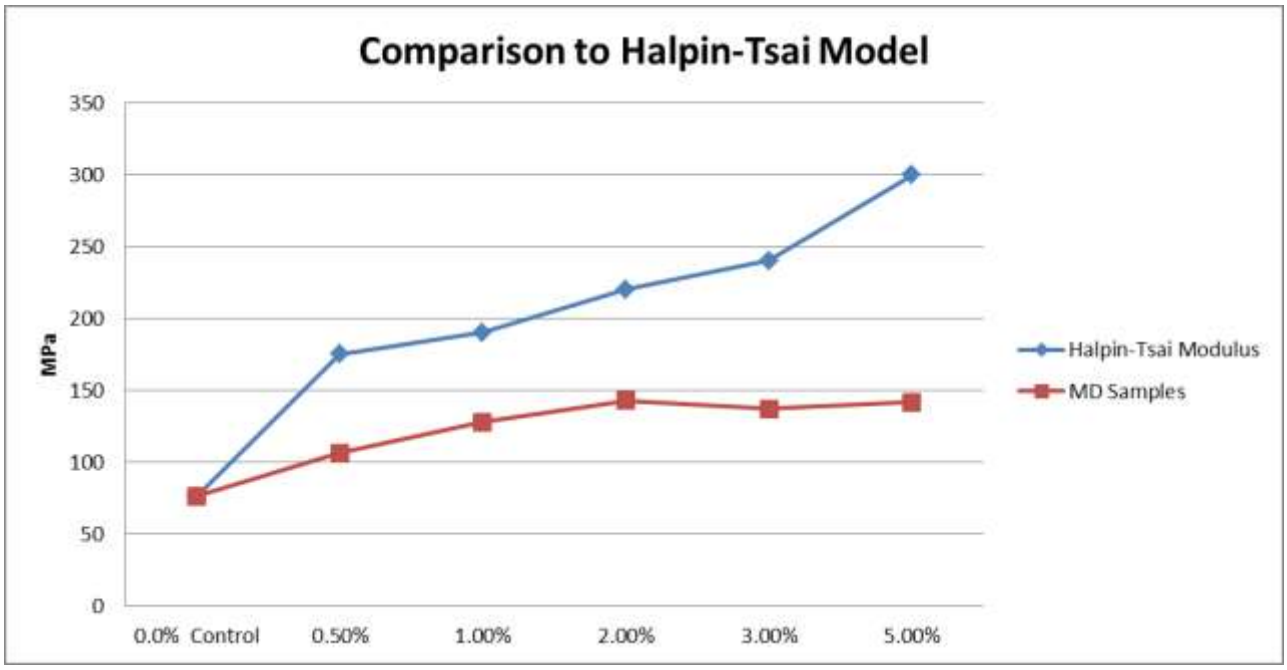

Figure 45: Comparison to Halpin-Tsai Modulus Evaluation

Figure 46 displays the comparison to the theoretical elastic modulus predicted by the Halpin Tsai equation displayed higher modulus values than the obtained experimental values. This may be due to several causes; the presence of agglomerations in the matrix weakening the structure, inhomogeneous distribution of the GNP reinforcement by single screw extrusion, and the weak interaction between the nonpolar filler and the nonpolar matrix. Improvements in any of these three facets should result in moduli that are more accurately predicted by the Halpin Tsai model.

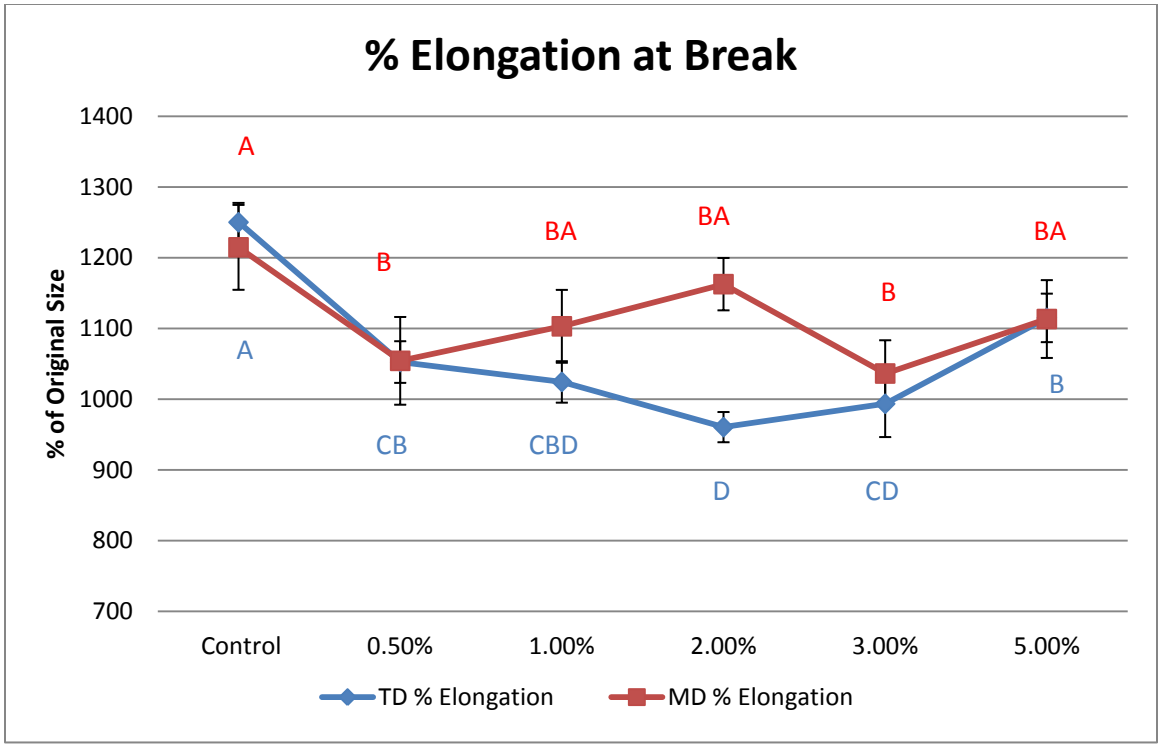

***Means with the same letter are not significantly different.

Figure 46: % Elongation to Break

Both tensile elongation to break in the MD and TD, as well as compressive extension prior to puncture were reduced with films containing a GNP content. Carotenuto, et al (2012) propose an explanation for this loss of plasticity in their study using LDPE-GNP films with GNP sized ~ 1µm in diameter by ~20nm in thickness. A complete loss of a cold drawing mechanism and necking region was observed in their study, resulting in fracture almost immediately after the yield point. Carotenuto, et al. claim this is due to the obstruction in polymer chain mobility, where the polymer chains are not allowed to unfold and rotate when stress is applied due to the uniform presence of GNP throughout the LDPE matrix. While the films in this study still display a prominent

necking region of significant elongation compared to Carotenuto's materials, the same principle proposed by Carotenuto may still apply, where GNP is reducing the elongation of the films prior to break. The GNP used by Carotenuto, et al's was likely more homogeneously distributed in the LDPE matrix than in this research, which would have a more pronounced effect on the resulting mechanical properties of the films.

Another consideration is that the GNP in this study are roughly one tenth the diameter of that used in Carotenuto, et al's study, which may possibly allow for greater polymer chain mobility with less obstruction, resulting in great elongation prior to break.

Electrical Conductivity

As an aside, electrical conductivity tests were performed since graphite is highly conductive in the planar direction. Film samples of 4" x 4" from the 5.0 GNP wt% film batch were conditioned at 25°C and 50% RH for 2 days. Surface conductivity was measured after the probe was in contact with the film surface for 1 minute. No sign of conductivity was exhibited.

Antistatic testing was also performed on 3.5" x 5.5" film samples from the 5.0 GNP wt% batch. Samples were cut in the MD and conditioned at 25°C for 2 days. Static decay time was measured for 90% dissipation of a 5 kV charge at 50% RH. Surface resistivity was measured on the film surface after the probe was in contact with the film for 1 minute. The film sample did not take the charge for testing, as surface resistivity was found too high to measure ($>10^{14}$ Ohms).

The GNP loading may either be too low or inadequate distribution of GNP in the film may be preventing GNP from forming a sufficient conductive network within the film samples.

CHAPTER 5

CONCLUSIONS

TEM imagery and optical microcopy revealed that the GNP was poorly distributed within the 20% GNP / 80 % LLDPE masterbatch. Single screw extrusion was unable to adequately distribute this poorly mixed masterbatch to impart significantly improved mechanical and barrier properties of the films. Some dispersion of GNP was observed with TEM imaging, but these regions were too limited in distribution to have a pronounced effect. A phase separated morphology was observed with TEM and confirmed with x-ray diffraction.

The DSC analysis revealed that the presence of GNP in the matrix acted as a nucleation agent on the LLDPE structure, where crystallization occurred 8.0°C higher in the 0.5% film sample and at a maximum of 11.0° C higher in the 2.0% and 5.0% sample. The LDPE crystallinity remained unchanged. While the presence of GNP facilitated nucleation, it also acted to slow the growth of crystallites, where LLDPE crystallization occurred over a much broader range of temperatures compared to the control sample.

Despite the inadequate dispersion and distribution, the films with a GNP content still displayed slightly improved barrier properties to oxygen. A maximum reduction in OTR observed in the 5% GNP sample, where the OTR was reduced from 166.4019 ± 2.434 CC / [100in² - day] to 135.2405 ± 7.38 CC / [100in² - day]. While the reductions in

OTR are statistically significant, they are not significant in the context of other flexible packaging materials. A simple 1 mil layer of OPET (oriented polyester) would reduce OTR to ~2-6 CC / [100in² - day] or adding a 1 mil layer of EVOH would reduce values to ~ 0.005 to .12 CC / [100in² - day]. WVTR results displayed no significant changes with added GNP content, which could be due to the presence of polar impurities or structural defects in the GNP.

Tensile analysis revealed a reduction in the plasticity of the films with added GNP content, where the elongation was reduced to 1036.3% from 1214.6% in the MD in the 3.0 % GNP sample and to 960.5% from 1250.1% in the TD in the 2.0 % GNP sample. Increases in 1% Secant moduli were observed in all samples containing GNP content, with a maximum increase of 87.5% in the 2.0 % GNP sample in the MD and 94.3% in the TD. Marginal reductions in tensile strength were observed in both the MD and TD of the films with GNP content. Puncture resistance testing displayed similar reductions in compressive extension prior to break, where an extension reduction of 4.88 ± 0.352 mm was observed in the 5.0 % GNP sample compared to the neat control. Maximum compressive load at puncture was also reduced from 603 ± 21.25gf to 479.81± 23.22 gf in the sample containing 5.0 % GNP. The reductions in elongations during puncture and tensile testing are likely due to the rigid GNP filler reducing polymer mobility. The reduction in tensile strength and puncture resistance is likely due to an inhomogeneous distribution of GNP agglomerates within the matrix, leading to premature cracking that is weakening the structure of the films. These agglomerates are likely present due to the

lack of shear applied by single screw extrusion and poor distribution of GNP within the masterbatch.

CHAPTER 6

FUTURE RESEARCH

There are many paths to be explored related to GNP-polyolefin nanocomposites. Future research should ensure that the GNP are homogeneously distributed in a masterbatch prior to letting down via single screw extrusion. Direct twin screw extrusion as a means to produce film samples that could be analyzed with the methods employed in this study could also be of interest. Lower initial masterbatch loading rates could also be investigated where a 5% or 10% GNP concentrated masterbatch could be let down by single screw extrusion. This may allow for improved distribution of a GNP-polymer masterbatch, as a smaller amount of GNP would be distributed over a greater volume of base resin, reducing the distributive forces required.

Further research should also investigate crystallinity changes that occur with GNP - polymer composites, as this was hindered in this study due to the GNP being let down into a LDPE-LLDPE blend, making an accurate percent crystallinity calculation difficult. Further investigation should also be performed to investigate the nucleation effect of GNP on separate linear and branched polyethylene structures, as a pronounced effect was observed on the LLDPE crystallinity, while the LDPE remained unchanged.

Other related research should also investigate introducing a polyethylene grafting compatibilizing agent, like maleic anhydride, as suggested by Carotenuto, et al, or vinyl

triethoxysilane, as used to obtain significant improvements by Wang, et al. Introducing a compatibilizing agent could improve interactions between a nonpolar matrix and the nonpolar GNP filler, potentially resulting in improved distribution and dispersion of GNP. Studies using a compatibilizing method should also investigate changes to polymer melt viscosity, as bonding a rigid filler to a polymer chain could impose processing limitations caused by viscosity changes to a polymer melt. This could hinder extrusion processing and limit mass production.

More broadly, additional commodity polymer - GNP composite materials could be investigated, especially those with polar functional groups, such as Nylon, as graphene oxide is capable of interacting with other organic functional groups. If a more packaging suitable material is obtained from GNP-polymer composites, studies should investigate the properties of the material before and after retort processing at 121°C, oxygen permeation analysis in high humidity environments, and heat sealability. Future studies should also investigate whether graphene or GNP escape the polymer matrix during decomposition of the polymer, as GNP and graphene could pose environmental and health risks if inhaled due to their small particulate size.

APPENDICES

Appendix A

X-Ray Diffraction Patterns

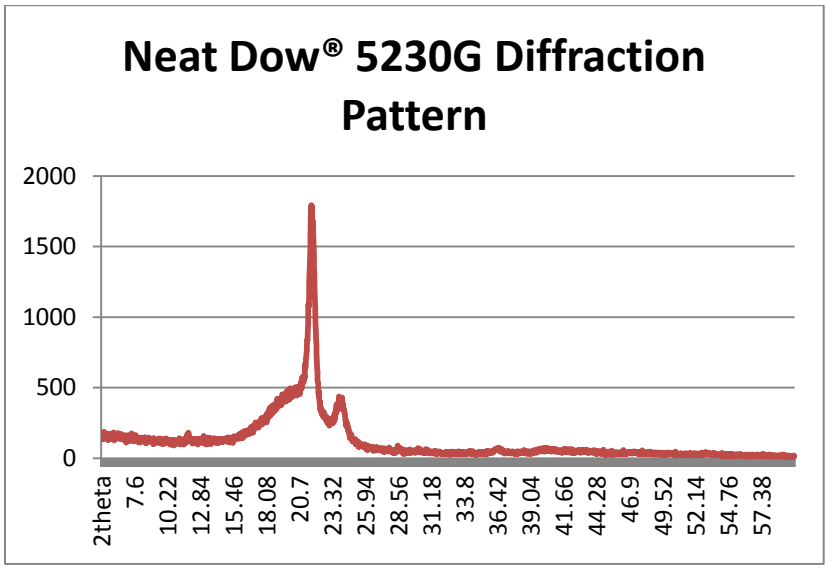

Figure A-1: Neat Control Film X-Ray Diffraction Pattern

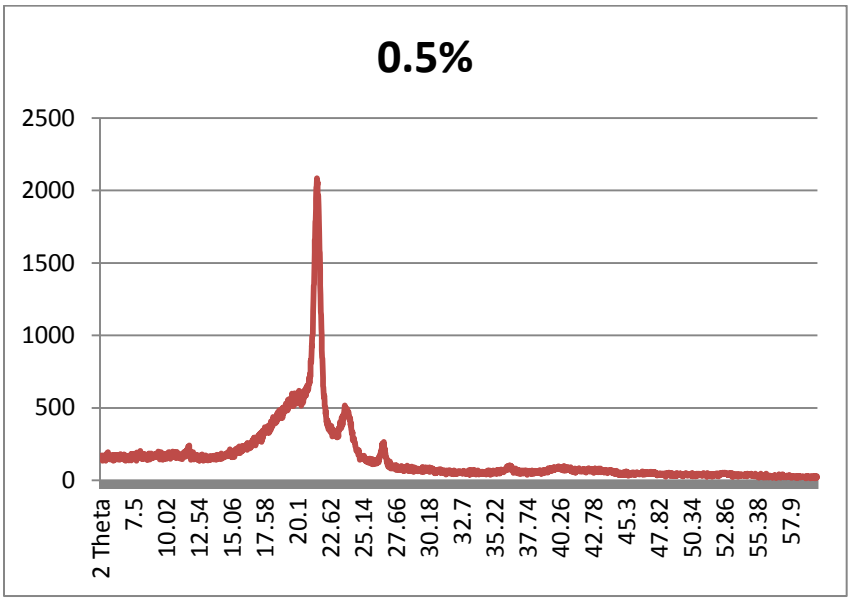

Figure A-2: 0.5% X-Ray Diffraction Pattern

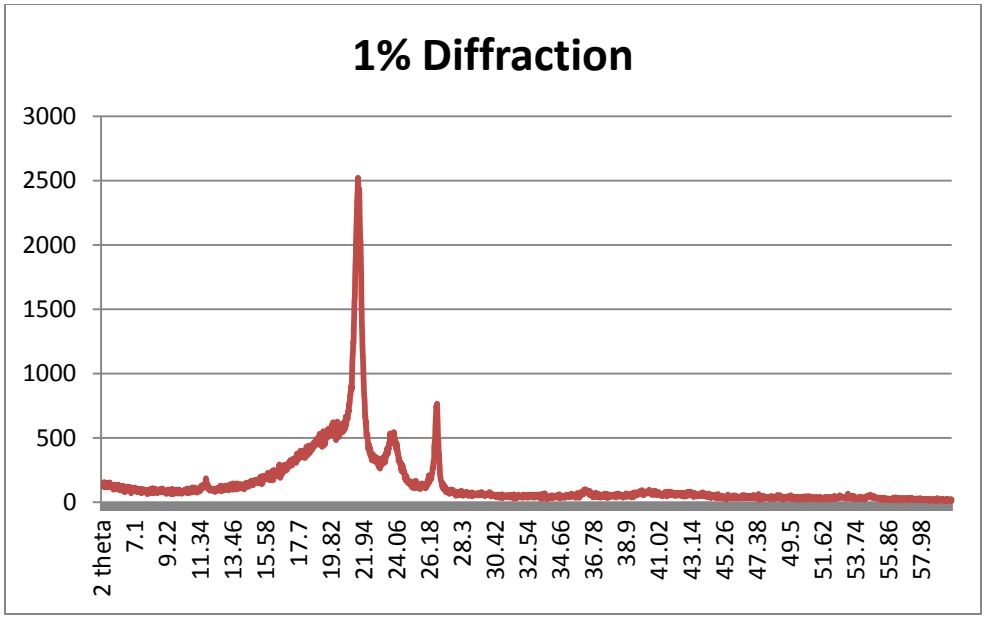

Figure A-3: 1.0% X-Ray Diffraction Pattern.

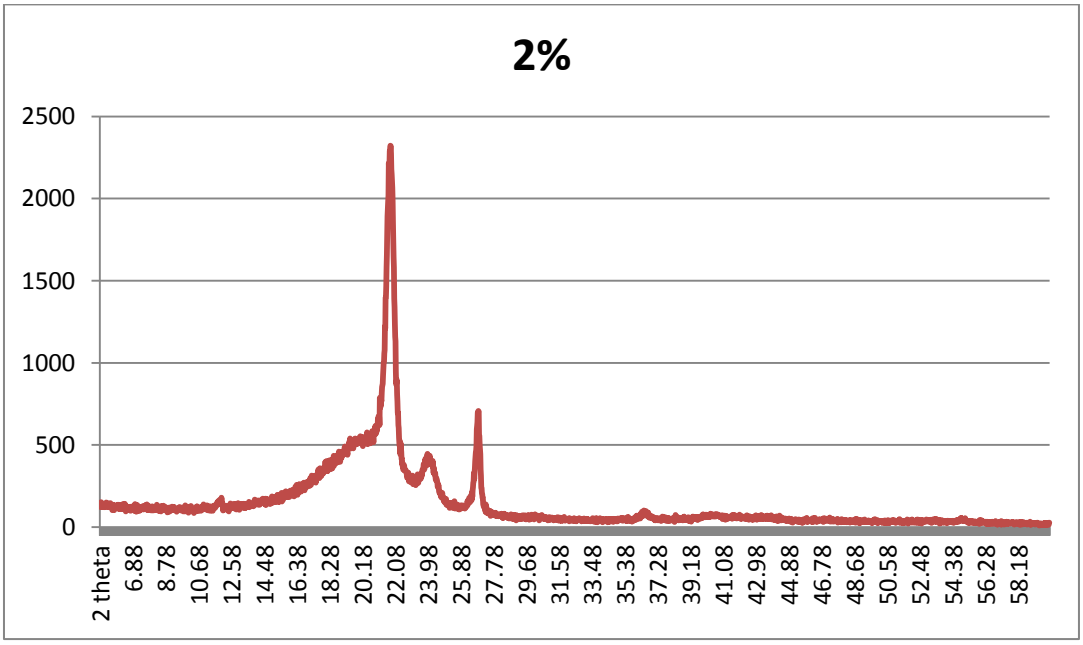

Figure A-4: 2.0% X-Ray Diffraction Pattern

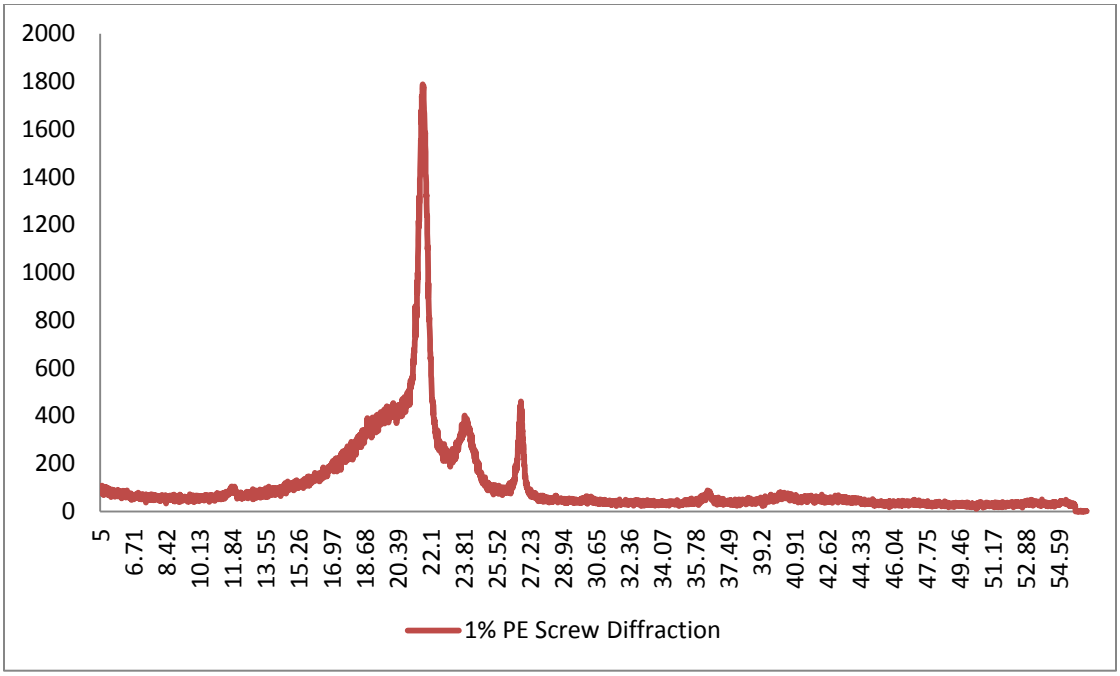

Figure A-5: 3.0% X-Ray Diffraction Pattern.

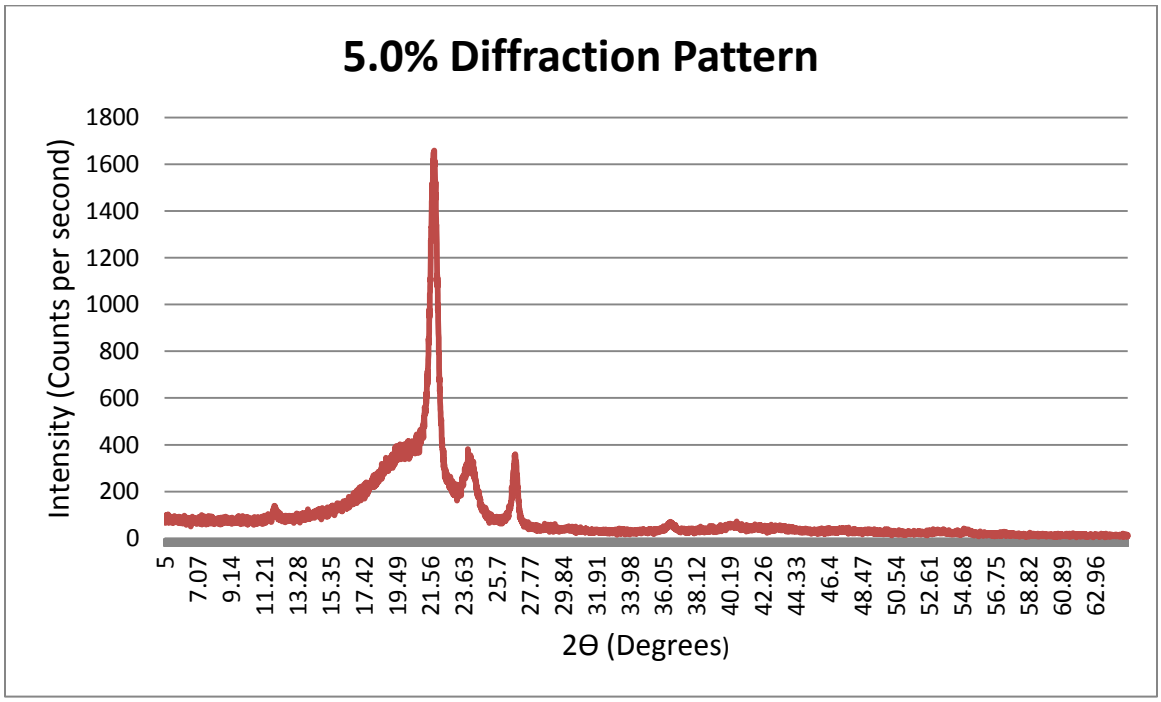

Figure A-6: 5.0% X-Ray Diffraction Pattern

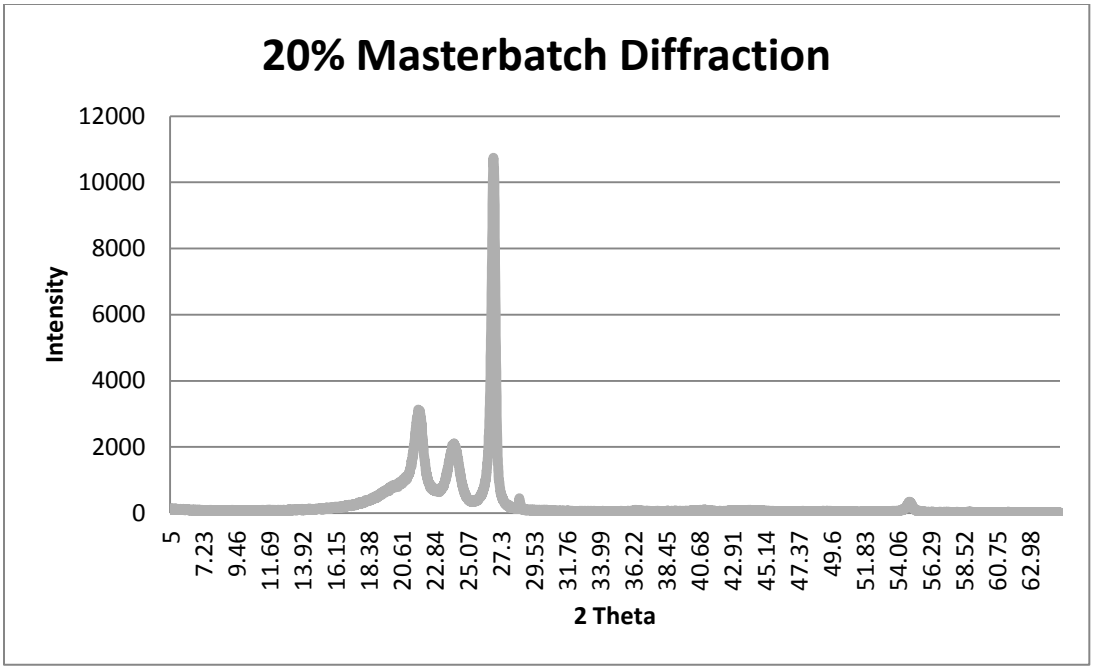

Figure A-7: Masterbatch X-Ray Diffraction Pattern

Appendix B

TD Stress Strain Curves of Film Samples

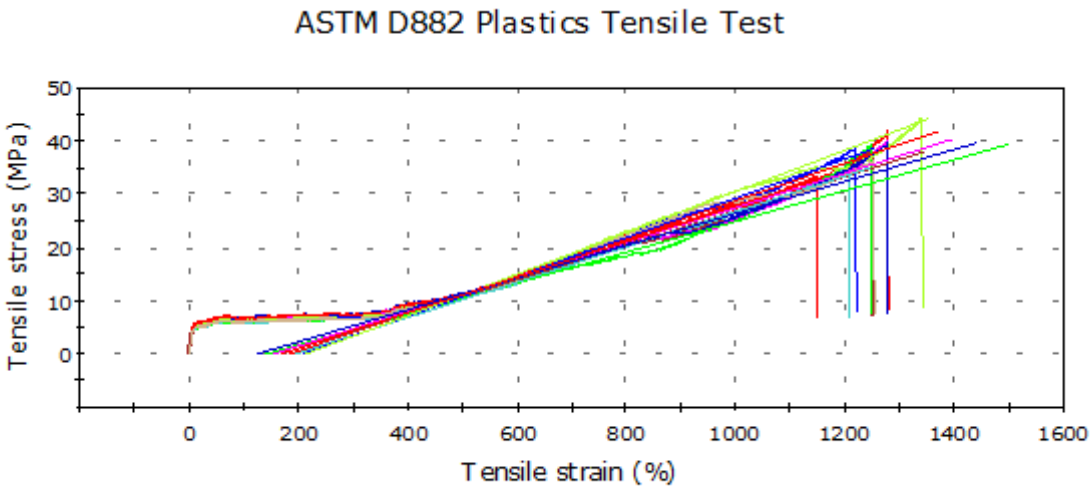

Figure B-1: 0.0% Control TD Stress Strain Curve

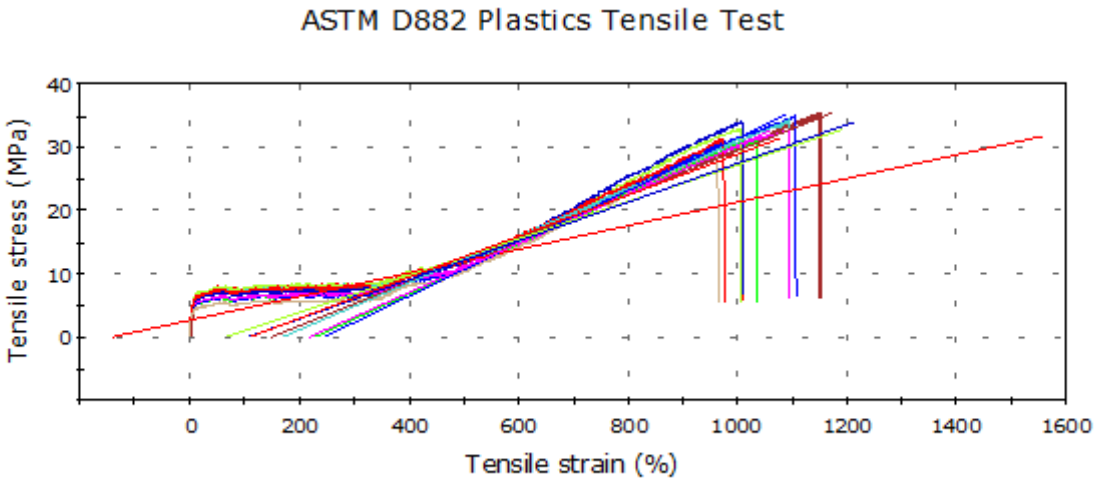

Figure B-2: 0.5% TD Stress Strain Curve

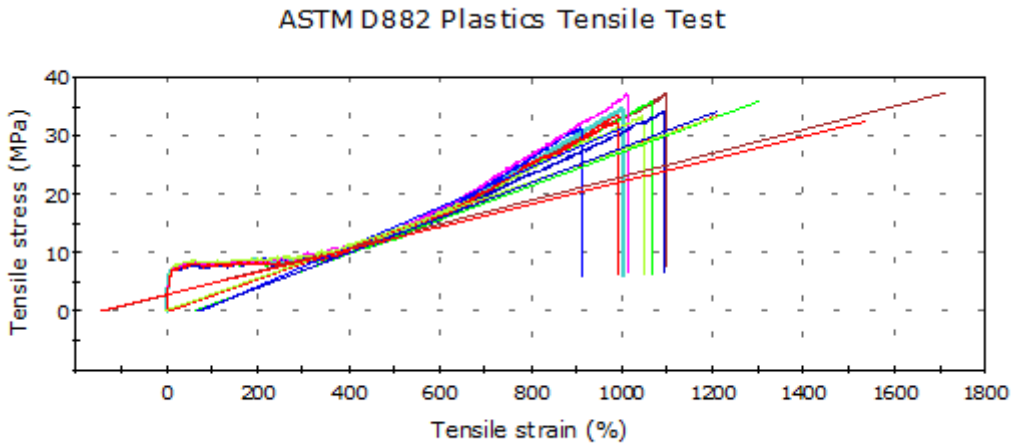

Figure B-3: 1.0% TD Stress Strain Curve

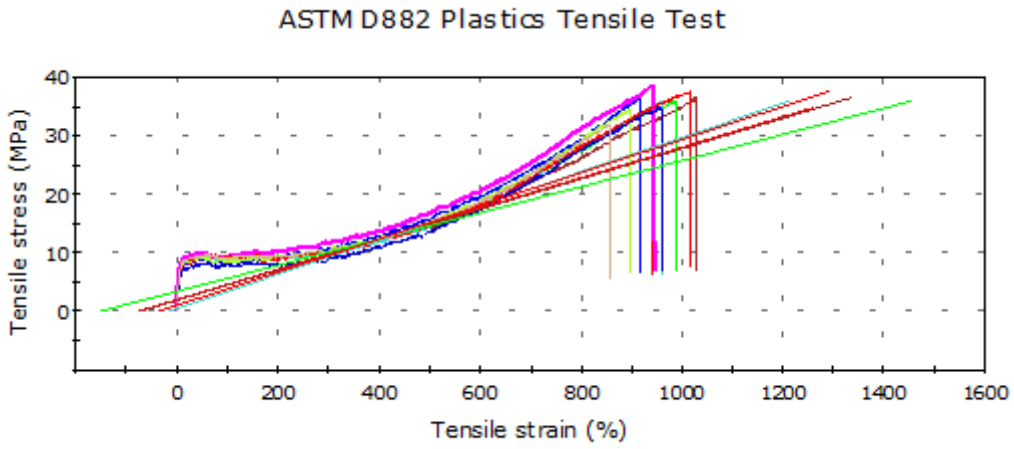

Figure B-4: 2.0% TD Stress Strain Curve

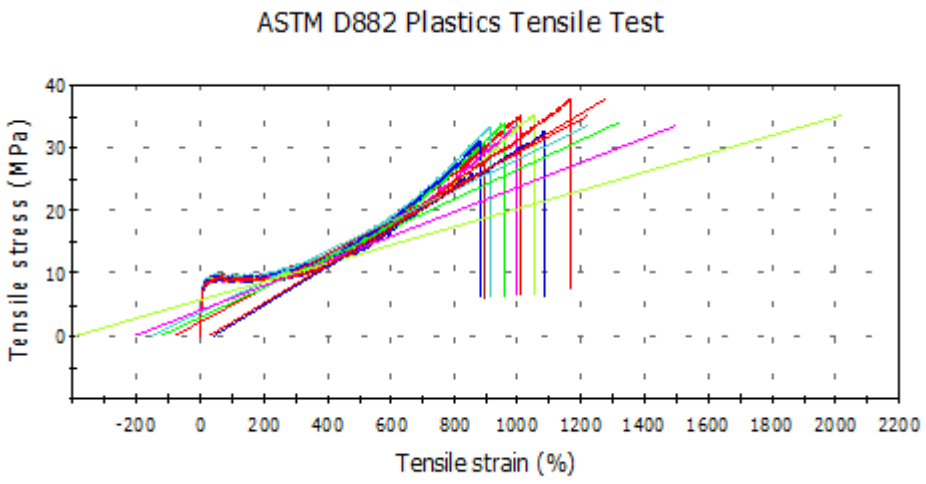

Figure B-5: 3.0% TD Stress Strain Curve

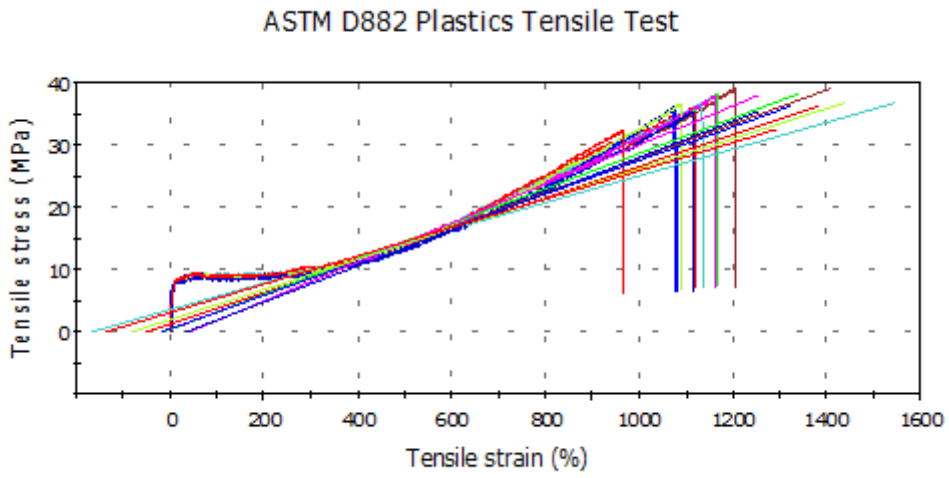

Figure B-: 5.0% TD Stress Strain Curve

Appendix C

MD Stress Strain Curves of Film Samples

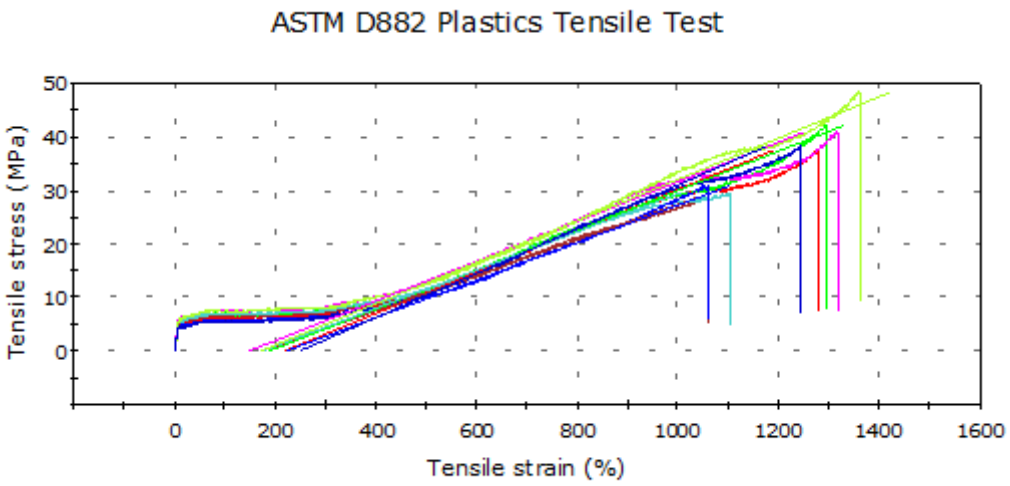

Figure C-1: 0.0% Control MD Stress Strain Curve

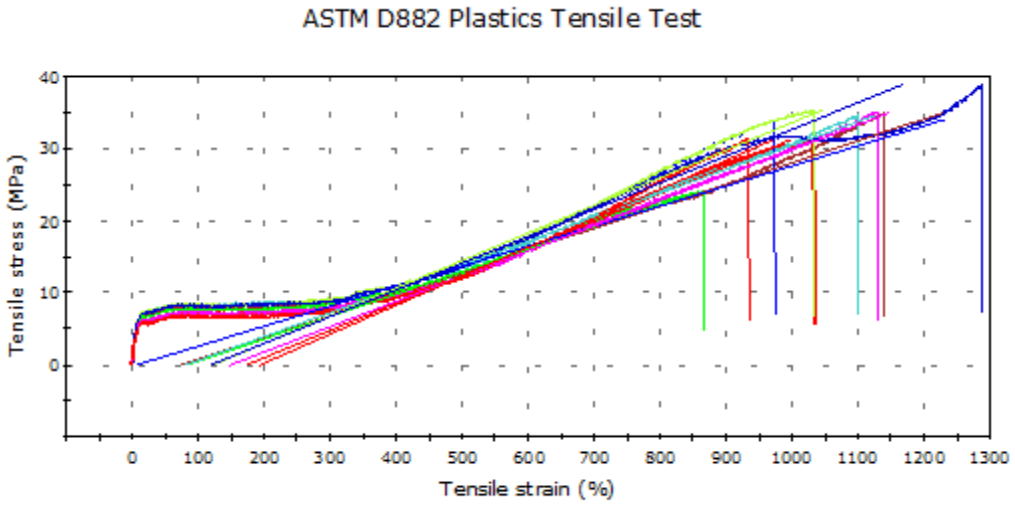

Figure C-2: 0.5% MD Stress Strain Curve.

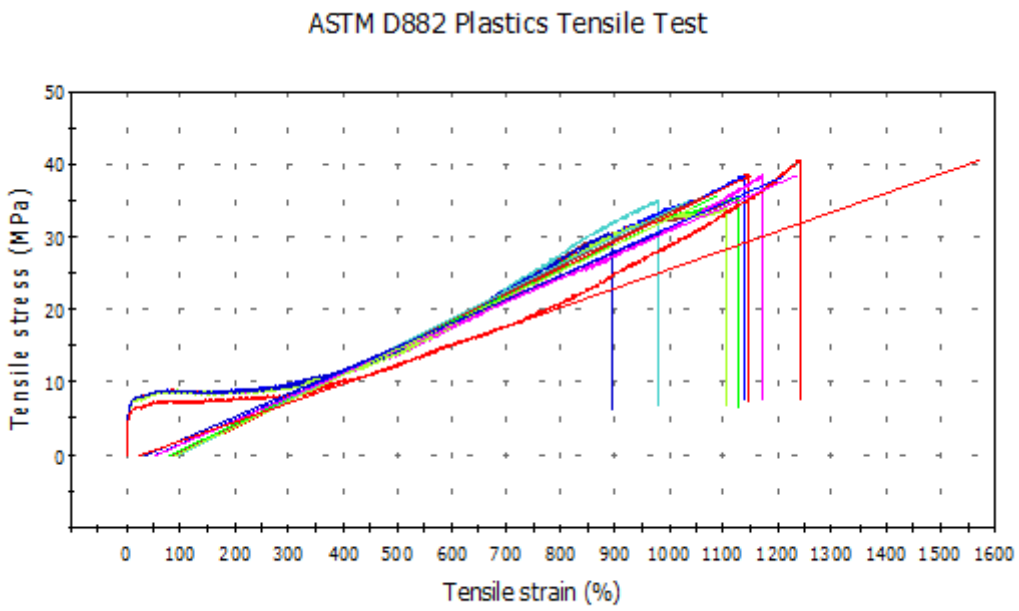

Figure C-3: 1.0% TD Stress Strain Curve

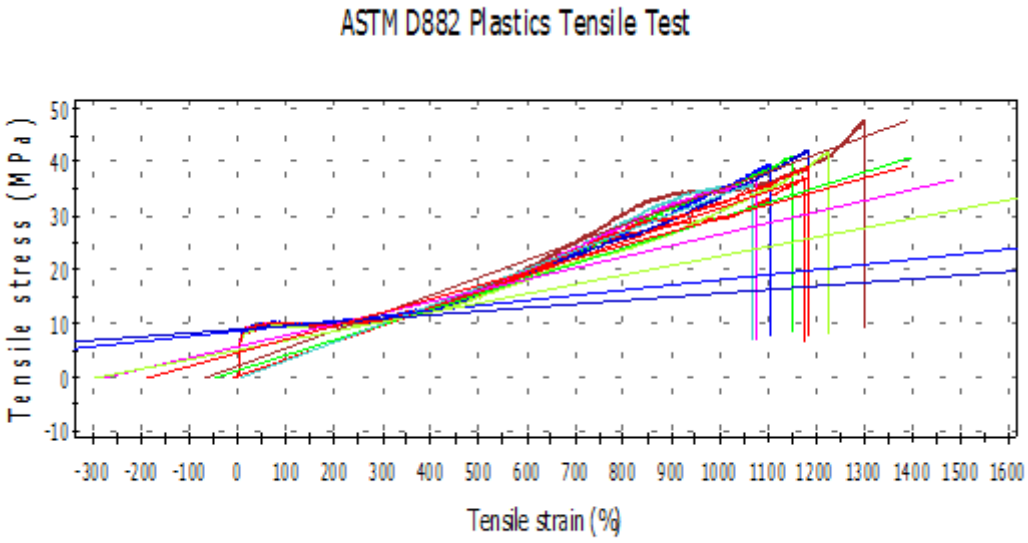

Figure C-4: 2.0% TD Stress Strain Curve

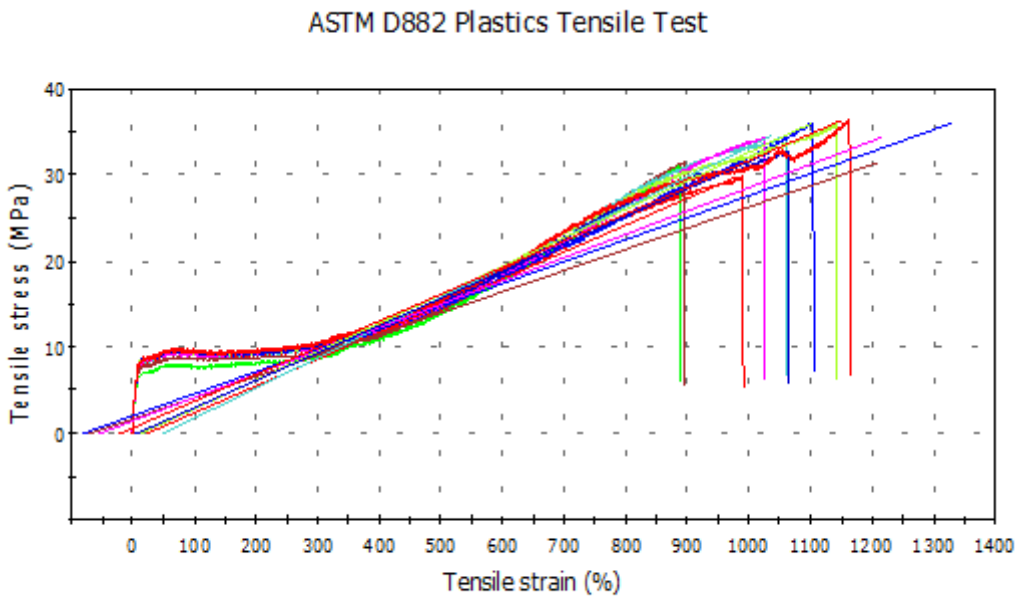

Figure C-5: 3.0% TD Stress Strain Curve

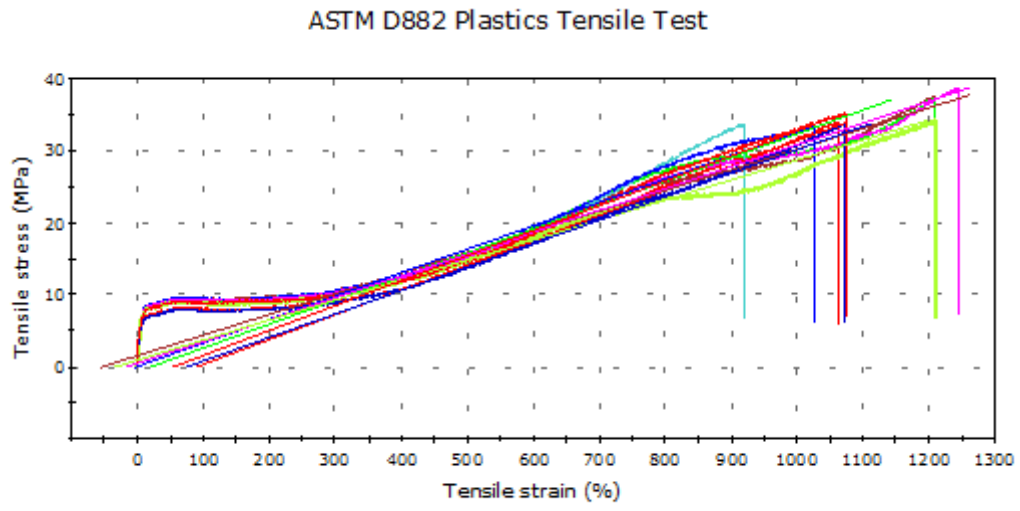

Figure C-6: 5.0% TD Stress Strain Curve

Appendix D

ASTM F 1306 Puncture Tests

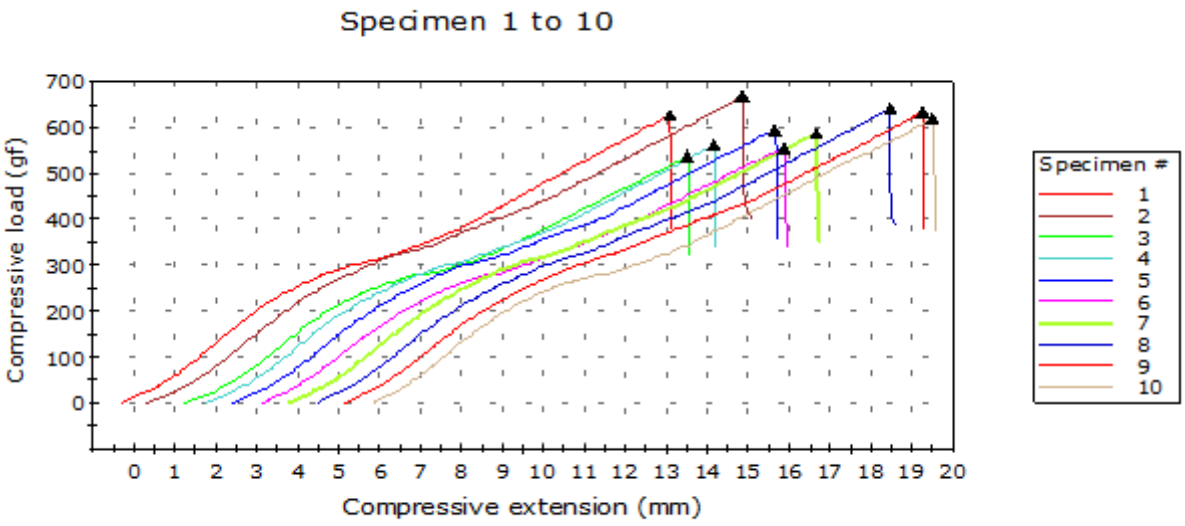

Figure D-1: 0.0% Control Sample Puncture Test

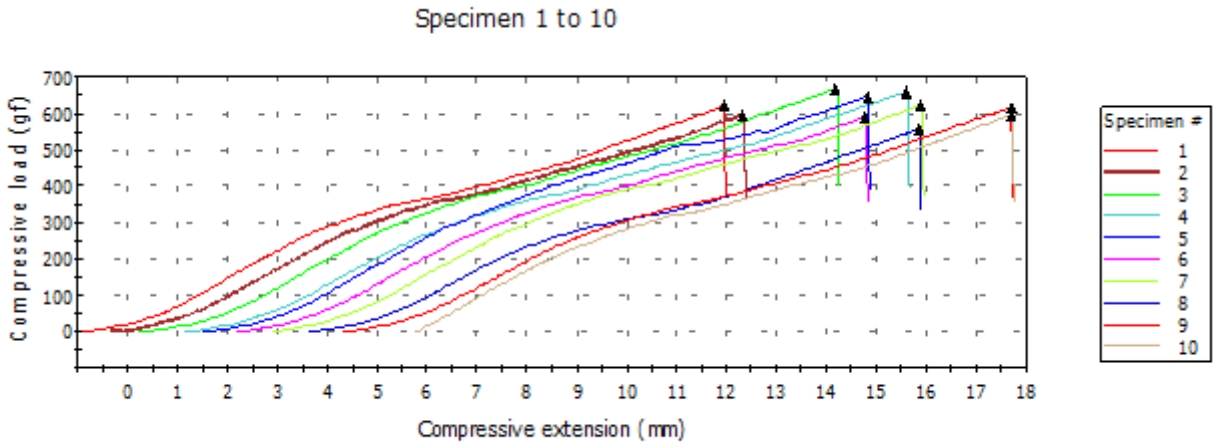

Figure D-2: 0.5% Puncture Test

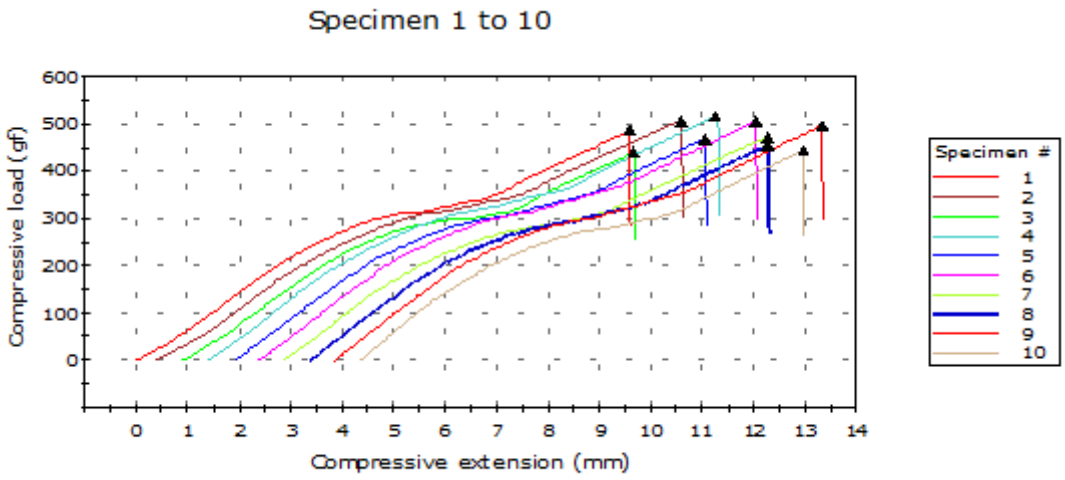

Figure D-3: 1.0% Puncture Test

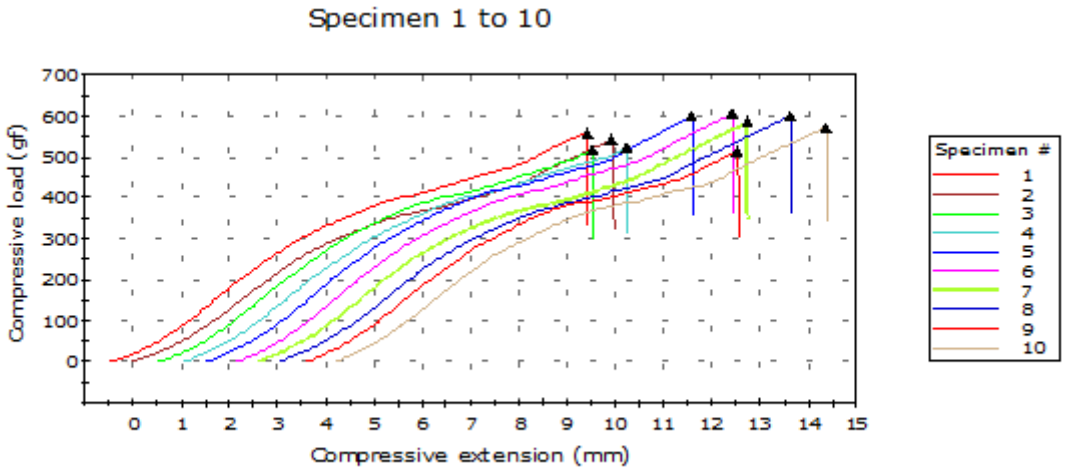

Figure D-4: 2.0% Puncture Test

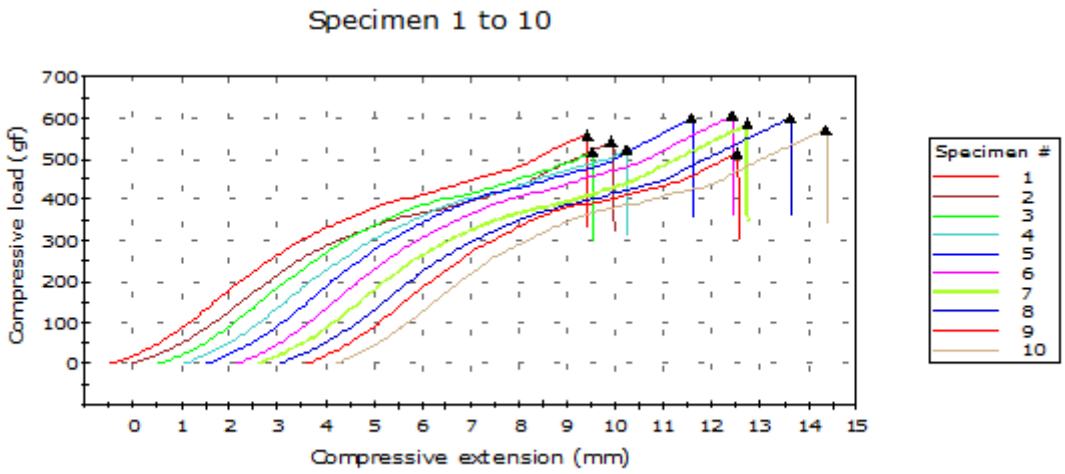

Figure D-5: 3.0% Puncture Test

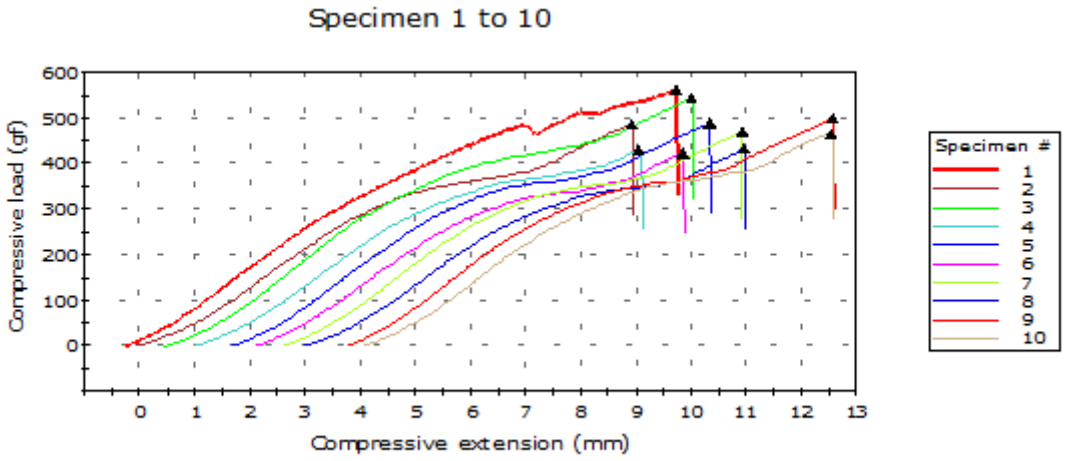

Figure D-6: 5.0% Puncture Test

Appendix E

Mechanical Property Summary Charts

	1% Secant Modulus (MPa)	Tensile Strength (MPa)	Elongation at Break (%)
0.0 % Control	76.14651	37.1	1214.6
0.50%	106.21593	33.3	1054.2
1.00%	127.92761	36.4	1103
2.00%	142.93131	40.2	1162.6
3.00%	136.96278	33.6	1036.3
5.00%	141.77457	35.4	1113.3

Figure E-1: MD Tensile Property Summary of Means

.

	1% Secant Modulus (MPa)	Tensile Strength (MPa)	Elongation at Break (%)
0.0 % Control	93.31438	38.9	1250.1
0.50%	111.0467	33.2	1052.5
1.00%	118.06865	34.6	1024.4
2.00%	147.99637	36.2	960.5
3.00%	141.5475	33.7	993.5
5.00%	145.215	36.6	1114.9

Figure E-2: TD Property Summary of Means

	Maximum Compressive Load (gf)	Elongation at Break (%)
0.0 % Control	93.31438	1250.1
0.50%	111.0467	1052.5
1.00%	118.06865	1024.4
2.00%	147.99637	960.5
3.00%	141.5475	993.5
5.00%	145.215	1114.9

Figure E-3: Puncture Resistance Testing of Means

Appendix F

DSC Curves

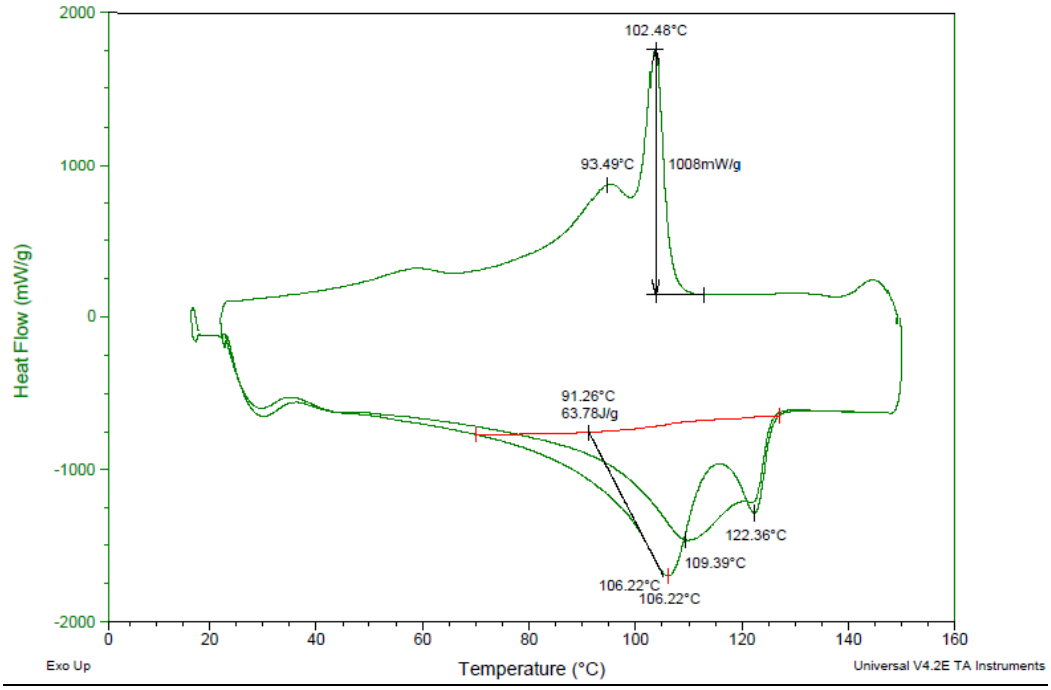

Figure F-1: 0.0% Control Sample DSC Curve

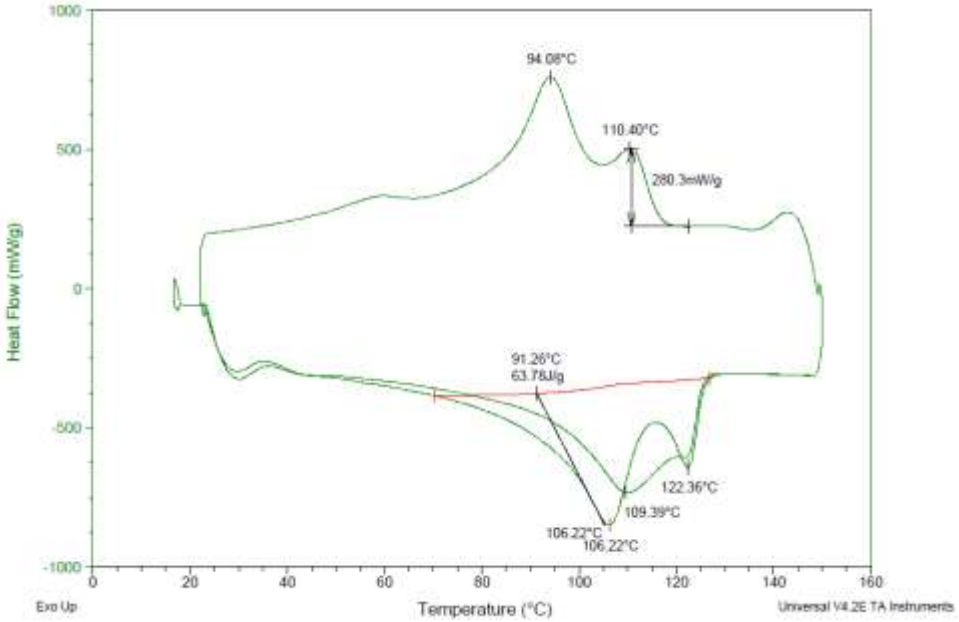

Figure F-2: 0.5% DSC Curve

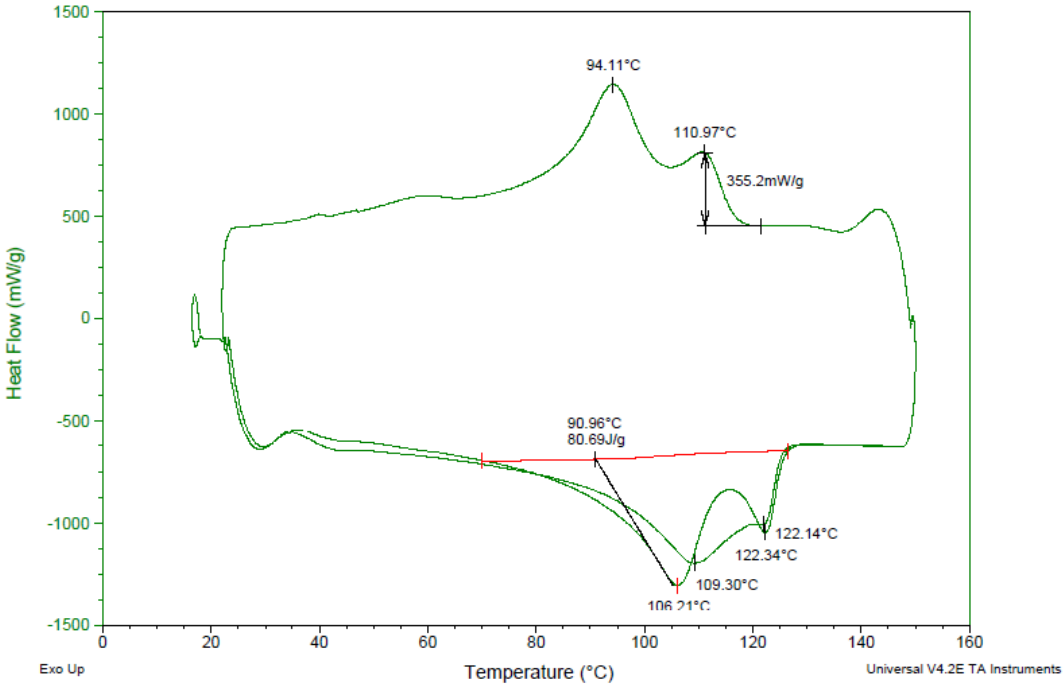

Figure F-3: 1.0% DSC Curve

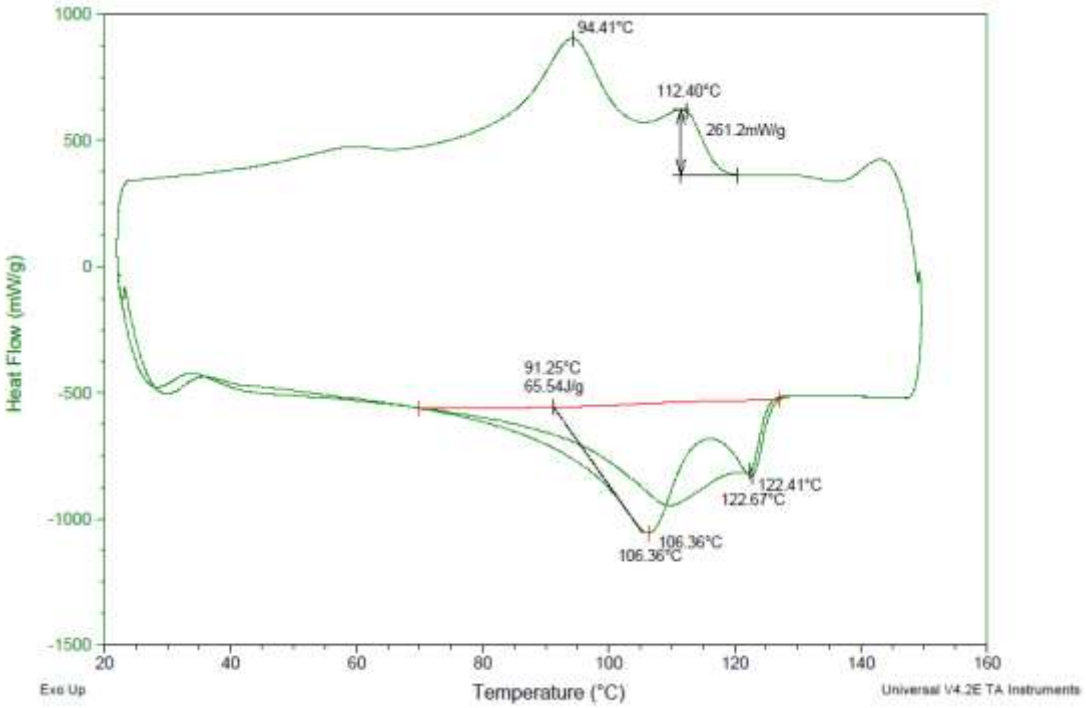

Figure F-4: 2.0% DSC Curve

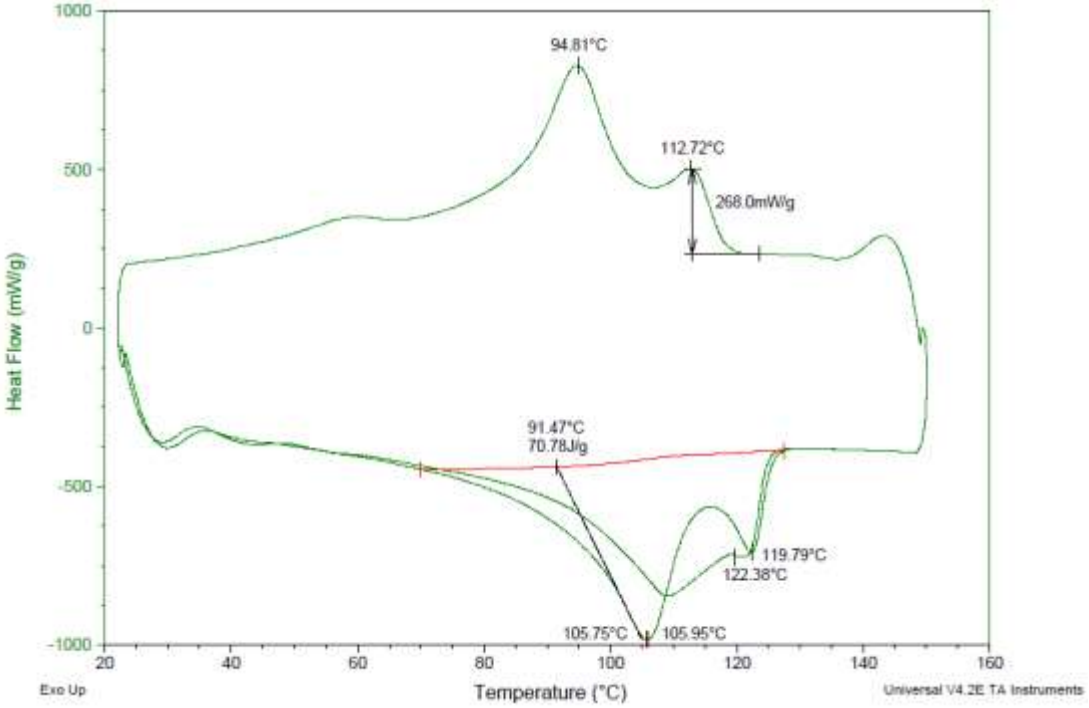

Figure F-5: 3.0% DSC Curve

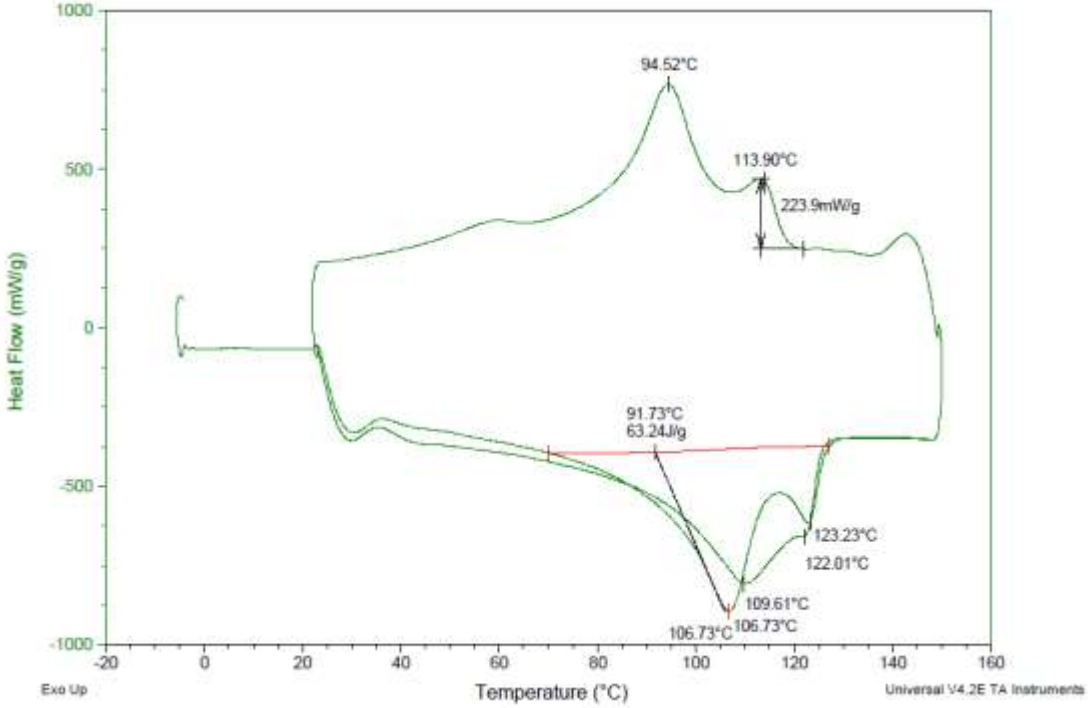

Figure F-6: 5.0% DSC Curve

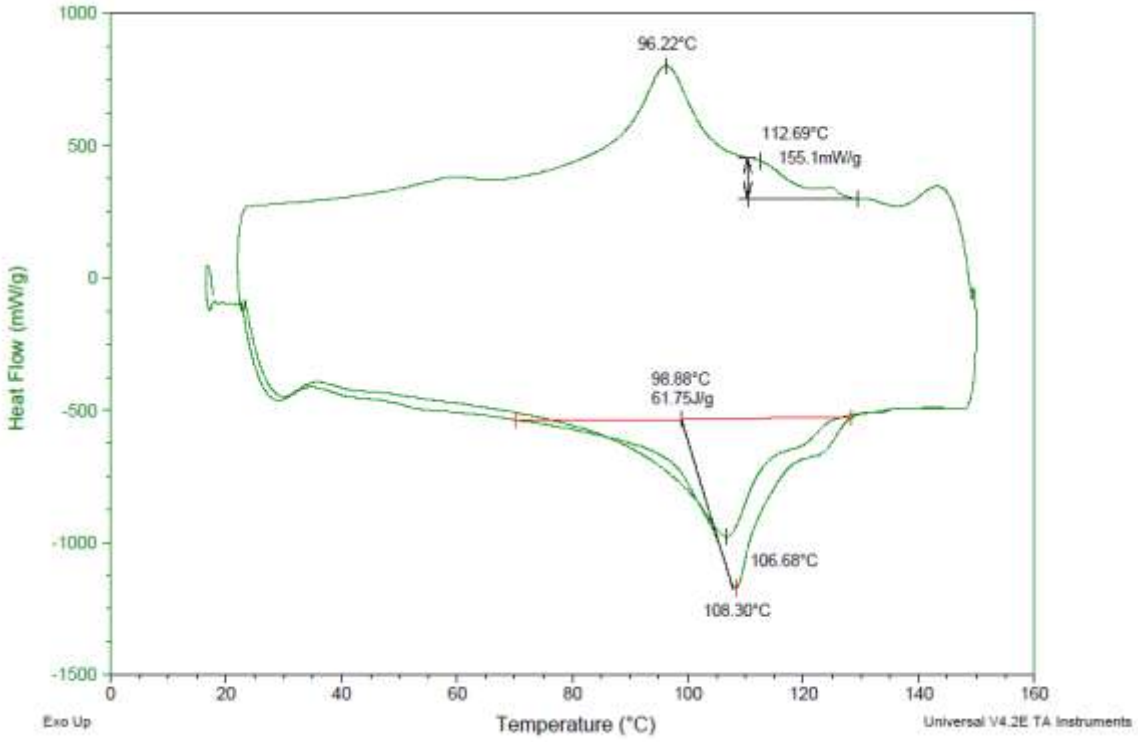

Figure F-7: 20% Masterbatch DSC Curve

REFERENCES

ASTM, (1993). "Standard Test Method for Water vapor Transmission of Materials.", Standard Designation E96-93. Annuel Book of ASTM, ASTM, 771- 778., Philadelphia, USA.

ASTM, (2001). "Standard Terminology Relating to Plastics.", Standard Designation D 883-00., Annual Book of ASTM Standards, ASTM, 169-178., Philadelphia, USA.

ASTM, (2002). "Standard Test Method for Oxygen Gas Transmission Rate Through Plastic Film and Sheeting Using a Coulometric Sensor.", Standard Designation D 3985-02., Annual Book of ASTM Standards, ASTM, Philadelphia, USA

Azeredo, H. M. (2009). Nanocomposites for food packaging applications. *Food Research International, 42*(9), 1240-1253. doi: 10.1016/j.foodres.2009.03.019

Bernard, C., Nguyen, T., Pellegrin, B., Holbrook, R. D., Zhao, M., & Chin, J. (2011). Fate of graphene in polymer nanocomposite exposed to UV radiation. *Journal of Physics: Conference Series, 304*, 012063. doi: 10.1088/1742-6596/304/1/012063

Callister, W. D., & Rethwisch, D. G. (2010). *Materials science and engineering: An introduction* (8th ed.). Hoboken, NJ: John Wiley & Sons.

Carotenuto, G., Nicola, S. D., Palomba, M., Pullini, D., Horsewell, A., Hansen, T. W., & Nicolais, L. (2012). Mechanical properties of low-density polyethylene filled by graphite nanoplatelets. *Nanotechnology*, *23*(48), 485705. doi: 10.1088/0957-4484/23/48/485705

Chaudhry, A., & Mittal, V. (2013). High-density polyethylene nanocomposites using masterbatches of chlorinated polyethylene/graphene oxide. *Polymer Engineering & Science*, *53*(1), 78-88. doi: 10.1002/pen.23241

Cheruvathur, R. (2009). *The Effect of Bond Strength of Flexible Laminates on Puncture Resistance.* (Unpublished master's thesis). Clemson University.

Cho, J., Logsdon, J., Omachinski, S., Qian, G., Lan, T., Womer, T. W., & Smith, W. S. (n.d.). Nanocomposites: A Single Screw Mixing Study of Nanoclay-filled Polypropylene. *ANTEC 2002*. Retrieved October 12, 2012, from http://www.tasmanmachinery.com.au/LinkClick.aspx?fileticket=L-ITcxQX5pQ%3D&tabid=79

Danzer, R., Supancic, P., Pascual, J., & Lube, T. (2007). Fracture statistics of ceramics – Weibull statistics and deviations from Weibull statistics. *Engineering Fracture Mechanics, 74*(18), 2919-2932. doi: 10.1016/j.engfracmech.2006.05.028

Darby, D., Cooksey, K., & Kimmel, R. (2007). Flavor and Aroma Permeation Concepts and Applications. *TAPPI PLACE*. Retrieved October 14, 2012, from http://www.tappi.org/content/enewsletters/eplace/2007/06PLA17.pdf

Darby, Duncan. Converting in Packaging (PKGSC 430) class notes

Etmimi, H. M. (2012). *New Approaches to the Synthesis and Exfoliation of Polymer/Functional Graphene Nanocomposites by Miniemulsion Polymerization* (Unpublished doctoral dissertation). University of Stellenbosch.

Frankland, J. (2010, May). Single-Screw Mixing 101 : Plastics Technology. Retrieved February 3, 2014, from http://www.ptonline.com/columns/single-screw-mixing-101

Frey, K. (2009). *Polyethylene and polypropylene in flexible barrier packaging*(Tech.). Retrieved August 01, 2014, from Tappi website: http://www.tappi.org/content/events/09PLACESY/Course_Papers/frey.pdf

Gennadios, A. and Weler, C. L. (1990). Edible films and coatings from wheat and corn proteins. Food Technol 44(10), 63-69.

Gupta, R. K., & Mukhopadhyay, P. (2011, January). Trends and frontiers in graphene-based polymer nanocomposites. *Plastics Engineering, 67*(1), 32. Retrieved July 20, 2014, from Academic OneFile.

Hofmann, D., Wartig, K., Thomann, R., Dittrich, B., Schartel, B., & Mülhaupt, R. (2013). Functionalized Graphene and Carbon Materials as Additives for Melt-Extruded Flame Retardant Polypropylene. *Macromolecular Materials and Engineering, 298*(12), 1322-1334. doi: 10.1002/mame.201200433

Jiang, X., & Drzal, L. T. (2011). Improving electrical conductivity and mechanical properties of high density polyethylene through incorporation of paraffin wax coated exfoliated graphene nanoplatelets and multi-wall carbon nano-tubes. *Composites Part A: Applied Science and Manufacturing, 42*(11), 1840-1849. doi: 10.1016/j.compositesa.2011.08.011

Kim, H., Abdala, A. A., & Macosko, C. W. (2010). Graphene/Polymer Nanocomposites. *Macromolecules, 43*(16), 6515-6530. doi: 10.1021/ma100572e

Kim, H., Kobayashi, S., Abdurrahim, M. A., Zhang, M. J., Khusainova, A., Hillmyer, M. A., ... Macosko, C. W. (2011). Graphene/polyethylene nanocomposites: Effect of polyethylene functionalization and blending methods. *Polymer, 52*(8), 1837-1846. doi: 10.1016/j.polymer.2011.02.017

Kobayashi, S., Kim, H., Macosko, C. W., & Hillmyer, M. A. (2013). Functionalized linear low-density polyethylene by ring-opening metathesis polymerization. *Polymer Chemistry, 4*(4), 1193. doi: 10.1039/c2py20883k

Kuila, T., Bose, S., Hong, C. E., Uddin, M. E., Khanra, P., Kim, N. H., & Lee, J. H. (2011). Preparation of functionalized graphene/linear low density polyethylene composites by a solution mixing method. *Carbon, 49*(3), 1033-1037. doi: 10.1016/j.carbon.2010.10.031

Kuila, T., Bose, S., Mishra, A. K., Khanra, P., Kim, N. H., & Lee, J. H. (2012). Effect of functionalized graphene on the physical properties of linear low density polyethylene nanocomposites. *Polymer Testing, 31*(1), 31-38. doi: 10.1016/j.polymertesting.2011.09.007

Kuilla, T., Bhadra, S., Yao, D., Kim, N. H., Bose, S., & Lee, J. H. (2010). Recent advances in graphene based polymer composites. *Progress in Polymer Science, 35*(11), 1350-1375. doi: 10.1016/j.progpolymsci.2010.07.005

Mhike, W., & Focke, W. W. (2013). Surface resistivity and mechanical properties of rotationally molded polyethylene/graphite composites. *Journal of Vinyl and Additive Technology, 19*(4), 258-270. doi: 10.1002/vnl.21316

Mukhopadhyay, P., & Gupta, R. K. (2013). *Graphite, graphene, and their polymer nanocomposites*. Boca Raton, FL: CRC Press.

Murray, L. (2006). The Impact of Foil Pinholes and Flex Cracks on the Moisture and Oxygen Barrier of Flexible Packaging. *TAPPI PLACE Conference*. Retrieved October 15, 2012, from http://www.tappi.org/content/enewsletters/eplace/2006/22-2murray.pdf

Nielsen, L.E. (1967) Models for the permeability of filled polymers systems. Journal of Macromolecular Science, Part A, vol. 1, no. 5, pp. 929–942.

O'neill, M. J., & Watson, E. S. (1694). *U.S. Patent No. 3263484 A*. Washington, DC: U.S. Patent and Trademark Office.

Potts, J. R., Dreyer, D. R., Bielawski, C. W., & Ruoff, R. S. (2011). Graphene-based polymer nanocomposites. *Polymer, 52*(1), 5-25. doi: 10.1016/j.polymer.2010.11.042

Richards, C. (2014, June 23). Defining graphene. Retrieved July 01, 2014, from http://www.rsc.org/chemistryworld/2014/06/defining-graphene-classification-grid

Selke, S. E., Culter, J. D., & Hernandez, R. J. (2004). *Plastics packaging: Properties, processing, applications, and regulations* (2nd ed.). Munich, Germany: Hanser Pub.

Silvestre, C., Duraccio, D., & Cimmino, S. (2011). Food packaging based on polymer nanomaterials. *Progress in Polymer Science, 36*(12), 1766-1782. doi: 10.1016/j.progpolymsci.2011.02.003

Siracusa, V. (2012). Food Packaging Permeability Behaviour: A Report. *International Journal of Polymer Science, 2012*, 1-11. doi: 10.1155/2012/302029

Stevens, M. (2012). Permeation and its Impact on Packaging. *Permeation and Its Impact on Packaging*. Retrieved March 02, 2014, from http://www.mocon.com/pdf/permeation/Perm%20%20Impact%20on%20Packaging.pdf

Thomas, S. (2012). *Polymer composites* (Vol. 1). Weinheim: Wiley-VCH.

Varma, V., Scheffer, D., Ginneman, C. R., & Lettow, J. S. (2012). *U.S. Patent No. EP2414286 A1*. Washington, DC: U.S. Patent and Trademark Office.

Vasileiou, A. A., Kontopoulou, M., & Docoslis, A. (2014). A Noncovalent Compatibilization Approach to Improve the Filler Dispersion and Properties of Polyethylene/Graphene Composites. *ACS Applied Materials & Interfaces*, 140122122451002. doi: 10.1021/am404979g

Verdejo, R., Bernal, M. M., Romasanta, L. J., & Lopez-Manchado, M. A. (2011). Graphene filled polymer nanocomposites. *Journal of Materials Chemistry, 21*(10), 3301. doi: 10.1039/c0jm02708a

Wang, J., Xu, C., Hu, H., Wan, L., Chen, R., Zheng, H., ... Wang, X. (210). Synthesis, Mechanical, and Barrier properties of LDPE/graphene nanocomposites using vinyl triethoxysilane as a coupling agent. *Journal of Nanoparticle Research*. Retrieved October 15, 2012, from http://link.springer.com/article/10.1007%2Fs11051-010-0088-y#page-1

Wang, L., & Pan, Y. (2011). Research frontiers and trends in graphene research. *Carbon, 49*(5), 1806. doi: 10.1016/j.carbon.2010.12.025

Yoo, B. M., Shin, H. J., Yoon, H. W., & Park, H. B. (2014). Graphene and graphene oxide and their uses in barrier polymers. *Journal of Applied Polymer Science, 131*(1), N/a-N/a. doi: 10.1002/app.39628

Zehetmeyer, G., Soares, R. M., Brandelli, A., Mauler, R. S., & Oliveira, R. V. (2012). Evaluation of polypropylene/montmorillonite nanocomposites as food packaging material. *Polymer Bulletin, 68*(8), 2199-2217. doi: 10.1007/s00289-012-0722-1

Zhong, Y., Janes, D., Zheng, Y., Hetzer, M., & Kee, D. D. (2007). Mechanical and oxygen barrier properties of organoclay-polyethylene nanocomposite films. *Polymer Engineering & Science, 47*(7), 1101-1107. doi: 10.1002/pen.20792

Zur Loye, H. (n.d.). X-Ray Diffraction: How it Works. *X-Rau Diffraction - An Overview*. Retrieved March 20, 2014, from http://www.chem.sc.edu/faculty/zurloye/xrdtutorial_2013.pdf